UNIVERSITÀ
DEGLI STUDI
FIRENZE

DOTTORATO DI RICERCA IN

NEUROSCIENZE

CICLO XXXV

COORDINATORE Prof.ssa Maria Pia Amato

Developing a genetic reporter to longitudinally study perineuronal nets *in vivo*

Settore Scientifico Disciplinare BIO/09

Dottorando

Dr. Calugi Francesco

Tutore

Prof.ssa Roberta Battini

Dr.ssa Laura Baroncelli

Coordinatore

Prof.ssa Maria Pia Amato

Anni 2019/2022

Index

1. Introduction

1.1 The key role of the extracellular matrix in the central nervous system

The central nervous system (CNS) is involved in the fascinating task of processing external stimuli to elaborate proper behaviors. This highly complex function is possible only through an extensive interconnection between neurons and glia through specialized structures such as the synapses. Historically, significant efforts have been made to understand CNS functions by focusing on the aforementioned cell populations and their constant dialogue without recognizing the importance of the space and the components in which they are embedded. Indeed, neurons, glia, and synapses are all surrounded and interact with the extracellular matrix, a heterogeneous and intricate network of glycoproteins, proteoglycans, and glycosaminoglycans that all together occupy nearly 20% of the entire CNS volume, a consistent fraction, that only recently is starting to gain the proper attention (Syková & Nicholson, 2008).

Far from being only a scaffolding structure that fills the extracellular space, the CNS extracellular matrix (ECM) is involved in many complex functions. In particular, the ECM is required for the complex coordination of the development of the CNS. From the proliferation of cells to their specialization, the acquisition of the proper shape and the migration, and the stabilization of the proper pattern of connections, many processes are regulated by the ECM (Long & Huttner, 2019). For instance, it has been shown that many ECM molecules and their receptors, such as the chondroitin sulfate proteoglycans (CSPGs), laminins, and integrins, are essential for the correct proliferation of neural progenitor cells and for their differentiation into neurons (Drago et al., 1991; Flanagan et al., 2006; W. Ma et al., 2008; Sirko et al., 2007; Stenzel et al., 2014). Moreover, laminins, integrins, and CSPGs are also involved in neurite outgrowth regulation, with laminins and integrins promoting this process, while CSPGs acting as inhibitors (Calof & Reichardt, 1985; Chen et al., 2009; Rolls et al., 2009). The inhibitory action of CSPGs is also observed in the adult stage. It has been observed, indeed, that following brain or spinal cord lesions, axonal growth is inhibited by the accumulation of CSPGs in the lesioned site. Accordingly, the enzymatic degradation of CSPGs promotes axon regeneration, axonal rewiring, and functional recovery, highlighting how the

comprehension of the different functions of the ECM is vital also from a clinical perspective (Bradbury et al., 2002; Moon et al., 2001; Rolls et al., 2009).

During postnatal development, the CNS acquires increasingly complex functions. The ECM, to sustain these needs, specializes in defined structures. For example, it has been demonstrated that the perinodal ECM develops postnatally around the nodes of Ranvier when myelination has been completed (Oohashi et al., 2002). The specific molecular composition and organization of the perinodal ECM reflect its function to help axons conduct electrical impulses at the proper velocity (Bekku et al., 2010).

Another striking ECM specialization that develops postnatally are perineuronal nets (PNNs). These honeycomb highly organized structures of extracellular matrix are tightly associated with different neuronal populations surrounding their soma and proximal processes. One characteristic that makes PNNs so intriguing is their close relationship with synapses, which are allocated in PNN-delimited holes (Sigal et al., 2019). In addition to delimiting synapse position, PNNs regulate synapses structurally and functionally (Frischknecht et al., 2009). The strict association between PNNs and synapses contributed to the development of a groundbreaking concept in neuroscience, the tetrapartite synapse model. Conventionally, the synapse is considered to be composed of three elements: the presynaptic element, the postsynaptic element, and the astrocytic projections that surround the synaptic active site (Araque et al., 1999; Lalo et al., 2021). In the last years, a growing literature has proposed to expand this model, including the ECM as another component of the functional synapse (Chelini et al., 2018; Dityatev & Rusakov, 2011).

In addition, many studies have demonstrated the involvement of PNNs in fundamental processes of the CNS, such as neuronal plasticity and memory (Gogolla et al., 2009; Pizzorusso et al., 2002), and alterations of these structures have been found in many pathologies related to the incorrect development of neuronal circuits or in neurodegenerative conditions (Wen, Binder, et al., 2018), thus demonstrating that PNNs represent a central part of the CNS.

Although many PNN functions in the physiology and the pathology of the CNS have been described, many questions remain open. In the present dissertation, I will describe in detail the role of PNNs in the CNS, focusing on their molecular composition, distribution, and the major findings regarding their involvement in physiological processes and pathological conditions. The ultimate goal of this introduction, however, will be to highlight that the study of these extracellular matrix structures has been strongly limited by the lack of reliable tools for the longitudinal visualization and analysis of PNNs *in vivo*.

1.2 Perineuronal nets

PNNs were first described by Camillo Golgi in the late 1800s as net-like structures tightly associated with neurons in the CNS. However, Ramon y Cajal dismissed these observations as a staining artifact, and PNNs were largely overlooked in the early 1900s due to Cajal's scientific influence. Only with the development of new staining techniques the interest in PNNs began to grow again. The study of PNNs underwent a turning point about 20 years ago with the discovery of their crucial role in neuronal plasticity and memory (Celio et al., 1998; H. H. Shen, 2018). To understand the many roles that these fascinating structures have in the CNS, it is necessary to introduce some fundamental information starting from their biochemical and molecular composition.

1.2.1 Structural components of PNNs

The highly organized PNN structure arises from the extended interconnection of its components, including chondroitin sulfate proteoglycans (CSPGs) of the lectican family, hyaluronan, tenascin-R, and structural stabilizers such as the hyaluronan and proteoglycan link proteins (Hapln) (fig.1a) (Oohashi et al., 2015).

Although it is still unclear which specific molecule guides the formation of PNNs *in vivo*, it has been reported that some components may be crucial in driving PNN assembly. An *in vitro* attempt to model PNNs has shown that the expression of the hyaluronan synthase 3 (HAS3) and of the link protein Hapln1 in HEK293T cells are essential in compacting the CSPGs in the pericellular space, suggesting that the same components may be crucial for PNN organization *in vivo* (Kwok et al., 2010). Indeed, similar results have demonstrated the key role of Hapln1 in guiding the appropriate maturation of PNNs *in vivo*, whereas it has been demonstrated that the genetic deletion of *Has3* does not impact the PNN number, without, however, demonstrating possible alteration in PNN organization (Arranz et al., 2014; Carulli et al., 2010). In other studies, the involvement of transgenic mouse lines deprived of tenascin-R and the CSPG aggrecan confirmed their key role in PNN organization. Indeed, tenascin-R KO mice show a tenuous PNN organization, whereas aggrecan KO mice show an almost absence of PNNs (Br&#xfffd;ckner et al., 2000; Morawski et al., 2014; Rowlands et al., 2018). Finally, the importance of hyaluronan on PNN organization has been demonstrated through an enzymatic approach. By injecting the bacterial enzyme hyaluronidase, PNNs

highlighted by a specific hyaluronan marker (HABP) disappeared (Yasuhara et al., 1994). To comprehend better how PNNs are organized, each major component will be introduced in the following paragraphs, starting from what is considered to be the backbone of the PNNs, the glycosaminoglycan (GAG) hyaluronan.

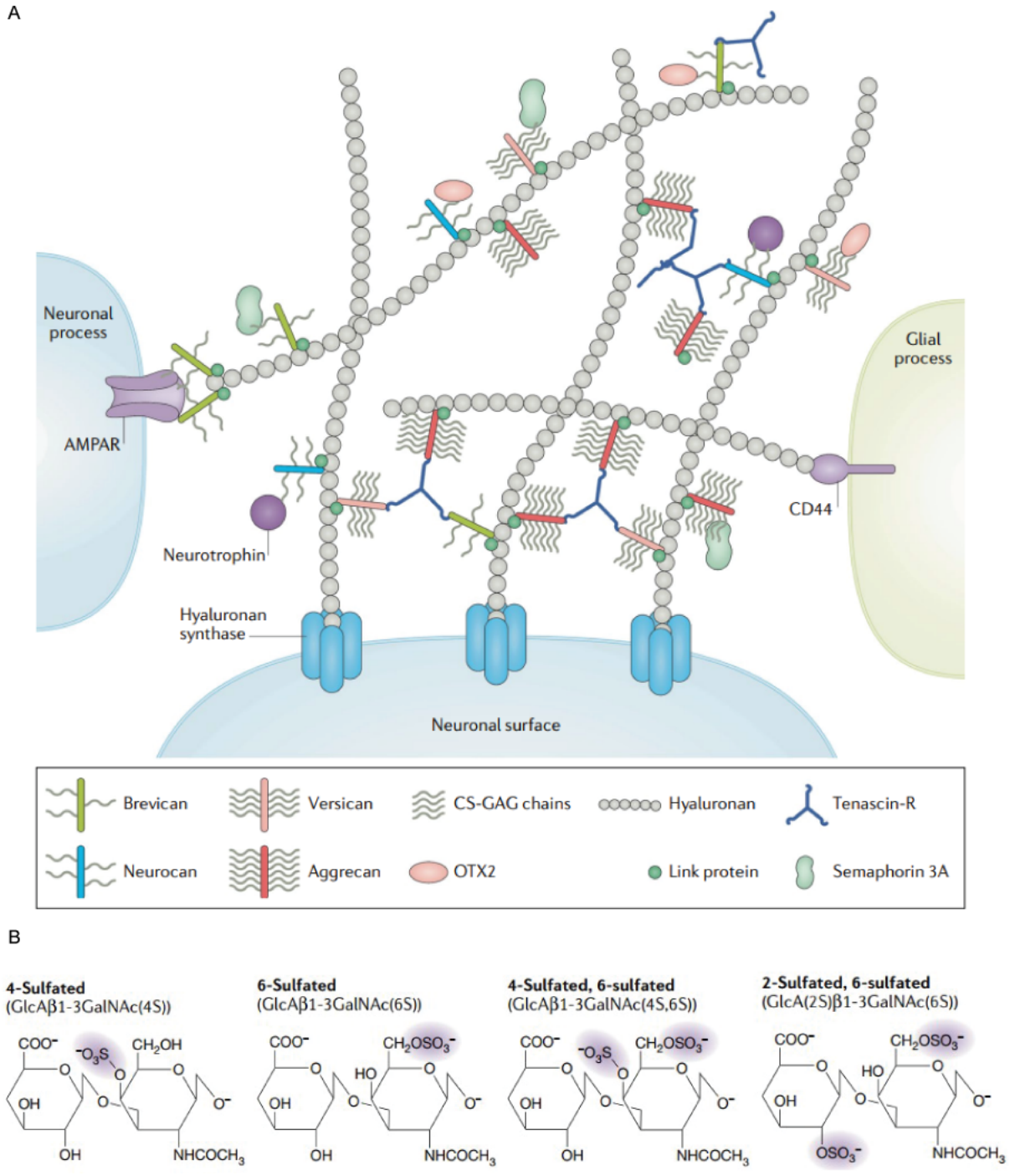

Fig.1: **(A)** Schematic representation of PNNs showing hyaluronan as an interaction site for the CSPGs, +which are strongly connected to it through the link proteins known as Hapln. In addition, the CSPGs are tightly packed together by tenascin-R, resulting in the characteristic alveolar structure of PNNs. **(B)** The "sulfation code" represented by the different sulfation patterns on the CSPGs provide binding sites for the interaction of different bioactive molecules (modified from Fawcett, Oohashi and Pizzorusso 2019).

Hyaluronan is a linear glycosidic polymer consisting of a repetition of disaccharide units of D-glucuronic and D-N-acetylglucosamine reaching weights from 5 to over 10,000 kDa (Li et al., 2017; Zimmermann & Dours-Zimmermann, 2008). Three different hyaluronan synthetases produce this GAG, which remains anchored to the cellular surface (Brückner et al., 1993; Itano & Kimata, 2002; Spicer & Tien, 2004; Tien & Spicer, 2005). Hyaluronan provides sites for the interaction of other ECM molecules, such as the CSPGs, whose binding is further stabilized by Hapln proteins, in particular Hapln1 and Hapln4 (Bekku et al., 2012; Carulli et al., 2010; Day & Prestwich, 2002; Kwok et al., 2010).

CSPGs are proteoglycans consisting of a core protein with branched chondroitin sulfate (CS-GAG) repeated units formed by N-acetylgalactosamine and D-glucuronic acid. The negative sulfated chemical groups of the CS-GAGs can be localized at different positions in the disaccharide units, forming different types of CS-GAG patterns as shown in fig.1b. The various CS-GAGs have biological relevance since the different distribution of the negative charges forms binding sites for transcription factors, neurotrophins, and other bioactive molecules, creating what is believed to be a “sulfation code” (Dick et al., 2013; Gama et al., 2006; Miyata et al., 2012; Vo et al., 2013). The importance of this code is also underlined by the difference in the sulfation pattern present in the CSPGs of the diffuse ECM and the PNN-CSPGs, suggesting that the molecules capable of binding PNNs may differ (Deepa et al., 2006). Moreover, the sulfation pattern changes throughout life, and alterations of this code may emerge in pathological conditions, reflecting a possible change in the pool of molecules capable of binding these extracellular matrix structures (Deepa et al., 2006; Scarlett et al., 2022). At birth, the CSPGs are mainly sulfated in position 6 (GalNAc6s) and less at position 4 (GalNAc4s). Then this ratio changes in favor of the 4 sulfated CS-GAGs and increases further with age (Foscarin et al., 2017; Miyata et al., 2012). The change in sulfation pattern significantly impacts neuronal functions since 6-sulfated CS-GAGs are known to be permissive for axon growth and plasticity, whereas 4-sulfated CS-GAGs are inhibitory (Lin et al., 2011; Miyata et al., 2012; H. Wang et al., 2008). Furthermore, the 4,6-sulfated chondroitin sulfate motif is recognized by the transcription factor OTX2, allowing it to act on the maturation and maintenance of PNNs (Beurdeley et al., 2012; Spatazza et al., 2013).

The most important PNN-associated CSPGs are aggrecan, neurocan, versican, and brevican, which share similar protein domains essential in interacting with other ECM components but differ from each other in a region where most of the GAG chains are linked (Zimmermann & Dours-Zimmermann, 2008). Among the PNN-CSPGs, aggrecan is the most represented, whereas the other PNN-CSPG may be present to a different extent (Dauth et al., 2016; Zimmermann & Dours-Zimmermann, 2008).

Aside from interacting with hyaluronan, the CSPGs also bind directly to membrane receptors, such as PTPσ receptors (RPTPσ), through the interaction with a positive amino acid motif in the first Ig-like domain present in the receptor sequence (Duan & Giger, 2010; Grumet et al., 1996; Y. Shen et al., 2009). Moreover, brevican is known to interact directly with AMPA receptors, promoting their clustering at excitatory synapses (Favuzzi et al., 2017).

The other two PNN molecular components, tenascin-R and the Hapln proteins, stabilize the interactions among the CSPGs and between the CSPGs and hyaluronan, respectively. Tenascin-R is a trimerized glycoprotein that interacts through its fibronectin III repeats domain to the CSPGs (Lundell et al., 2004). Among the four PNN-CSPGs, tenascin-R has the highest affinity for brevican, even though it is not clear the extent of this interaction for other CSPGs (Aspberg et al., 1997; Hagihara et al., 1999). As a trimer, Tenascin-R may interact with three different CSPGs cross-linking different PNN components and generating the typical organized structure of the PNNs (Kwok et al., 2011). Indeed, mice lacking tenascin-R show less condensed PNNs due to their impaired development (Br�ckner et al., 2000; Weber et al., 1999)(Brückner et al., 1993; Itano & Kimata, 2002; Spicer & Tien, 2004; Tien & Spicer, 2005)(Br�ckner et al., 2000; Weber et al., 1999). Since the last fundamental components of PNNs, i.e, Hapln proteins will be of great interest in this dissertation, their discussion will be detailed in the next section.

1.2.1.1 The Hapln link protein family

The Hapln link proteins are a family of four small proteins of 38-43 kDa that stabilize the interaction between the CSPGs and hyaluronan (Faltz et al., 1979; Kwok et al., 2011). The resulting molecular complex consists of one CSPG and one link protein interacting with the hyaluronic acid chain on average every 100 hyaluronan monosaccharides (Faltz et al., 1979). While Hapln1 and Hapln3 are widely expressed in the organism, Hapln2 and Hapln4 are specific for the CNS (Hirakawa et al., 2000; Spicer et al., 2003). All the four members of the Hapln link family share similar features, such as a putative signal peptide at the N-terminus, an Ig domain to interact with the CSPGs, and two consecutive link modules to bind hyaluronan (fig.2a) (Deák et al., 1999; Heinegård & Hascall, 1974; Spicer et al., 2003). The four link proteins are identical for nearly 50% of their amino acid sequence, with similarities reaching more than 60% (Hirakawa et al., 2000; Spicer et al., 2003). Moreover, the amino acidic sequence of the link proteins is conserved between mice and humans, with

the lowest percentage of identity for Hapln3 (81%) and the highest identity for Hapln1 (96%) (fig.2c) (Spicer et al., 2003). The functional differences between the four link proteins are unclear. One possibility is that they interact to different extents with the CSPGs, generating specific ECM structures. Indeed, Hapln2 is part of the perinodal ECM, whereas Hapln1 and Hapln4 are localized in PNNs and expressed by PNN-associated neurons (Bekku et al., 2010; Carulli et al., 2006, 2010; Galtrey et al., 2008; Oohashi et al., 2002). Single-cell transcriptomic analysis have revealed that Hapln1 is expressed in the cortex by many interneurons, including the parvalbumin (PV) and Lamp5-positive subsets and astrocytes, whereas Hapln4 is expressed by excitatory and inhibitory neurons but not from astrocytes (Tasic et al., 2018).

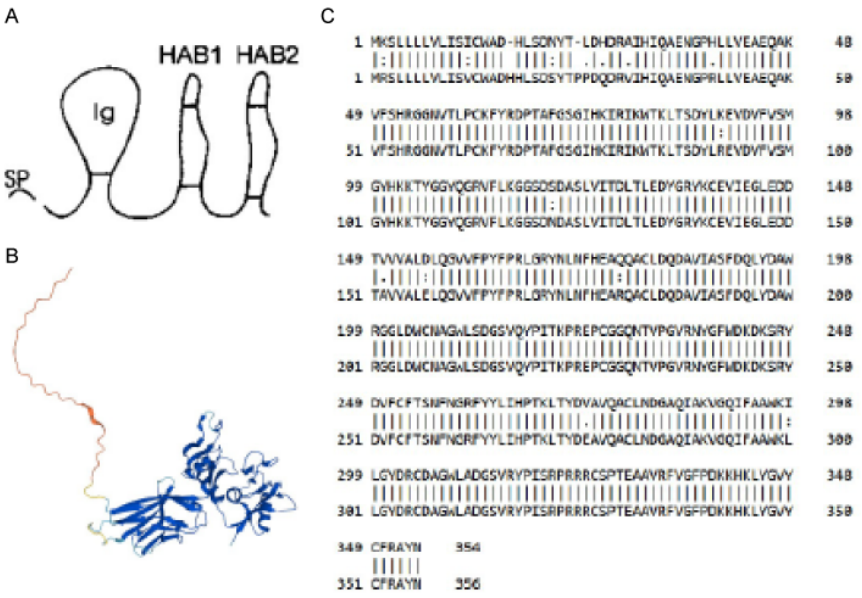

Fig.2: **(A)** Schematic representation of the Hapln1 link protein . SP signal peptide; Ig immunoglobulin domain; HAB hyaluronan binding domain (Deák et al., 1999). **(B)** 3D hypothetical model of the Hapln1 predicted by AlphaFold. The color code represents the confidence in the 3D reconstruction with low confidence in red and very high confidence in blue (Jumper et al., 2021). **(C)** Alignment between human (above) and mouse (bottom) Hapln1 protein sequences. Note the extensive homology represented by the vertical bars.

Once secreted in the extracellular space, link proteins are very stable, with Hapln1 having a turnover of over 80 days (Fornasiero et al., 2018). This very low turnover rate could remark the importance in stabilizing PNNs and guiding their formation and maintenance. In an attempt to create an *in vitro* model of PNNs in cell cultures, it was demonstrated that the expression of Hapln1 and HAS3 in HEK293T cells is essential to condense aggrecan near the cell surface, revealing a likely similar function for Hapln1 *in vivo* (Kwok et al., 2010). Accordingly, it has been also reported that mice lacking Hapln1 in the CNS show less condensed PNNs, reflecting an impairment in their development (Carulli et al., 2010). Unlike the CSPGs, which have both high biochemical variability due to the heterogeneity in their sulfation pattern and high variability in the molecular PNN composition, there are no reports describing the absence of Hapln1 in PNNs. This feature may be crucial since, as previously

described, PNNs may undergo various modifications making their unique identification difficult (Ueno, Fujii, et al., 2018)

1.2.2 The long journey towards the understanding of PNN heterogeneity

The different biochemical composition of PNNs, represented by the different sulfation patterns of the CSPGs, poses the challenge of recognizing all PNNs (Fawcett & Kwok, 2022). Indeed, for PNN visualization, several molecules are involved. Among PNN markers, one class consists of plant lectins, among which the *Wisteria Floribunda Agglutinin* (WFA) is considered the standard marker for PNNs (Härtig et al., 1992; Kosaka & Heizmann, 1989). This lectin is known to recognize both non-reducing and internal residues of N-acetylgalactosamine located in the GAG chains of the CSPGs, and it has been shown that these residues are devoid of sulphation (Nadanaka et al., 2020). Moreover, some antibodies that detect aggrecan and label PNNs (Cat-315 and Cat-316) recognize different CS-GAGs than the WFA (Lander et al., 1997; Matthews et al., 2002). Interestingly, it has been demonstrated that although both WFA and anti-aggrecan antibodies can recognize many PNNs, some PNNs are recognized by only one of these markers, making it challenging to recognize PNNs uniquely (Miyata et al., 2018; Ueno et al., 2017; Ueno, Fujii, et al., 2018). Accordingly, many classes of PNNs exist, but this number is probably underestimated, and eventually, it will increase with the introduction of additional markers or by labeling these structures genetically.

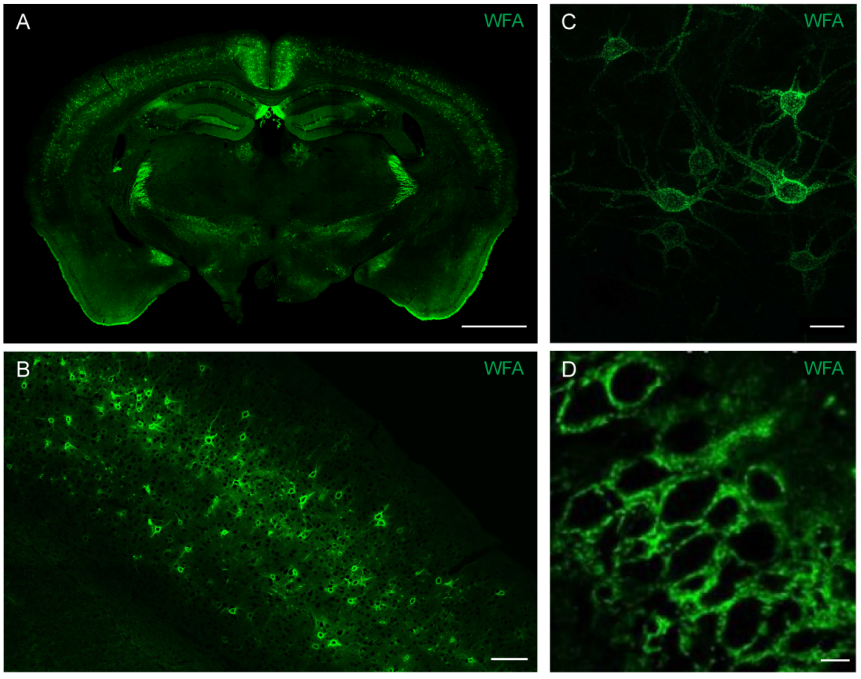

Fig.3: Representative images of PNN distribution and different morphologies across the CNS. (A) PNNs are unevenly distributed across the brain. Note the different density between brain areas. Scale bar 1mm **(B)** PNNs are not homogeneously distributed in the cortex. In the visual cortex PNNs are more dense in layer 4 and less in layer 2/3 and 5. Scale bar 100µm **(C-D)** Representative images of the different PNN morphologies in the visual cortex (C), and in the CA2 region of the hippocampus (D). Scale bar 20µm in C and 10µm in D. In D image modified from Lensjo et al. 2017.

Regardless of the marker used, the results of the different labeling methods converge in the concept that PNNs are not distributed homogeneously in the CNS, as shown in the representative image of fig.3a. If in some regions of the CNS PNNs are abundant, such as in the cortex, in deep nuclei of the cerebellum and in some deep structures of the brain, in others such as the hippocampus PNNs are sparser. Moreover, it is important to note that even in the same brain region PNNs have an irregular distribution. For instance, PNNs are more abundant in layer 4 of the cortex, while they are less present in the superficial and deep layers (fig.3b). The reason for such a heterogeneous PNN distribution in the CNS is still unclear. What we know is that PNNs are associated with particular cell types having a peculiar fast-spiking profile and that this association is decisive in the functionality of the structures and circuits in which they are present (Carulli & Verhaagen, 2021).

In addition, PNNs present various morphologies (fig.3c-d). If, on the one hand, PNNs are structurally complex and extensively localized around the soma and proximal processes of neurons, on the other hand, some PNNs look more like particularly pronounced pericellular matrix aggregates. However, even in this case, the reason for this diversity is still to be determined.

The already vast heterogeneity of PNNs from a biochemical, distribution, and morphological perspective is further incremented by the different associations these structures have with the various neuronal populations. In the spinal cord, both excitatory and inhibitory neurons are surrounded by PNNs to various extents according to the specific layer or structure (Galtrey et al., 2008; Irvine & Kwok, 2018; Tansley et al., 2022). Similarly, in the brain neuronal subsets surrounded by these structures change based on the region. For instance, in the deep cerebellar nuclei (DCN) of the cerebellum, PNNs are localized around large excitatory neurons, whereas in the cerebellar cortex, PNNs surround Golgi cells (Carulli et al., 2006). In the visual thalamus PNNs are absent in the dorsal lateral geniculate nucleus (LGN), whereas in the ventral region of the LGN, two different classes of PNNs cluster in separate regions. The Cat315-positive PNNs are localized in the outer region of the vLGN around parvalbumin-positive (PV) interneurons. In contrast, WFA-positive PNNs are confined to the inner region of the vLGN, surrounding an unknown neuronal subset (Sabbagh et al., 2018). In the amygdala of adult mice, most of the neurons associated with PNNs are excitatory (Morikawa et al., 2017), whereas in the hippocampal CA2 region, both pyramidal excitatory neurons and PV interneurons are ensheathed by PNNs (Carstens et al., 2016; Lensjø, Christensen, et al., 2017; Morikawa et al., 2017).

Although PNNs associated with excitatory neurons are also documented in the cortex, most of the neurons ensheathed by these structures are PV interneurons (Härtig et al., 1994; Lensjø, Christensen, et al., 2017). An extensive quantification of the colocalization between PV interneurons and PNNs throughout the cortex is not available yet. However, it is known

that in regions such as the primary visual cortex, about 75% of parvalbumin neurons are associated with PNNs (Lensjø, Christensen, et al., 2017; Ye & Miao, 2013). Interestingly, the colocalization between PNNs and PV interneurons changes across the visual cortical layers (Faini et al., 2018; Ye & Miao, 2013). Moreover, a differential distribution across the cortical layers is also observed for WFA-positive PNNs and Cat-315 positive PNNs, with the first primarily localized in layers IV and V and the second most in layers V and VI (Lensjø, Christensen, et al., 2017; Miyata et al., 2018; Pizzorusso et al., 2002; Ye & Miao, 2013).

Although the heterogeneity of PNNs in terms of biochemical composition, distribution, and association with various neuronal populations has been known for a long time, it is only in recent years that their complexity has begun to be recognized. Efforts to analyze the meaning of such differences are only at the beginning, and reliable tools that can help to dissect this complexity would be fundamental in this challenging task. Since the markers used up to now cannot definitively address the problem of the heterogeneity of PNNs, new methods must be developed. As evident from the topics covered above, one of the most intriguing questions regarding PNNs is their association with the different neuronal populations, comprising not only neurons belonging to different categories, such as excitatory and inhibitory neurons but also neurons belonging to the same neuronal subpopulation, such as PV interneurons. The existence of two different cortical populations of PV interneurons, one associated with PNNs and one not surrounded by these extracellular matrix structures, suggests that they might be differently involved at a microcircuit level. As explained in the following paragraphs, the maturation of PNNs significantly impacts circuit development and stability, so understanding why they mature only around some specific neurons would answer key questions that have been intriguing the scientific community for a very long time.

1.3 The constant dialogue between PNNs and experience

One of the fascinating features of the CNS is that it can be shaped by experience to adapt to the ever-changing environment. This fundamental property, called experience-dependent plasticity, includes several functional and structural neuronal modifications essential for the post-natal development of circuits but also for learning and memory in the adult brain. PNNs are key structures in the regulation of plasticity (Carulli et al., 2010; Pizzorusso et al., 2002). Traditionally, PNNs have been considered stable brakes of plasticity, limiting the impact of experience on neuronal circuits. However, recent evidence suggests that experience regulates extracellular matrix structures even after their full development, introducing new and exciting aspects regarding PNNs and their functions. In the following paragraphs, the reciprocal influence between PNN and experience will be treated, starting with the role of PNNs in the post-natal development of the CNS.

1.3.1 PNNs and developmental plasticity

Experience has a significant impact on post-natal circuit development in temporally defined periods called critical periods (Berardi et al., 2000; Hensch, 2005). The existence of such periods has been demonstrated using classical paradigms based on sensory deprivation to evaluate the impact of such manipulations on neuronal circuit rearrangements. In the visual cortex of rodents, it has been observed that monocular deprivation (MD) leads to massive changes in binocular-responsive neurons to process visual stimuli only in a period spanning from the around post-natal day (P) 19 to P35. In particular, after a brief period of MD, a weakening of the responses to visual stimuli coming from the deprived eye is associated to the strengthening of the responses coming from the eye that has remained open, defining a process known as ocular dominance plasticity (Gordon & Stryker, 1996; Hubel & Wiesel, 1970; Wiesel & Hubel, 1963). If the same paradigm is carried out in adult mice, the effects are strongly attenuated and are characterized by different physiological and molecular mechanisms (Lehmann & Löwel, 2008; Ranson et al., 2012; Sato & Stryker, 2008). The strict temporal limitation of these periods of heightened plasticity implies the existence of

mechanisms for their definition, among which the maturation of inhibitory circuits, and in particular PV interneurons, and the maturation of PNNs are key events for their opening and their closure (Fagiolini et al., 2004; Fagiolini & Hensch, 2000; Hensch et al., 1998; Pizzorusso et al., 2002; Yazaki-Sugiyama et al., 2009).

The prominent role of PNNs in regulating the closure of developmental plasticity was long debated since, from the first evidence of the ECM involvement in limiting developmental plasticity, it was not possible to understand whether the effect was mediated by the diffuse ECM or by PNNs (Pizzorusso et al., 2002). Indeed, in the seminal study of Pizzorusso and colleagues, the injection in the rat adult visual cortex of a bacterial enzyme that degrades the CSPGs, the chondroitinase ABC (ChABC), restored juvenile-like ocular dominance plasticity. However, since the enzyme activity was not specifically directed towards PNNs, it was not possible to understand the different contributions in limiting plasticity between PNNs and the diffuse ECM (Pizzorusso et al., 2002). Supporting the role of PNNs as plasticity regulators, transgenic animals depleted in some fundamental PNN components such as Hapln1 or aggrecan show impaired PNNs and persistent plasticity in adulthood but only animals lacking the Hapln1 link protein present an overall content of the CSPGs not different from WT mice, suggesting that the impairment in the aggregation of the CSPGs in PNNs is important in restricting plasticity (Carulli et al., 2010; Rowlands et al., 2018).

Although PNNs limit the influence of experience in shaping neuronal circuits, the experience itself drives the maturation of these structures. Indeed, sensory activity plays a fundamental role for the expression of some PNN components such as aggrecan and Hapln1 prior to PNN aggregation and without these molecules PNNs can't form properly (Carulli et al., 2010; McRae et al., 2007; Pizzorusso et al., 2002; Ye & Miao, 2013). In fact, alongside the decrease of the aforementioned PNN components, in rodents raised in darkness it was observed an impairment in PNN formation and persistent plasticity in adulthood (Carulli et al., 2010; Pizzorusso et al., 2002).

In addition to the induction of PNN aggregation, experience also drives PNN development. As a mediator of experience, the homeobox transcription factor OTX2 promotes the maturation of PNNs (Beurdeley et al., 2012; Hou et al., 2017; Sugiyama et al., 2008). OTX2 is expressed in the retina and transported along the visual pathway in an experience-dependent manner and, after reaching the visual cortex, OTX2 interacts with the CSPGs in the PNNs (Beurdeley et al., 2012; Sugiyama et al., 2008). It has been demonstrated that OTX2 accumulation in PNNs is promoted by the developmental change in the CSPG sulfation pattern (Miyata et al., 2012). During the critical period, the GAG-CS are mostly sulfated in position 6, which is associated with a more plastic state. Then the sulfation changes in favor of the more inhibitory sulfation in position 4 and it is this shift that promotes the association between PNNs and OTX2 (Miyata et al., 2012). After being internalized by

PV interneurons, OTX2 promotes the expression of aggrecan, so further promoting the expression of one of the fundamental components of PNNs (Beurdeley et al., 2012; Hou et al., 2017; Sugiyama et al., 2008). Interestingly, OTX2 is also essential in the maintenance of adult PNNs. Interfering with OTX2 expression in the choroid plexus of adult mice leads to a decrease in PNNs and to a reopening of an adult plastic period (Spatazza et al., 2013).

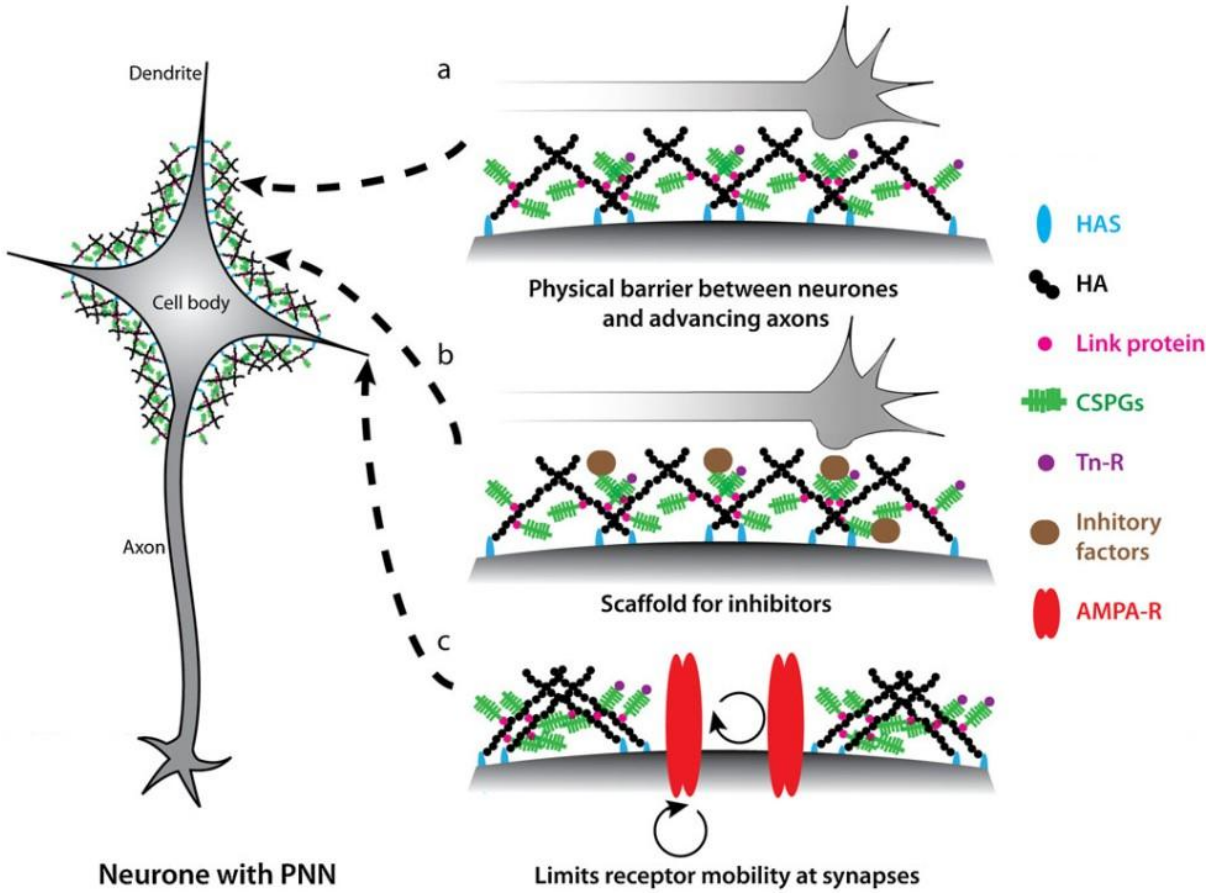

Fig.4: Illustration of PNN possible inhibitory actions on plasticity. PNNs may act as mere physical barriers preventing the formation of new connections. The sulfation pattern on the CSPGs are binding sites for inhibitory factors, such as the axon repulsive molecule Sema3a. PNNs restrict synaptic AMPA receptor trafficking limiting synaptic functional plasticity. The interaction between the PNN-CSPGs and PTPσ receptors limit plasticity in adulthood. Modified from Wang et al., 2012.

Despite the involvement of PNNs in limiting plasticity has been extensively described in the literature, the mechanisms through which these structures exert their control are still not well understood (fig.4). One hypothesis is that the PNNs act as a physical barrier preventing the rearrangement of neuronal circuits, limiting the formation of new contacts between neurons. The molecular composition of PNNs is rich in CSPGs and these molecules are known to be axonal repulsive and inhibit axonal growth after injury (Bradbury et al., 2002; Cheah et al.,

2016). Another possible mechanism by which PNNs inhibit plasticity may lie in their ability to limit AMPA receptors mobility, thus preventing functional and structural synaptic plasticity (Frischknecht et al., 2009). Aside from creating a physical barrier for neuron's interaction and receptor mobility, it has been demonstrated that PNNs are capable of binding, through specific sulfation patterns, inhibitory factors for neurite growth and targeting such as Sema3a (Dick et al., 2013). Indeed, the specific disruption of the Sema3a signaling leads to a reopening of plasticity in adulthood, confirming the important role of PNNs as a hub for bioactive axonal inhibitory molecules (Boggio et al., 2019). Another mechanism through which PNNs exert their negative action on plasticity is through their association with RPTPσ. Indeed, the association between the PNN-CSPGs and the RPTPσ promotes the dephosphorylated status of the receptor TrkB repressing its intracellular signaling. PNN degradation promotes TrkB phosphorylation leading to a new period of plasticity in adulthood (Lesnikova et al., n.d.).

1.3.2 Experience as a long-lasting regulator of PNNs

The need for the central nervous system to change based on experience cannot be limited to specific developmental periods only. Some degree of plasticity must remain into adulthood to allow the CNS to adapt to the ever-changing environment. Traditionally, PNNs have been considered highly stable and immutable due to their function as brakes of plasticity. However, mounting evidence shows that these structures are modified by various factors even after the end of the critical period. Indeed, PNNs have been observed in adult mice to change in a circadian manner in different brain areas involved in emotional memory processing (Pantazopoulos et al., 2020). Although the meaning of this rapid remodeling is not completely understood yet, circadian modifications of PNNs could be linked to a temporary increase in plasticity to allow, for example, the formation and stabilization of new memories (Pantazopoulos et al., 2020). A change in PNNs associated with heightened plasticity was indeed observed in adult animals reared in an enriched environment characterized by high levels of social interactions and enhanced cognitive, sensory, and motor stimulations (Sale et al., 2007). Amblyopic adult rats reared under such conditions show not only a reduction of PNNs in the visual cortex but also a recovery of visual acuity, effects otherwise absent in amblyopic animals reared in standard conditions (Sale et al., 2007).

It is worth noting that the environment can be a double-edged sword in influencing the development and the functions of the CNS. Impoverished environments characterized by isolation or social stress can lead to cognitive impairment and depressive states (Von Frijtag et al., 2000). It has been shown that adult rats subjected to a paradigm of social defeat associated with prolonged social isolation show impaired hippocampal plasticity mirrored by an increase in PNNs in this region, which seems to be essential in determining the cognitive impairments observed in these animals (Riga et al., 2017).

The mechanisms through which the environment impacts PNNs are not clear. It has recently been observed that changes in neuronal activity can lead to modifications of PNNs in adulthood (Carstens et al., 2021; Devienne et al., 2021). It is likely that experience, influencing the activity of neuronal circuits, may cause a change in the expression of PNN components and PNN degrading enzymes. Indeed, a decrease in the mRNAs of aggrecan and Hapln1, paralleled by an increase in ECM protease activity, have been observed in the cerebellum of adult-enriched animals (Foscarin et al., 2011).

Other environmental factors affecting PNNs in adulthood are nutrition and diet. After being fasted overnight, the re-fed mice showed increased PNN in the medial eminence, which is a key structure involved in energy homeostasis (Kohnke et al., 2021). Interestingly, the enzymatic degradation of PNNs led to increased food intake behavior, suggesting that PNNs may have a regulatory role in energy balance (Kohnke et al., 2021). Moreover, rodents fed with a hypercaloric diets show alterations on PNN density in brain regions related to energy homeostasis, decision-making, and cognitive function, such as the hypothalamus, prefrontal cortex, and hippocampus (Dingess et al., 2018; Reichelt et al., 2021; Zhang et al., 2021). Furthermore, mice genetically deprived of the hormone leptin show impaired PNN maturation in the arcuate nucleus of the hypothalamus, suggesting that altered metabolic conditions such as overnutrition or related diseases may impact PNNs even in adulthood (Mirzadeh et al., 2019).

In summary, positive stimulations, such as environmental enrichment, or negative stimulations, such as social defeat and social isolation, can modify PNNs. As a result, PNNs can be continuously reshaped throughout life. Interestingly, PNNs have also been shown to change with age. In particular, in sensory cortices, the number of neurons surrounded by PNNs increases in 12 months aged mice compared to 2 months aged mice (Ueno, Takao, et al., 2018). Moreover, during aging, a constant reduction of the plastic 6 sulfated CSPGs in favor of the inhibitory 4 sulfated CSPGs takes place, which may reflect impairments in adult plasticity (Foscarin et al., 2017).

In order to adapt to the continuous changes in the environment, organisms need to modulate their state of plasticity throughout life. This need is demonstrated by regulating PNNs in response to various stimuli. Given the different outcomes that PNN regulation may have,

monitoring PNN structural changes longitudinally and the effects these changes might have on neuronal activity would help us better understand the impact of the various stimuli on the CNS. It is currently impossible to carry out this type of *in vivo* longitudinal study due to the lack of adequate means. In designing a methodology for visualizing PNNs *in vivo*, however, it is necessary to consider the constant change of PNNs from a biochemical perspective. Indeed, as demonstrated by the change in the sulfation pattern during aging, different experiences may also induce changes in PNN sulfation, thus possibly making it challenging for the already-known markers to visualize these important extracellular matrix structures (Foscarin et al., 2017). One of the most interesting applications of visualizing PNNs *in vivo* chronically could be related to memory. Indeed, the balance between plasticity and stability could be a fundamental mechanism by which memories are acquired and then stored, thus possibly involving PNNs modulations that could be monitored. Indeed, as discussed in the next paragraph, several findings have associated PNN manipulations with alterations in long-term memory stability.

1.3.3 PNNs and memory

Past experiences are used to plan future actions. If an experience is salient, this is retained in the form of long-term memory. Memory formation involves plastic changes in the functionality and connectivity of synapses (Takeuchi et al., 2014). Since the pioneering works done by Kandell, Bliss, and Lømo, it was evident that changes in the synaptic strength are one of the fundamental mechanisms by which the brain encodes information. The LTP and the LTD are part of this functional synaptic change and are altered by PNN manipulations. Different effects following PNN degradation have been found throughout the brain and in various areas belonging to the same brain structure, such as the hippocampus. For example, if, on the one hand, a decrease in LTP has been observed after PNN enzymatic degradation in the CA1 area of the hippocampus, on the other hand, an increase in LTP has been observed in the CA2 area (Carstens et al., 2016; Shi et al., 2019). Moreover, following enzymatic degradation of the PNNs, a decrease in the LTD was observed in the hippocampal CA1 region, whereas an increase was observed in the perirhinal cortex (Khoo et al., 2019; Romberg et al., 2013). The effects of PNN degradation on synaptic plasticity in the various brain areas give a glimpse of the different effects that PNN degradation has on memories.

1.3.3.1 The stabilizing role of PNNs on long-term memories

The manipulation of PNNs impacts the recall memories. Depending on the region and the memory modality considered, PNNs changes can have different effects. Many findings regarding the effect of PNN manipulation on memory have been observed in associative learning studies. Associative learning is one of the most utilized paradigms to study memory. These paradigms rely on presenting two stimuli, the conditioned stimulus (CN) and the unconditioned stimulus (UN), separated by minimal time latency. The CN is a neutral stimulus, such as a tone, a context, or a visual cue. In contrast, the UN could be aversive (electric shock in fear conditioning) or induce a physiological response (air puff in the eye in eyeblink conditioning). After a phase during which the two stimuli are presented simultaneously, the CN only elicits the response, such as freezing in fear conditioning or eyeblink in eyeblink conditioning.

In the cerebellum's deep nuclei, the PNN enzymatic degradation affects the acquisition and recall of associative memories in mice subjected to eyeblink conditioning (Carulli et al., 2020). In particular, it has been observed an increment in the learning process and a reduction during the recall when the animals were tested after three weeks from the learning phase (Carulli et al., 2020). In other forms of associative learning, such as in fear conditioning, the removal of PNNs elicits similar impairments in the recall of memories. In particular, the injection of ChABC in the secondary visual cortex of adult rats impaired the recall of remote visual fear memories. In contrast, no consequences have been observed if the animals were tested only after one week (Thompson et al., 2018).

Different effects have been reported using other learning modalities, such as in auditory fear conditioning and contextual fear conditioning experiments. In both cases, PNNs were disrupted enzymatically in the auditory cortex and the hippocampus respectively, but the recall of the fear memory was impaired just 24h after the learning phase (Banerjee et al., 2017; Hylin et al., 2013; Shi et al., 2019) Interestingly, it was reported that the recall of contextual fear memories was incremented by augmenting the number of PNNs in the CA1 region of the hippocampus through the overexpression of the Hapln1 protein, suggesting a significant role of PNNs in modulating the extent of the recall of memories (Shi et al., 2019).

PNNs degradation not only affects the recall of acquired fear memories but can also induce the complete erasure of the memory trace. Adult animals with degraded PNNs in the basolateral amygdala exhibit a juvenile phenotype regarding the stability of fear memories (Gogolla et al., 2009). If subjected to an extinction protocol, adult animals with intact PNNs and re-exposed to the fear context display a renewal in fear expression. On the contrary,

adult animals without PNNs subjected to the same protocol did not display fear renewal. The same outcome was observed in juvenile animals where PNNs were not mature yet (Gogolla et al., 2009). The extinction protocol causes the erasure of the previously acquired fear memory in juvenile animals lacking PNNs, and in adult animals depleted in PNNs. Therefore, PNNs in the basolateral amygdala have a role in adult animals to protect fear memories from erasure (Gogolla et al., 2009).

Novelty detection is a spontaneous behavior in mice. When animals are placed in front of new objects or new subjects, they prefer to explore the new ones instead of the familiar ones. This behavior is based on forming a memory of the encounter with the familiar element. These two types of memories are called spontaneous object recognition (SOR) and social memory. They are encoded in different brain areas, such as the perirhinal cortex and the hippocampal CA1 area for spontaneous object recognition memory (SOR) and the CA2 hippocampal region for social memory, and in both cases, alterations in the recall of such memories have been observed in animals depleted of PNNs (Cinalli et al., 2020; Hitti & Siegelbaum, 2014). Animals genetically depleted in the CNS of the PNN components Hapln1 or aggrecan or with PNNs enzymatically degraded in the perirhinal cortex show enhanced object recognition memory (Romberg et al., 2013; Rowlands et al., 2018), whereas animals with the PNNs enzymatically disrupted in the CA2 region of the hippocampus show impairments in social memory (Domínguez et al., 2019).

Spatial memory requires several highly interconnected and interdependent brain areas, such as the hippocampus and the medial entorhinal cortex, for spatial and context encoding (E. I. Moser et al., 2008; M.-B. Moser et al., 2015). In the medial entorhinal cortex, grid cells provide a metric representation of the space thanks to their stable and regular activity pattern over time and in different environments (E. I. Moser et al., 2014). Each grid cell only fires at discrete animal locations in a given space, resulting in a regular firing pattern with a typical hexagonal shape (E. I. Moser et al., 2014). The origin of such regular firing fields has yet to be fully understood, but recently PV interneurons have been described as the main players in their development (Christensen et al., 2021). This inhibitory cell population is highly represented in the medial entorhinal cortex and is strongly associated with PNNs (Lensjø, Christensen, et al., 2017). Enzymatic disruption of mature PNNs in the medial entorhinal cortex results in alterations of grid cell representations. When animals are placed in a novel environment, grid cells, that generally exhibit regular patterns of activity, show altered firing fields (Christensen et al., 2021). Furthermore, when animals are relocated to a familiar environment after the exposure to a novel one, the already encoded familiar representation is also altered, suggesting that PNNs could provide a rigid framework through which grid cell network spatial representations are maintained (Christensen et al., 2021).

In summary, PNN manipulation has different effects depending on the type of memory under consideration. In particular, it is interesting to note that removing PNNs, generally, determines deficits in memory recall, suggesting a role for PNNs as stabilizers of long-term memories. It has been hypothesized that PNNs constitute a physical framework for storing long-term memories (Tsien, 2013). Indeed, synapses are allocated in PNN holes and are regulated structurally and functionally by these extracellular matrix structures (Frischknecht et al., 2009; Sigal et al., 2019). The removal of PNNs could induce a generalized increment in the plasticity state that could impact the stability of synapses and, therefore, the recruitment of the memory engram. Indeed, in the amygdala, an actual return to a plastic juvenile phenotype has been observed in which memory traces are even eliminated (Gogolla et al., 2009). Furthermore, the grid cell network undergoes an increase in plasticity after PNN degradation. This effect is exemplified by the alteration in the otherwise regular pattern of activity of grid cells when animals are exposed to a novel environment (Christensen et al., 2021). The removal of PNNs from PV interneurons in the medial entorhinal cortex impacts PV interneurons firing, which in turn impacts the high regularity in the grid cells activity, making it more susceptible to changes induced by novel contexts (Christensen et al., 2021). Generally, PNN depletion disrupts the recall of long-term memories, but for SOR memories, this manipulation leads to an increase (Romberg et al., 2013; Rowlands et al., 2018). Although it might be hard to reconcile this effect to an increase in plasticity, it has been observed that the expression of such memory requires LTD in the perirhinal cortex, which is, indeed, enhanced by PNN depletion (Griffiths et al., 2008; Romberg et al., 2013). While it seems clear that limiting plasticity is crucial in protecting long-term memories, Thompson et al. have proposed that alterations in PV interneuron network activity could be another mechanism involved in impairing long-term memory recall. In particular they observed an impairment in the coherency of the theta oscillatory activity between the basolateral amygdala and the secondary visual cortex during the recall of remote visual fear memory (Thompson et al., 2018). As described in the following paragraphs, PNNs contribute to the correct generation of circuit oscillatory activity, since they sustain the proper firing of PV interneurons (Wingert & Sorg, 2021). In order to finally dissect how PNNs promote the stabilization of long-term memories, finding a way to visualize and record specifically the activity of PNN-associated neurons during, for instance, the acquisition and the recall of memories with intact of degraded PNNs would help us to better understand the important role of these structures in such a fundamental property of the brain as the retention of memories.

1.4 The impact of PNNs on neuron physiology

Among the neuronal populations, PV interneurons are most extensively associated with PNNs in the brain, especially in the cortex (Härtig et al., 1994; Lensjø, Christensen, et al., 2017). Indeed, many studies concerning the impact of PNNs on neuron physiology concern this neuronal population. Therefore, a detailed discussion regarding PV interneurons and their electrophysiological properties will be introduced to comprehend better how PNNs support their activity and functions.

1.4.1 Parvalbumin interneurons

PV interneurons represent nearly 20% of the total GABAergic neurons (Markram et al., 2004). They are characterized by at least three main features: the peculiar morphology, the characteristic high-frequency firing profile, and the expression of the calcium-binding protein parvalbumin (Celio, 1986; DeFelipe & González-Albo, 1998; Kawaguchi et al., 1987; Kawaguchi & Kubota, 1993; Klausberger & Somogyi, 2008). These morphological, electrophysiological, and molecular characteristics give PV interneurons a major role in controlling the activity of entire circuits (Agetsuma et al., 2018; Bartos et al., 2007).

PV interneurons present long and extensively ramified dendrites allowing them to receive multiple inputs from the surroundings, especially from other PV interneurons (Galarreta & Hestrin, 2002; Gulyás et al., 1999). Indeed, PV interneurons are either chemically or electrically interconnected, creating a highly synchronized inhibitory network, which is fundamental for the emergence of oscillatory activity in the gamma and theta range and for the coordination and control of principal neurons activity (Amilhon et al., 2015; Cardin et al., 2009; Galarreta & Hestrin, 1999; Sohal et al., 2009). The tight control that PV interneurons exert on principal neurons is due to the position in which these interneurons take contact. Through particular axonal structures, a morphological feature that divides PV interneurons into basket and chandelier cells, PV interneurons form synapses on the soma and the axonal initial segment of principal neurons (Okhotin & Kalinichenko, 2002; Petilla Interneuron Nomenclature Group et al., 2008; Y. Wang et al., 2016). These regions are involved in the generation of action potentials, so PV interneurons are in a perfect position to strictly control

the activity of principal neurons (Di Cristo et al., 2004; Hu et al., 2014). The extensive connectivity with principal neurons and the extensive PV network these interneurons form, makes this neuronal population essential in balancing the excitation and the inhibition in neuronal circuits.

This critical function arises from another important feature of PV interneurons, their fast-spiking profile (Caillard et al., 2000; Hu & Jonas, 2014; Rudy & McBain, 2001; Sommeijer & Levelt, 2012). In particular, PV interneurons show a short duration of the action potential, a fast repolarization period, high-frequency action potentials with minimal adaptation, and are the most excitable among the neuronal populations (Avermann et al., 2012; Descalzo et al., 2005; Pala & Petersen, 2015; Rudy & McBain, 2001). These functional characteristics allow PV interneurons to exert a strong and temporally precise inhibition, which sculpts the activity of principal neurons and their computation. PV interneurons are involved in feedback, feedforward, and lateral inhibitory circuits, which are basic functional architectures for many computational functions, such as limiting the time window for the summation of excitatory inputs and, therefore, the generation of the output by principal neurons (Pouille & Scanziani, 2001).

In the framework of cortical computation, in the visual cortex, PV interneurons regulate the gain of visual responses (Atallah et al., 2012). Excitatory and PV interneurons display a non-linear relationship between their firing activity and the response to visual stimuli with increasing contrast levels. This relationship can be modulated selectively by activating or inhibiting PV interneurons, revealing their key role in modulating this signal processing (Atallah et al., 2012). In contrast to principal neurons, the vast majority of PV interneurons do not show a preference for visual stimuli orientations, possibly due to their extensive connections through which they integrate the responses from differently oriented stimuli responsive principal neurons (Isaacson & Scanziani, 2011; W.-P. Ma et al., 2010; Niell & Stryker, 2008). The broadening tuning of PV interneurons is a feature not present since birth but arises only during postnatal development and is led by visual experience (Kuhlman et al., 2011).

The last important feature that characterizes PV interneurons is the expression of the calcium-binding protein parvalbumin. This protein is differentially expressed among the PV interneuron population and reflects different plastic conditions (Donato et al., 2013). Indeed, shifts in the expression of this protein (PV state) have been reported in the CA3 region of the hippocampus associated with different learning and plastic paradigms (Donato et al., 2013). Environmentally enriched mice show a low PV state characterized by low parvalbumin expression, low GAD67 enzyme (a GABA synthesizing enzyme), and an increase in inhibitory contacts onto PV interneurons. In contrast, fear-conditioned mice show a high PV state characterized by high parvalbumin expression, high GAD67 levels, and an increase of

excitatory contacts. The two configurations are correlated to a more permissive or a more restricted plasticity state, respectively. Animals involved in a trial and error learning paradigm show a progressive shift from a low PV state, so when the animal needs to be more plastic in order to learn the task, to a high PV state when the task is acquired, and the memory needs to be retained (Donato et al., 2013). Interestingly, in the same work, the injection of ChABC leads to a low PV configuration, with increased inhibitory contacts and decreased parvalbumin expression, therefore associated with a more plastic state (Donato et al., 2013). Thus, PV interneurons are essential in balancing the excitation and inhibition state of the brain, in the processing of stimuli and in plasticity. PNNs are extensively associated with these interneurons and play a critical role in supporting this neuronal population in all these delicate functions.

1.4.2 The essential role of PNNs in sustaining parvalbumin interneuron physiology

PNNs sustain PV interneuron activity and function in several ways. One possibility is the protective function that PNNs have on PV interneurons against oxidative stress and damage. The extensive activity of PV interneurons requires a high metabolic activity, which renders these interneurons more prone to oxidative insults (Carter & Bean, 2009; Kann et al., 2014). It has been shown, either in WT mice or transgenic lines more prone to oxidative stress, that PNN-associated neurons are more protected from oxidative insults than neurons lacking PNNs (Cabungcal et al., 2013; Suttkus et al., 2012, 2014). Although the PNN protective mechanisms are not fully understood, it has been demonstrated that PNNs are particularly capable of binding Fe^{3+}, a cation extensively used to induce oxidative insults, thanks to the extensive presence of negative charges (Morawski et al., 2015; Suttkus et al., 2012). Hence, PNNs may have neuroprotective actions against oxidative agents through their particular biochemical composition, and by protecting PV interneurons, they may sustain their functionality.

Furthermore, the anionic coating represented by PNNs may act as an ion sorting filter, creating local micro milieus of cations such as Ca^{2+} and Na^{+}, essential for supporting the high activity of PV interneurons (Morawski et al., 2015). Indeed, it is generally accepted that PNNs actually are essential in sustain the fast-spiking profile of PNN-associated neurons as many studies have shown that after PNN degradation their firing is reduced, although some studies have reported no change in firing after PNN manipulation possibly due to different

experimental condition (Balmer, 2016; Chu et al., 2018; Favuzzi et al., 2017; Tewari et al., 2018).

PNNs control PV interneuron activity also by regulating their recruitment by excitatory or inhibitory inputs. Indeed it has been shown in the hippocampus that the genetic deletion of the PNN protein brevican leads to a reduction in the excitatory inputs on PV interneurons paralleled by a reduction in their firing frequency (Favuzzi et al., 2017). Moreover, in supporting PV interneuron activity and functionality, brevican promotes the proper clusterization of synaptic glutamate receptor GluA1 AMPA and the voltage-gated potassium Kv3.1b channels, which are essential for the emergence of PV interneuron fast-spiking activity (Du et al., 1996; Favuzzi et al., 2017). In contrast to what has been observed in Favuzzi et al., the enzymatic degradation of PNNs leads to a change of the inhibitory inputs onto PV interneurons both in the hippocampus and in the cortex (Carceller et al., 2020; Donato et al., 2013). In particular, the PNN enzymatic degradation in the CA3 region of the hippocampus led to an increase in inhibitory contacts, whereas in the prefrontal cortex, it was shown a decrease associated with an increase in gamma activity (Carceller et al., 2020; Donato et al., 2013).

As previously reported, changes in the excitatory or inhibitory inputs reaching PV interneurons can be observed following PNN degradation depending on the region under consideration. This different recruitment of PV interneurons can also be observed at the level of different layers of the same structure, which can lead to different outcomes in PV interneuron activity and functionality as explained in more detail below. Indeed, two different effects *in vivo* are reported in the literature after PNN degradation in the visual cortex. In one study, LFP recordings from the visual cortex of adult rats have shown a decrease in the firing rate of spontaneous and visually-evoked activity and an increase in the spiking variability after PNN enzymatic degradation. Moreover, during spontaneous activity an increase in gamma and theta activity has also been observed after PNN degradation (Lensjø, Lepperød, et al., 2017). In contrast, another study reported an increase in PV interneurons activity after ChABC treatment (Faini et al., 2018; Lensjø, Lepperød, et al., 2017). Two main findings support the increase in PV interneuron activity in this study. In the *in vivo* experiments, animals subjected to visual stimulation reported a decrease in the gain of visual responses and an increase in the gamma oscillatory activity, which both have been previously linked to an increase in PV interneuron activity (Atallah et al., 2012; Faini et al., 2018; Sohal et al., 2009). In the *in vitro* experiments, patch-clamp recordings from PV interneurons in layer 4 show an increase in sEPSP and mEPSP, suggesting increased thalamic recruitment of PV interneurons and, thus, supporting the observed increase of PV interneuron activity in the *in vivo* experiments (Faini et al., 2018). Although there are differences in the experimental conditions between the two studies, such as species and the use or not of anesthesia, the

different outcomes observed could be due to the different layers in which the recordings were made. In Lensjø et al., LFP recordings have been made in layer 2/3. In contrast, in Faini et al., LFP recordings have been made in layer 4 of the visual cortex. It is well known that thalamic afferents mainly reach layer 4 of the visual cortex and less layer 2/3 (Niell & Scanziani, 2021). Since an increase in PV activity is observed only in layer 4 of the visual cortex and an increase in thalamic recruitment has been observed, PNN degradation may induce different outcomes on PV interneuron activity depending on the layer in which these structures are degraded. In layer 2/3 it is possible to speculate that such recruitment does not take place and possibly the decrease in PV interneuron activity observed may simply be due to the lack of a structure that sustains their activity. Leaving aside the diversity of the outcomes of the activity of PV interneurons, the degradation of PNNs leads to an altered processing of the visual stimuli and a change in the oscillatory activity of the circuit, highlighting how PNN degradation might alter circuit functions and computations (Faini et al., 2018; Lensjø, Lepperød, et al., 2017).

Interestingly, none of the studies mentioned above could perform specific recordings from PNN^+ PV interneurons. Since it is known that in the visual cortex exist PV interneurons with or lacking PNNs, it would be exciting to dissect and compare the functional consequences of PNN remotion in both PV interneurons subpopulations after, for example, the presentation of visual stimuli (Lensjø, Christensen, et al., 2017; Ye & Miao, 2013).

Recently, an effort has been made to dissect the functional differences between PNN^+ and PNN^- PV interneurons by highlighting PNNs directly *in vivo* (Benbenishty et al., 2023). By injecting the WFA conjugated with different fluorophores directly in the somatosensory cortex, PNNs have been observed longitudinally *in vivo* for the first time. Moreover, in the same study, calcium imaging was performed specifically from PNN^+ and PNN^- PV interneurons. Although the functional differences between the two populations have not been extensively investigated, a difference in the mean and median area under the curve of the calcium trace between the two populations has been observed upon whisker stimulation (Benbenishty et al., 2023). Despite the remarkable results of Benbenishty and colleagues, the WFA recognizes only a part of the entire population of PNNs due to its limited capability of recognizing only a particular sulfation status of the PNNs (Miyata et al., 2018). Therefore, for an accurate functional study of PNN^+ and PNN^- PV interneuron populations, an alternative tool capable of labeling all PNNs regardless of their sulphation status needs to be developed.

The study of the different involvement of the two PV subpopulations in response to stimuli is only at its beginning. As previously described, PNNs sustain PV interneurons activity and functionality and their disruption leads to impairments in cortical processing. The longitudinal *in vivo* visualization of PNNs and the activity recordings of PNN-associated neurons will

open a completely new field of research not only in the study of PNNs but also on how the brain processes stimuli.

1.5 PNNs and brain disorders: from neurodevelopmental to neurodegenerative diseases

The previous paragraphs described the importance of PNNs in the correct development of inhibitory circuits and their key role in supporting PV interneuron physiology. In the last decades, a growing literature has been describing PNN alterations in many pathological conditions characterized by the disruption of PV interneurons functionality.

The proper development of the CNS requires a constant dialogue between genetic and environmental factors, which leads to the correct postnatal maturation of neuronal networks characterized by an intrinsic delicate balance between excitation and inhibition. Aversive events may induce incorrect wiring and connectivity, causing an alteration in this balance which is a hallmark of several neuropathological conditions, such as epilepsy, schizophrenia, and neurodevelopmental disorders (Khoshkhoo et al., 2017; Rubenstein & Merzenich, 2003; Sohal & Rubenstein, 2019; Yizhar et al., 2011).

Subjects affected by Rett syndrome, a severe X-linked neurodevelopmental disorder caused by the mutation of methyl-CpG-binding protein 2 (MeCP2), show a plethora of symptoms, including cognitive, motor, and visual dysfunctions as well as stereotyped movements and high incidence of seizures (Hagberg, 2002). These symptoms are shared by another neurodevelopmental disorder such as the cyclin-dependent kinase-like 5 disorder (CDKL5). However, unlike in Rett syndrome, many symptoms start in the first stage of development (Villard, 2013). In these pathological conditions, it is not easy to understand which is the cause of the onset of the symptoms; indeed, alterations have been observed both in the excitatory and in inhibitory circuits (Kadam et al., 2019). An interesting aspect of Rett syndrome concerns the onset of the symptoms, which occurs relatively late and parallels the maturation of PV interneurons. In mice, the specific deletion of MeCP2 from PV interneurons is sufficient to recapitulate most symptoms (Ito-Ishida et al., 2015). Moreover, the visual critical period is completely abolished in mice lacking MeCP2 in PV interneurons (He et al., 2014). In contrast, in global KO mice, the critical period is present but accelerated and characterized by a precocious closure which may be responsible for the aberrant processing

of visual stimuli (Durand et al., 2012; Krishnan et al., 2015). Altered visual processing is also observed in CDKL5 KO mice, suggesting an improper development of PV interneurons, which was confirmed in a study showing an increase in PV interneurons density and connectivity (Mazziotti et al., 2017; Pizzo et al., 2016). Given the alterations observed in PV interneurons, it is not surprising that many alterations have also been observed in PNNs for both the disorders mentioned above. In particular, in global MeCP2 KO mice, it was observed a precocious maturation of PNNs and an increase in mature PNN density (Krishnan et al., 2015; Patrizi et al., 2020). Similarly, CDKL5 KO animals show an aberrant organization of PNNs. In particular, at the end of the visual critical period (P35), CDKL5 KO mice show an increase in PNN density paralleled by a decrease in their organization as revealed by a decrease in the WFA staining (Pizzo et al., 2016).

Altered PNN maturation has also been observed in a Fragile X syndrome mouse model. Subjects affected by this neurodevelopmental disorder show autistic traits ranging from sensory hyperarousal, attention deficits, intellectual and developmental disability, social anxiety, and repetitive behaviors (Hagerman & Hagerman, 2008; Protic et al., 2022). Acoustic hypersensitivity in Frm1 KO mice seems to be associated with an imbalance between excitation and inhibition, and, indeed, the delayed maturation of PV interneurons has been observed in the auditory cortex of this Fragile X syndrome mouse model (Lovelace et al., 2016; Wen, Afroz, et al., 2018). Similar to PV interneurons, PNNs display the same maturation delay. However, interestingly, genetic ablation of MMP9 reverses PNN maturation and the hyper-responsiveness of Frm1 KO neurons to WT levels, suggesting that the precocious alteration in PV interneurons circuitry and, in particular, PNNs proper maturation may impact life-long sensory processing (Wen, Afroz, et al., 2018).

One psychiatric illness associated with an alteration between inhibition and excitation is schizophrenia (Liu et al., 2021). The disease manifests in adulthood, and it is believed that incorrect brain development during early life stages may cause the pathology onset (Bitanihirwe & Woo, 2014). Although the mechanisms underlying the pathophysiology of the disease are not fully understood, alterations in the functionality of the inhibitory circuits have been demonstrated (Woo et al., 2010). In particular, a decrease in PV interneurons density has been observed in the prefrontal cortex of human subjects affected by this pathology. At the functional level, alterations in the gamma oscillatory activity have also been demonstrated, possibly due to an alteration in PV interneurons functionality (Gandal et al., 2012; Kaar et al., 2019; Woo et al., 2010). In addition to the alterations observed at the level of PV interneurons, analyses conducted on human post-mortem brain tissues have shown PNN alterations in different brain regions (Mauney et al., 2013; Pantazopoulos et al., 2010). As previously stated, the pathophysiology of schizophrenia is unfortunately largely unknown; therefore, it is difficult to consider PNNs as significant actors in its development. However, it

is possible that the alteration of these structures in schizophrenic subjects could have significant effects on the functionality of PV interneurons. As described in the previous paragraphs PNNs protect against oxidative stress, and, indeed, redox dysregulation has been observed in patients affected by this pathology (Cabungcal et al., 2013, 2014; Do et al., 2000; Flatow et al., 2013).

The PNN protective function towards PV interneurons could also play a key role in other brain disorders such as epilepsy. The etiology of this disorder is unclear, but an imbalance between excitation and inhibition could be a key event in its development (Righes Marafiga et al., 2021). In fact, in animal models and subjects affected by this pathology, a decrease of both PV interneurons and PNNs has been found following epileptic events (Andrioli et al., 2007; Drexel et al., 2011). Furthermore, following the onset of seizures, an increase in matrix proteases capable of degrading PNNs has been observed. Interestingly, MMP9 KO animals show an improvement in the epileptic phenotype, suggesting that the degradation of PNNs could concur with the altered functionality of PV interneurons (Wilczynski et al., 2008).

The PNN protective function seems important also in Alzheimer's disease. The clinical expression of this pathology is associated with intracellular neurofibrillary tangles (NFT) made of the hyperphosphorylated Tau protein and the extracellular deposition of amyloid plaques which are thought to be involved in neuronal toxicity and degeneration. The idea of a possible PNN neuroprotective function in Alzheimer's came from a seminal work in which a higher survival rate was associated with primary cortical neurons ensheathed by PNNs compared to PNN- neurons after the application of exogenous β amyloid peptide (Miyata et al., 2007). Indeed, analog findings were also observed in Alzheimer's post-mortem human brain tissues in which PNN+ neurons were devoid of NFT and associated with amyloid plaques without any apparent damage (Brückner et al., 1999; Morawski et al., 2010). Despite these interesting findings, many studies observed a reduction in PNNs in many areas of the human brain. However, conflicting results have emerged in human subjects and various animal models of the disease (Scarlett et al., 2022). These contradictory results could emerge from the different PNN markers used in the studies and their capability of highlighting different classes of PNNs. Indeed, emerging results have shown that during the disease progression, PNNs could change the CS-GAG sulfation pattern towards a super-sulfated status, which is correlated with the presence of hyperphosphorylated Tau (Logsdon et al., 2022). The progressive change in PNN composition could explain the conflicting results regarding PNN degradation that emerged in patients and in the different animal models. Moreover, a change in the sulfation code represented by the different composition of the CS-GAG may impact the PNN binding capability and affinity for growth factors and other proteins such as Tau that could impact both PNN function, stabilization, and also the survival of PNN-associated neurons (Huynh et al., 2019). Unfortunately, a

detailed study regarding PNN composition and sulfation in Alzheimer's disease is lacking due to technical limitations for visualizing all the different classes of PNNs with a single reporter. Hence, developing a method for visualizing all PNNs could be fundamental for studying the impact of these extracellular matrix structures not only in physiological conditions but also in pathologies.

2. Aim of the study

PNNs are highly organized extracellular matrix structures associated with different neuronal populations throughout the CNS, and in the cortex, they are mostly associated with PV interneurons. However, not all PV interneurons are enwrapped by these extracellular matrix structures (Lensjø, Christensen, et al., 2017). This heterogeneity is further accentuated by the biochemical composition of the PNNs, which can vary according to the region of the CNS and during development, making their unambiguous identification challenging (Miyata et al., 2012, 2018; Sabbagh et al., 2018). Indeed, PNNs are dynamic structures constantly remodeled by experience allowing the CNS to oscillate between a more plastic and stable state to adapt to the ever-changing environment (Riga et al., 2017; Sale et al., 2007). In fact, the degradation of these structures leads to renewed periods of juvenile-like plasticity in adulthood and to the destabilization of long-term memories (Gogolla et al., 2009; Pizzorusso et al., 2002). Furthermore, PNNs sustain the electrophysiological properties and computations of PNN-associated neurons such as PV interneurons (Faini et al., 2018; Favuzzi et al., 2017). Indeed, in the visual cortex, PNNs degradation leads to an altered gain of visual responses (Faini et al., 2018). Finally, alterations in PNNs have been found in several neurodevelopmental disorders characterized by alterations in circuits balance, underlining the potential fundamental role of PNNs in the correct functioning of brain circuits (Patrizi et al., 2020; Pizzo et al., 2016).

Much of the current knowledge of PNNs and their key functions derive from applying methodologies for their manipulation. Via their enzymatic degradation, genetic deletion, or overexpression, fundamental functions such as limiting plasticity in the CNS or supporting the physiology of PV interneurons have been demonstrated (Faini et al., 2018; Pizzorusso et al., 2002). Although the outcomes of PNN manipulation are known, such as, for instance, ocular dominance shift, alteration of visual stimuli processing, or impairment in the recall of long-term memories, the underlying mechanisms have not been extensively elucidated. This lack of knowledge was mainly due to the inability to study *in vivo* the neuronal populations associated with PNNs specifically. Furthermore, the observed alterations in the different outcomes following PNNs degradation may involve gradual changes in activity that should be investigated. Being able to longitudinally monitor the impact of PNN degradation on neuronal circuit activity would be fundamental in understanding these phenomena.

The methodologies used so far for PNN studies involved their manipulation, not allowing the study of PNNs from a physiological non-altered condition. The first efforts to understand

PNN functions *in vivo* without altering these structures have been made by labeling PNNs through the cortical injection of the PNN marker WFA (Benbenishty et al., 2023). However, the WFA recognizes only some of the PNNs in the brain, limiting the application of this methodology to particular areas without the certainty of displaying all the PNNs present (Miyata et al., 2018).

Indeed, changes in the sulfation pattern of the CSPGs have been observed during development and aging, and different experiences might likely induce changes as well (Foscarin et al., 2017; Miyata et al., 2012). In pathological conditions it has been observed that Alzheimer's and schizophrenic patients show an alteration in the CS-GAG sulfation pattern (Enwright et al., 2016; Logsdon et al., 2022). Moreover, in Alzheimer's subjects, a generalized shift towards a super-sulfated status has been observed, leading to the inability of the WFA to label PNNs reliably (Logsdon et al., 2022). Therefore, a different method to visualize PNNs *in vivo* needs to be developed. A possible strategy to visualize PNNs *in vivo* without the involvement of exogenous markers is by modifying PNN components. In particular, making one of the PNN components fluorescent could allow the visualization of any class of PNNs regardless of their sulfation status. Hence, this thesis aimed to develop a genetic method to visualize PNNs allowing long-term functional and morphological studies *in vivo*, either in physiological or pathological conditions.

3. Materials and methods

3.1 Animals

All the animals used in the experiments were house grouped and maintained at 22 °C in a light/dark cycle of 12h/12h. Animals were housed in standard cages according to the regulation about animal welfare. Food (standard diet Mucedola 4RF25) was available ad libitum. All the experiments were approved by the Italian Minister of Health.
Animals were of the C57Bl/6J strain for the ubiquitous and neuron-specific construct validation. For every experiment P90 or P60 animals have been used. For the conditional construct validation and characterization B6.129P2-Pvalbtm1(cre)Arbr/J strain mice (JAX stock #017320) have been used and all the experiments have been performed on P20 or P60 animals.

3.2 Stereotaxic injections

Mice have been anesthetized with isoflurane (Forane, 3% induction, 1% maintenance) and fixed on a stereotaxic support. The skin has been cut, and a perforation has been done in the skull using a surgical drill 3mm lateral from lambda for adult mice (P60 or P90) and 2.5mm for juvenile mice (P20). A glass microcapillary has been stereotaxically inserted in the primary visual cortex reaching the maximum depth of 600μm for adult mice and 500μm for P20 animals. A total of 250nl for viral solutions or 700nl for PNN-fluorescent marker solutions have been injected manually into the left cortex at 600μm/500μm, 400μm/350μm and 200μm below the dura. At each injection step a third of the volume has been delivered in 5 (for the AAV solutions) or 15 (PNN-fluorescent marker solutions) minutes and waited 5 minutes between each steps. The skin has been sutured, and a physiological solution has been injected subcutaneously to prevent dehydration.

3.2.1 PNN fluorescent marker solutions

To reveal PNNs *in vivo* using PNN fluorescent markers, two different solutions have been injected in P90 animals during the cranial window surgery procedure. The first contained Wfa-fluorescein (Vector laboratories, # FL-1351) diluted in PBS 1X 1:10 from a stock solution of 2 mg/ml. The second solution contained anti-aggrecan-568 200 µg/ml. For both solutions 700 nl have been injected. To conjugate the anti-aggrecan AB1031 (Sigma-Aldrich, #AB1031) to the fluorophore Alexafluor568 the kit Alexa Fluor 568 Antibody Labeling Kit (Invitrogen, #A20184) has been used.

3.2.2 AAV solutions

Single AAV injections have been performed for immunohistochemistry experiments, whereas two injections 2.5mm and 3.5mm lateral from lambda have been performed for two-photon imaging sessions. From the starting viral titer different dilutions have been performed to verify the tagging efficiency of the ubiquitous, the neuron-specific and the conditional AAVs. All the AAVs have been produced by the Viral Core Facility (VCF) of the Charité Universitatsmedizin in Berlin.
For immunohistochemistry experiments the AAV solutions have been diluted in PBS 1X. From a starting viral titer of 1,6 x 10^{12} vg/mL the ubiquitous AAV CAG_HAPLN1-mRuby2 (serotype PHP.eb) has been diluted 1:100 in PBS 1X. The neuron-specific AAV hSyn1_HAPLN1-mRuby2 (serotype PHP.eb) has been injected 1:1000 from a starting solution 2,32 x 10^{13} vg/mL. The conditional AAV CAG_DiO_HAPLN1-mRuby2 (serotype PHP.eb) has been diluted 1:30, 1:100 and 1:300 from the starting titer 5,04 x 10^{12} vg/mL. For the *in vivo* imaging sessions the same dilutions of the Hapln1-mRuby2 AAV have been maintained and coinjected with AAV-Syn-Flex-GCaMP6s-WPRE-SV40 (Addgene, #100845) 5.5 x 10^{12} vg/mL. After injection, 40 days have been waited prior to every experiment.

3.3 Retro orbital injections

Adult mice (P60) have been anesthetized with isoflurane (Forane, 3%) and an unilateral manual injection has been performed retro orbitally with a 80ul of a PBS 1X solution with 1,6 x 10^{11} vg of the conditional AAV. The injection has been performed carefully in order to

prevent any bleeding from the injection site. After the injection, animals have been left to recover on a heating platform. In the following days mice have been checked to reveal any possible eye infection.

3.4 Two-photon imaging

3.4.1 Surgery

Cranial windows have been implanted on P80 mice previously injected with the AAV solutions at P60. Animals were anesthetized with isoflurane (3% induction; 1% maintenance). Dexamethasone (subcutaneous 0.2 mg/kg) and Lidocaine (2%, 15-20 µL, subcutaneous, scalp area) were administered. After a few minutes, the scalp has been cleaned with three swabs of povidone-iodine and a large portion of skin, covering both the hemispheres, has been removed. The skull was cleaned from the periosteum by initially using saline and then by carefully scraping it with a scalpel blade. A circular area has been drawn of 3 mm of diameter centered 3 mm lateral, 1 mm anterior to lambda to mark the craniotomy area. A thin layer of a light-curing dental cement has been applied on the rest of the exposed skull (3M Vitrebond™ plus). A metal head-plate was fixed to the skull by using more dental cement. By carefully using a dental drill and a biopsy punch, a 3 mm circular groove has been thinned until almost transparent on the previously marked area, then a few drops of cold sterile ACSF were applied to the area. A circular island of bone was removed with the tip of a sharp forceps without damaging the dura. A circular 3 mm coverslip has been placed and held in place on the craniotomy and secured to the skull by using dental resin (Lang Contemporary Ortho Jet™). Then the skull and the head-plate have been covered with more dental resin to finish the surgery. The animals have been allowed to recover in a heated box and monitored to ensure the absence of any sign of discomfort. Before any other experimental procedure, mice have been left to recover for 12-16 days to reduce inflammation in the surgical area, thus increasing the optical access to the tissue. The same surgical procedure has been conducted In animals (P90) used in the PNN fluorescent marker *in vivo* experiments even though with some differences. In particular, after the skull removal and before the cranial window implantation, animals have been injected with the PNN fluorescent marker solutions with the procedure previously reported (section 3.2.1). In these experiments live imaging sessions have been performed

immediately after cranial window implantation, a day and a week after the surgery in animals in which the inflammation did not alter the optical access.

3.4.2 Imaging

Imaging has been performed using a Bruker Ultima Investigator™ microscope equipped with a GaSsP Photomultiplier tube and controlled by the scanning software Prairie View. Laser excitation was provided by a tunable Ti:Sapphire pulsating LASER (Chameleon Ultra™, Coherent) tuned at 920 nm for GCaMP6s excitation and at 1040 nm for mRuby2 excitation. Excitation power was controlled with a Pockels Cell. LASER power has been maintained under a maximum of 40 mW on the sample.
Images has been acquired using a 20x long WD water immersion objective (Olympus XLUMPlanFL N 20x N.A. = 1.00). For each mouse, fields have been acquired both in layer 2/3 and IV of the cortex (1024x1024 pixels, x-y resolution: 0.307 µm/px). The images acquired at 920 nm and 1040 nm then have been merged with the software ImageJ.

3.5 Cloning

To generate the ubiquitous and the neuron-specific constructs (fig.5a,b), the human coding sequence of *hapln1* was cloned in two different pAAV plasmids, respectively pAAV_CAG-mRuby2 (Addgene #99123) and pAAV_hSyn1-mRuby2 (Addgene, #99126) containing the mRuby2 fluorophore sequence. The human *hapln1* coding sequence was PCR amplified from the plasmid pDONR223_HAPLN1_WT (Addgene, #81757) using the primers Pf-HAPLN1, ATTGGTACCGCCACCATGAAGAGTCTACTTCTTCTG, and Pr-HAPLN1, TATGGTACCCTTAAGCAATTGGTTGTATGCTCTGAAGCAGTAGAC containing the KpnI restriction enzyme sequence. After digesting the ubiquitous and neuron-specific plasmids with KpnI (New England Biolabs, KpnI # R0142), the amplified hapln1 sequence was ligated in the two different backbones pAAV_CAG-mRuby2 and pAAV_hSyn1-mRuby2. To verify the correct orientation, colony PCRs were performed using the related primers Pf-HAPLN1, ATTGGTACCGCCACCATGAAGAGTCTACTTCTTCTG and Pr-orient, GCAATTGGTTGTATGCTCTG. For the generation of the conditional construct (fig.5c), the sequence hapln1-mRuby2 taken from the previously generated plasmid pAAV_CAG-Hapln1-mRuby2 was amplified by PCR using the primers Pf-NheI-DiO, TATAGCTAGCGCCACCATGAAGAGTCTAC and Pr.BsrGI-DiO, AATAATGTACAGCTCATCCATTCCTC. The amplified hapln1-mRuby2 sequence and the

backbone pAAV_CAG-DiO-mRuby2 (Addgene, #104058) have been digested with the restriction enzymes NheI and BsrGI. After the ligation, all the resulting plasmids have been sequenced using the primers Prevseq2 TGAAGCTAGTGGCAAGAATG and Pseq4 TTACGAGGATGGTGGTGTG. After the sequencing validation, all plasmids have been amplified and extracted with QIAGEN Plasmid Maxi Kit (Qiagen, #12162).

A

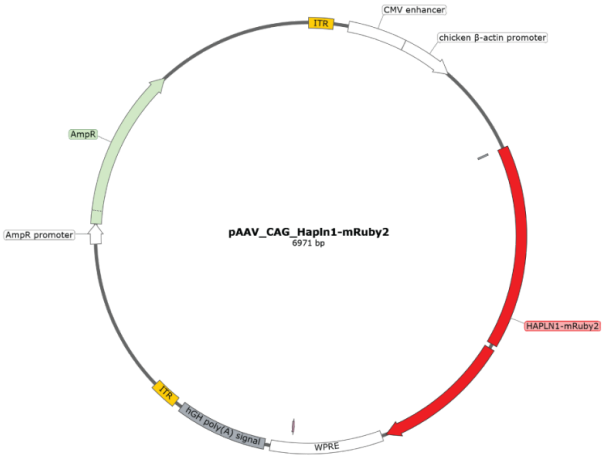

B

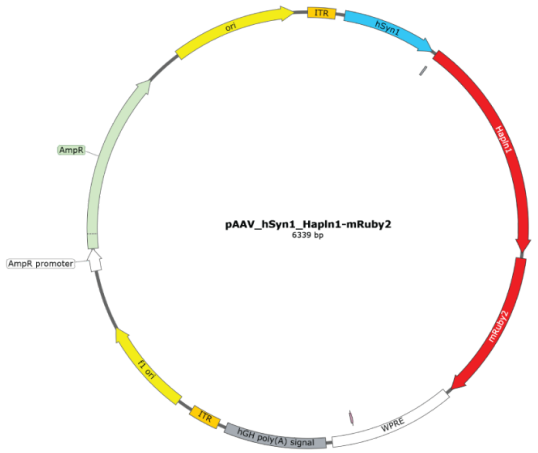

C

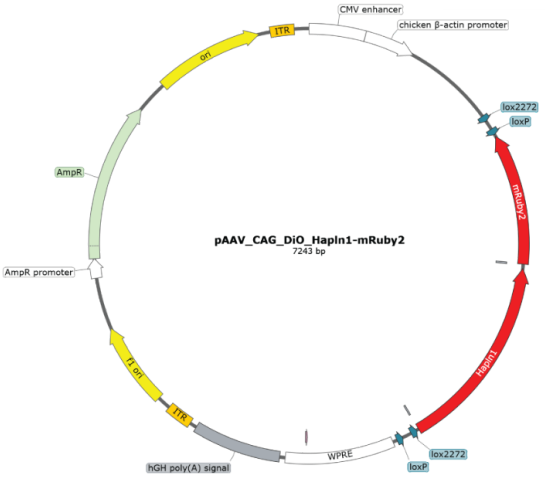

Fig.5: Plasmid maps of the ubiquitous (A) neuron-specific (B) and conditional constructs.

3.6 Transfection

HEK293T cells and the stable transfected HAS3-HEK cell line (Kwok et al., 2010) have been plated for immunocytochemistry experiments in glass coverslips previously treated with 0.1% gelatine in 12-well plastic dishes and in a 10 cm petri dish for western blot (WB) experiment. Cells were cultured with DMEM low glucose (Euroclone, #SH30021FS), 10% fetal bovine serum (FBS) and penstrep 1X. The antibiotic selection of the HAS3-HEK cell line has been performed by adding to the culture medium G418 50 mg/mL (Euroclone, #ECM0016C). Cells were brought to 70% confluency prior to lipofection using lipofectamine 2000 (Thermo Fisher Scientific, #11668019). A total of 500 ng of plasmid has been used for single transfection or in a the cotransfection protocol using pAAV_CAG-DiO-Hapln1-mRuby2 and pAAV_Cre-GFP (Addgene, #68544) (250 ng + 250 ng). After transfection, cells have been left to grow for 36h or 48h prior to immunocytochemistry or WB experiment respectively. The culture medium of cells plated for WB experiment have been replaced after transfection with DMEM low glucose (Euroclone, #SH30021FS), 0.1% FBS and pen-strep 1X.

3.7 Immunocytochemistry

Cells plated in glass coverslip were fixed in 2% paraformaldehyde (PFA, wt/vol, dissolved in 0.1 M phosphate buffer, pH 7.4) for 10 min at RT. Cells then were rinsed three times in PBS 1X solution. Cells were pre-incubated 2 h at RT in blocking solution of 3% bovine serum albumin (BSA) in PSB1X and incubated O/N at 4°C with a PBS 1X solution of anti-Hapln1 antibody 1:100 (R&D Systems, #AF2608), 1% BSA and 0.1% Triton X-100 (vol/vol) for membrane permeabilization. Cells then were rinsed three times in PBS (10 min each) at RT and incubated for 2 h with a PBS 1X solution of secondary anti-goat-488 1:500 (Molecular Probes, #A11055), 1% BSA and 0.1% Triton X-100 (vol/vol). Finally, cells were rinsed three times with PBS 1X, coverslipped in mounting medium (Fluoroshield ™ with DAPI, Sigma #F6057), and stored at 4°C until the acquisition session.

3.8 Western blot

Proteins have been extracted from the cell lysates of HEK293T transfected with pAAV_CAG-Hapln1-mRuby2 or untransfected. For tissue protein extraction, liver and cerebral cortex samples have been homogenized in modified RIPA buffer (50 mM Tris pH8, 150 mM NaCl, 5 mm EDTA, 15 mM MgCl2, 1% NP40) plus protease inhibitors. Samples have been sonicated for 1 min on ice (10 s on/10 s off) and centrifuged for 15 min at 14,000×g, at 4 °C. The supernatant has been recovered and the protein concentration has been determined by Bradford assay (Biorad #5,000,006) using a Nanodrop Spectrophotometer (Thermoscientific 2000 C). For proteins extracted from the culture medium, proteins have been previously concentrated using centrifugal filters Amicon Ultra-4 (Merck, #UFC801024). 8% SDS-PAGE have been performed to check Hapln1-mRuby2, Hapln1 and β-tubulin presence. The samples have been blotted onto nitrocellulose membranes (Biorad) and blocked in 5% BSA in Tris-buffered saline (TBS) for 1 h at RT. The nitrocellulose membrane have been incubated at 4 °C overnight with the following antibodies: anti-Hapln1 1:1000 (R&D Systems, #AF2608), anti-β-tubulin 1:5000 (Sigma, #T8328). Blots have then been washed 3 times in TTBS for 30 min, incubated in HRP conjugated anti-mouse (Santa Cruz, # sc-516102) or anti-goat (Santa Cruz, # sc-2354) antibodies diluted (1:8000) in 2.5% BSA in TTBS for 1 h at RT. The membranes were then rinsed three times in TTBS and incubated in enhanced chemiluminescent substrate (Millipore) and acquired through a Chemidoc XRS instrument.

3.9 Immunohistochemistry and image acquisition

3.9.1 Immunohistochemistry

3.9.1.1 PNNs immunostaining

Mice have been anesthetized with chloral hydrate (1 ml/50 g) and perfused via intracardiac infusion with PBS and then 4% paraformaldehyde (PFA, wt/vol, dissolved in 0.1 M

phosphate buffer, pH 7.4). Brains have been quickly removed and post-fixed overnight in PFA, then transferred to 30% sucrose (wt/vol), 0.05% sodium azide (wt/vol) solution, and finally stored at 4°C. 45-µm coronal sections have been cut on a freezing microtome (Leica), and one free-floating section every 90µm have been processed for immunohistochemistry. Slices have been pre-incubated 2 h at RT in blocking solution of 3% bovine serum albumin (BSA) in PSB and incubated 4 h at RT with a PBS solution of WFA 1:200 (Biotinylated Wisteria floribunda lectin, Vector Laboratories). Then, slides have been rinsed three times in PBS (10 min each) at RT and incubated for 2 h with a PBS solution of fluorescent streptavidin 1:400 (Streptavidin Alexa Fluor 488 conjugate, Thermo Fisher Scientific). Finally, slides have been rinsed three times with PBS and used for parvalbumin staining. A pre-incubation in a blocking solution of 10% BSA plus 0.2% of Triton in PBS 1X has been done at RT for 1 h. Slices have been incubated O/N at 4°C in the primary antibody solution of PBS 1X, anti-parvalbumin 1:1000, BSA 1% and triton 0.1% (Synaptic System, #195004). Slices were then rinsed three times in PBS 1X (5 min each) and incubated with a secondary antibody solution of PBS1X, anti-guineapig-647 1:500 (Invitrogen, #A21450), BSA 1% and triton 0,1% for 2 h at RT. Slices have been then rinsed three times in PBS (5 min each), coverslipped in mounting medium (VECTASHIELD® antifade mounting medium, Vector Laboratories, cat.no. H-100), and stored at 4°C until the acquisition session.

3.9.1.2 Hapln1 immunostaining

Mice were anesthetized with chloral hydrate (1 ml/50 g) and perfused via intracardiac infusion with PBS 1X and then 4% paraformaldehyde (PFA, wt/vol, dissolved in 0.1 M phosphate buffer, pH 7.4). Brains were quickly removed and post-fixed overnight in PFA, then transferred to 30% sucrose (wt/vol), 0.05% sodium azide (wt/vol) solution, and finally stored at 4°C. 45-µm coronal sections were cut on a freezing microtome (Leica), and free-floating sections were processed for immunohistochemistry. Brain slices have been pre-incubated 2 h at RT in blocking solution of 3% bovine serum albumin (BSA) in PSB 1X and incubated O/N at 4°C with a PBS 1X solution of anti-Hapln1 antibody 1:100 (R&D Systems, #AF2608). Then, slides have been rinsed three times in PBS (10 min each) at RT and incubated for 2 h with a PBS 1X solution of secondary biotinylated anti-goat antibody 1:500 (Vector laboratories, #BA-9500). Then slides have been rinsed three times with PBS 1X and incubated with a PBS 1X solution of streptavidin-488 1:500 (Streptavidin Alexa Fluor 488 conjugate, Thermo Fisher Scientific). Slices were then rinsed three times in PBS 1X (10 min each), coverslipped in mounting medium (VECTASHIELD® antifade mounting medium, Vector Laboratories, cat.no. H-100), and stored at 4°C until the acquisition session.

3.9.2 Image acquisition

3.9.2.1 Epifluorescence acquisition

Images for the in vitro validation of the ubiquitous construct have been acquired using a 63X oil objective (Plan-Apochromat 63X/1.40 NA Oil M27). Images have been acquired in a z-step of 3.36 µm acquring every 0.24 µm. Image size was 1338 x 1040 pixels (pixel size 0.102 µm x 0.102 µm). Representative images to reveal the colocalization between the native Hapln1 and Hapln1-mRuby2 have been acquired at Axio Imager.Z2 microscope (Zeiss, Oberkochen, Germany) using a 20X air objective (EC Plan-Neofluar 20X/0.5 NA) from 45µm brain sections. A z-stack has been performed, acquiring one image every 1.28 µm for a total of 14 images (17.94 µm total z-step). Every image was 1038 x 1040 pixels (pixel size 0.323 µm x 0.323 µm). The maximum projection function was then applied to reduce the three dimensional acquisition to 2D. For the representative images showing the injection site of the ubiquitous AAV in the visual cortex and the brain-wide expression of the conditional AAV injected retro orbitally, a tile region including all the brain or the cortex has been acquired using a 10X air objective (EC Plan-Neofluar 10X/0.30 NA). The tiled acquired image was then stitched with the ZENblue software.

3.9.2.2 Confocal acquisition

Confocal images were acquired using LSM 900 confocal microscope (Zeiss, Oberkochen, Germany). For the representative images of the colocalization between the ubiquitous construct Hapln1-mRuby2, WFA and anti-PV antibody (fig.7b) images have been acquired using a 63X oil objective (Plan-Apochromat 63X/1.40 NA Oil M27). A z-stack was performed acquiring images every 0.5 µm for a total of 10.5 µm. The maximum projection function was then applied to create a 2D image. An analog z-stack approach (24 images with a step of 1,2 µm fro a total of 30,36 µm) have been used to take the representative image of the colocalization between the neuro specific construct, the WFA and anti-PV (fig.8a) at a magnification 40X (Plan-Apochromat 40X/1.40 NA Oil).

For the image acquisition of the conditional AAV characterization experiments, images have been acquired at a magnification 20X (Plan-Apochromat 20X/0.8). A tile region has been

acquired including the injection site and the homolog region in the non-injected contralateral cortex. Images have been acquired only in one focal plane corresponding to the highest peak of intensity of the WFA signal. The tiled images have then been stitched with the ZENblue software and exported in a TIFF format for further analysis.

3.10 Data analysis

3.10.1 PNNs and PV interneuron quantification

To count PNNs and PV interneurons a ROI has been drawn around every injection site. The drawn ROI has been then applied to the contralateral non-injected cortex. Based on the ROI a mask has been applied to limit the count only in the defined region. For PV interneurons and PNNs, an unbiased count method has been applied using a neural-network previously published (Ciampi et al., 2022) and applied for PNNs and PV interneurons count (Lupori et al., 2023). In contrast, PNNs highlighted by Hapln1-mRuby2 have been counted manually due to the low signal to contrast ratio. The x and y coordinates have been saved automatically with a custom software in Python (3.8) for density, intensity and colocalization analysis. All the statistical analysis has been performed using the software Graphpad Prism 8.

3.10.1.1 PNNs and PV interneuron density

The metric density represents the number of PNNs or PV interneurons in a unit of area (mm^2).To calculate the mean density of WFA+ PNNs and PV interneurons in the injected or control cortex for each mouse, the density of WFA+ PNNs and PV interneurons was first calculated by dividing the number of WFA+ PNNs or PV interneurons by the ROI area in each slice. Then an average density value was calculated for the injected cortex and control cortex for each mouse averaging the density values obtained in each slice. A RM Two-way ANOVA analysis has been performed to verify the effect of the viral injection so the treatment and the different titers injected on the density of PNNs and PV interneurons. Sidak correction has then been applied in the multiple comparison analysis.

3.10.1.2 PNNs and PV interneurons intensity

Quantification of the intensity of PNNs or PV cells has been performed on 80x80 pixels image tiles centered on the center positions of each PNN/cell (x,y coordinates). Within each tile, pixels belonging to the cell or the background have been segmented, and the intensity of each PNNs/cell has been defined as the mean value of the pixels belonging to that structure/cell. The segmentation has been performed using a random forest pixel classifier implemented with the MATLAB Treebagger class and including other custom MATLAB functions (Cicconet et al., 2019). Single pixels belonging to the background or foreground are classified with this approach. Classifying all the pixels in an image tile results in a binary segmentation mask. The features considered for pixel classification were the contrast-adjusted pixel intensity (using the imadjust MATLAB function), the position of the pixel relative to the center of the tile in the horizontal and vertical axes, and the pixel intensity in 16 versions of the image tile filtered with 16 Gabor filters. The wavelength and orientation of each Gabor represented one of the possible combinations of four different wavelength values (2.8, 5.6, 11.3, 22.6 pixels/cycle) and four different orientations (0°, 45°, 90°, 135°). Wavelengths were sampled in increasing powers of 2 starting from 4 $\sqrt{2}$ up to the hypotenuse length of the input image tile, while orientations were sampled from 0° to 135° with a step of 45° (Jaini et al.,1991). Each random forest model for segmentation of PNNs and PV cells was trained on 69600 pixels from 626 tiles for PNNs and for PV interneurons were 609 (60 pixels randomly chosen for each tile). To calculate the mean intensity of WFA+ and PV staining for each mouse in the injected and control cortex, the individual intensity values in each cortex have been summed and divided by the total number of WFA+ PNN or PV interneurons. Then the mean values of intensity of the treated cortex has been normalized to the contralateral part due to the intrinsic variability of the immunohistochemistry technique. One sample t-tests have been performed to test possible differences between the treated and the control cortex.

3.10.1.2 PNNs and PV interneurons colocalization

PV cells and PNNs were counted with three distinct deep learning models on separate channels. We defined the colocalization of WFA+ PNN and a Hapln1-mRuby2+ PNN based on their x,y coordinates in the starting image using the following criteria. We selected one cell/PNN at a time as a reference object. For each reference object, we selected only objects in other channels with a distance equal to or smaller than 20 pixels (9.675µm). If in addition

to one object also other objects satisfy this criterion, only the closest object is defined as colocated. Otherwise, the reference object has been defined as non-colocalized if there were no other objects in the nearby 20 pixels (i.e. a PV-negative PNN or a WFA-negative PV cell).I computed different metrics to describe Hapln1-mRuby2+ PNNs, WFA+ PNNs and PV interneurons colocalization. It has been evaluated the percentage of Hapln1-mRuby2+ WFA+ PNNs over the total of WFA+ PNNs, the percentage of WFA+ Hapln1-mRuby2+ PNNs over the total of Hapln1-mRuby2+ PNNs, the percentage of WFA+ PV interneurons over the total of PV interneurons, the percentage of WFA+ PV+ PNNs over the total of WFA+ PNNs and the percentage of WFA+PV- PNNs over the total of WFA+ PNNs.

Significant differences of WFA+PV interneurons, PV+ PNNs and PV- PNNs have been tested for each condition between the injected and the control cortex using a paired t-test.

4. Results

4.1 Injecting fluorescent PNN markers *in vivo* does not allow to perform chronic imaging of PNN-like structures

A fluorescent reporter would need some key features to enable the *in vivo* visualization of PNNs. The first characteristic is a different emission wavelength with respect to the genetically encoded calcium sensors belonging to the GCaMP family. Indeed, separating the two signals would allow me visualizing PNN structures and recording the activity of PNN-associated neurons, likely without interference. The second fundamental feature concerns the specificity of the reporter in tagging PNNs avoiding the specific recognition of some sulfation patterns. Finally, the fluorescent reporter would be expected to have the capability to allow the longitudinal visualization of PNNs to maximize its possible applications.

The first strategy I decided to undertake to prove the possibility to visualize PNNs *in vivo* involved molecules known to bind these extracellular matrix structures in *ex vivo* conditions. Among these, the WFA and aggrecan antibodies are widely used for PNN visualization in histological preparations. In particular, the anti-aggrecan antibody AB1031 is directed against the core protein of CSPGs, therefore its binding capability is not influenced by the sulfation status of PNNs (Ueno, Fujii, et al., 2018). Therefore, the injection *in vivo* of the fluorophore-conjugated antibody AB1031, represented a promising strategy for the *in vivo longitudinal* visualization of PNNs. In a pilot experiment, I injected in the visual cortex of adult mice the WFA conjugated to fluorescein, a fluorophore that emits green light. In this experiment, I wanted to test the hypothesis that a single injection of a fluorescent PNN marker would have allowed longitudinal PNN visualization. Following the injection, three two-photon imaging sessions have been performed. The first session has been performed immediately after the injection (day 0), the second the following day (day 1), and the last a week later (day 7, fig.6a). As shown in fig.6b, the WFA-fluorescein highlighted extracellular matrix structures strongly resembling PNNs. These structures remained visible even a day later but were utterly absent a week later.

I repeated the same experiment using the anti-aggrecan AB1031 antibody previously conjugated to the red fluorophore Alexafluor568 so, compatible with GCaMP6 applications and recognizing the core protein of aggrecan so not affected by the sulfation status of the PNNs. The anti-aggrecan-568 antibody highlighted PNN-like structures similarly to what was

observed with the WFA-fluorescein complex (fig.6c). Unfortunately, the next day, these structures appeared more tenuous and they were completely absent a week later.

Thus, the direct injection *in vivo* of PNN markers allowed me to visualize structures resembling PNNs, but the tagging capability did not last. The incapability to perform chronic imaging of the PNN-like structures led me to change strategy for visualizing PNNs *in vivo*.

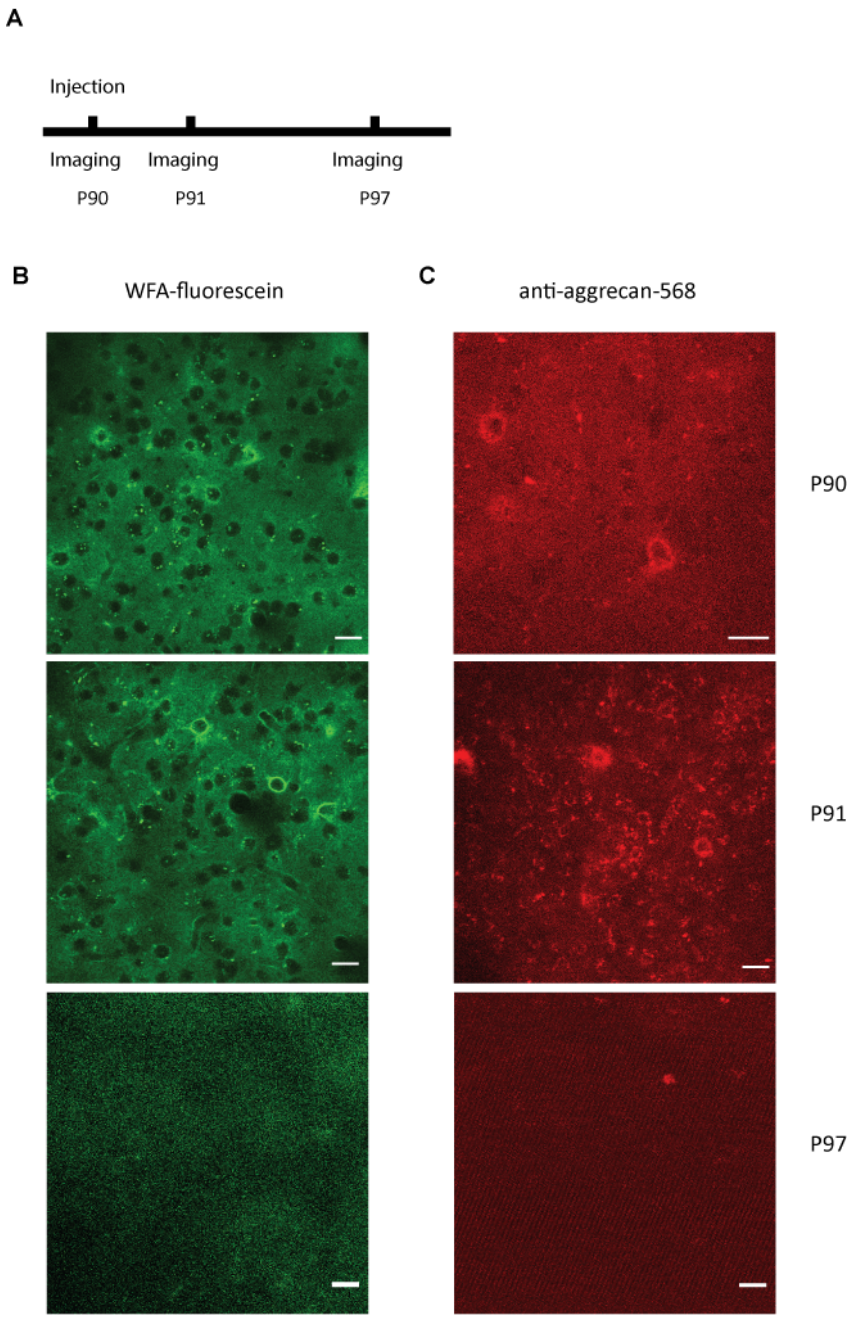

Fig.6. Direct injection of PNN markers for PNN *in vivo* visualization: (A) Schematic diagram representing the experimental protocol. Animals have been injected at P90 and immediately imaged. Two more imaging sessions have been performed the day after (P91) and after a week from the injection (P97). **(B-C)** Representative *in vivo* images of PNN-like structures highlighted by WFA-fluorescein in B and anti-aggrecan-568 in C at different time points (P90, P91, P97). No signal was detected after a week (P97) for either of the PNN markers. Scale Bar: 20μm.

4.2 Developing of a genetic PNN fluorescent reporter

Given the results observed following the injection *in vivo* of the PNN fluorescent markers, I have considered making one of the PNN components fluorescent to obtain longitudinally visible PNNs *in vivo*. The approach taken into consideration was to convey this fluorescent component through an adeno-associated virus (AAV). These vectors are widely used to deliver exogenous genes into murine or human organisms by replacing the viral native genes with a gene of interest. It is known that the AAV technology has many advantages, such as the low immunogenicity, the very low rate of integration into the host genome, the stable long-term expression and the capability to infect non dividing cells such as neurons (Bessis et al., 2004; Haberman et al., 1998). The major drawback of such technology is the low viral genome capacity, meaning that the gene to insert in the AAV must be limited in size. Among PNN components, the Hapln link protein genes have a small size. Moreover, among the Hapln link proteins, Hapln1 has an essential role in PNN organization suggesting its potential presence in all PNNs and making it the perfect candidate to highlight all PNNs (Carulli et al., 2010). To make Hapln1 fluorescent, I decided to fuse it As coding sequence to the gene mRuby2, which is a fluorophore that emits in the red spectrum of the light and it was successfully used simultaneously with the GCaMP6s calcium sensors in *in vivo* imaging experiments (Rose et al., 2016). The new fusion construct Hapln1-mRuby2 has been put under the control of the ubiquitous and strong promoter CAG in order to maximize its expression (fig.7a).

To validate the Hapln1-mRuby2 fusion protein, I decided to use a stably transfected cell line, the HEK293T-HAS3 (HAS3) cell line. Previously, it has been reported that transfecting the HAS3 cells with a plasmid containing the hapln1 gene it was possible to obtain a stable double transfected cell line capable of aggregating the CSPGs in the pericellular matrix mimicking PNN formation *in vivo (Kwok et al., 2010)*. Following the transfection of HAS3 cells with the ubiquitous Hapln1-mRuby2 plasmid, it was possible to verify the expression of Hapln1-mRuby2 as shown in fig.7b-c. To verify that the construct was expressed in an intact and non-degraded form, I performed an immunocytochemistry experiment using an antibody directed against the Hapln1 protein. Fig.7b-c allows to appreciate the high degree of colocalization between the signal of the mRuby2 fluorophore and the signal of the antibody directed against the Hapln1 protein, suggesting that the fusion protein was expressed in an intact form. However, it was not possible to verify the presence of Hapln1-mRuby2 either in extracellular medium or in the pericellular matrix since no apparent deposition of Hapln1-mRuby2 has been observed.

To understand whether Hapln1-mRuby2 was secreted, I decided to perform a Western blot experiment on the proteins collected from the culture medium to reveal the presence of Hapln1-mRuby2 using an antibody against Hapln1.

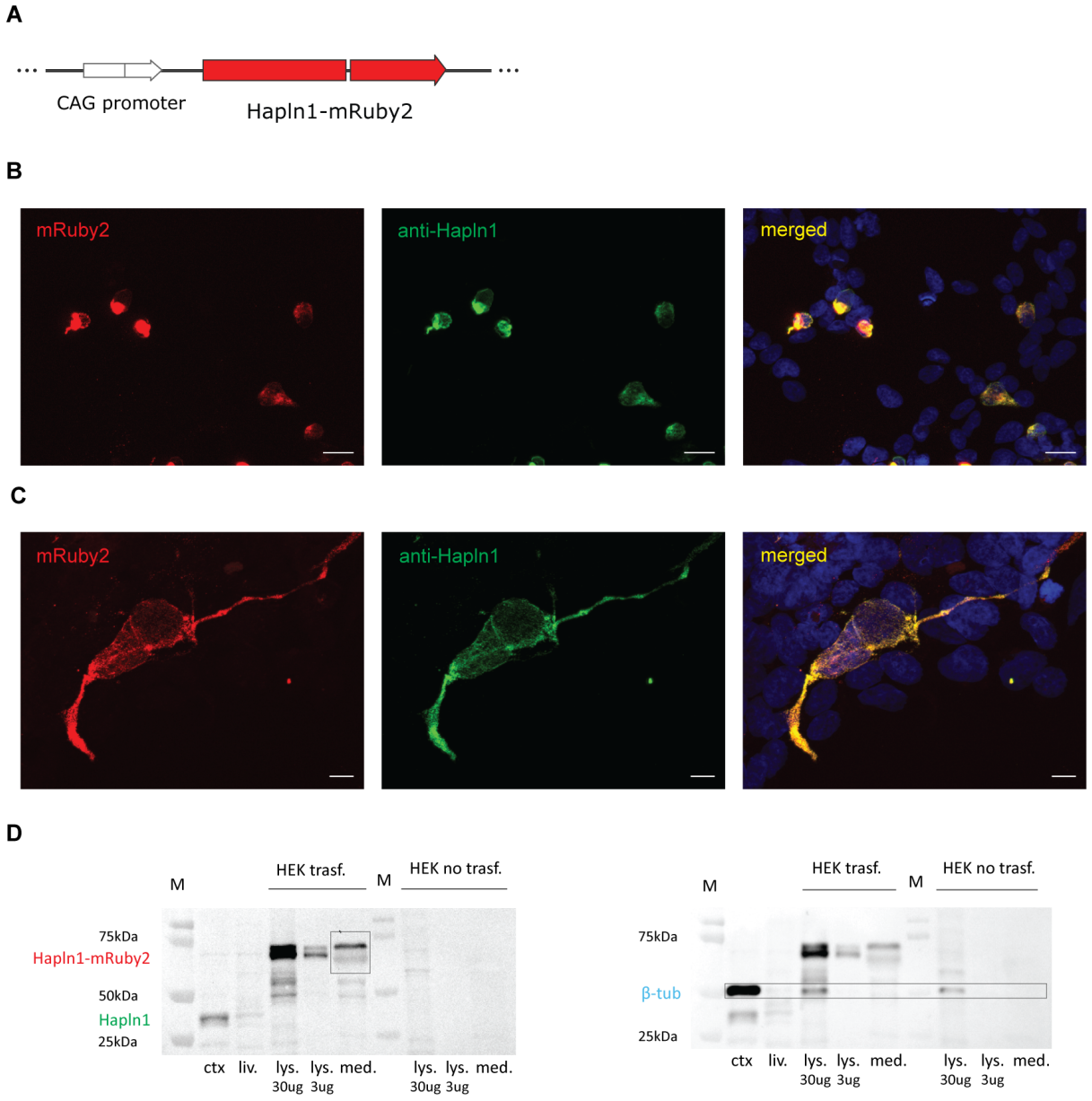

Fig.7. Hapln1-mRuby2 *in vitro* validation: (A) Schematic representation of the plasmid. The sequence of the hapln1 gene has been fused to the fluorophore mRuby2 and cloned under the control of the CAG promoter. **(B-C)** Immunocytochemistry experiment for Hapln-mRuby2 validation in a low (B) and higher (C) magnification. The signal of Hapln1-mRuby2 and of anti-Hapln1 antibody colocalize almost perfectly. Scale Bar: 20μm in B, 10μm in C. **(D)** Western blot experiment to validate Hapln1-mRuby2 secretion. Left, Hapln1-mRuby2 is present in the culture medium of transfected HAS3 cells. Note the different position with respect to the native cortical Hapln1 protein. Left, β-tubulin is present in the cell lysate of the HAS3 cells but not in the culture medium. The apparent no presence of β-tubulin is also observed in the lane with 3μg of cell lysate protein (M, marker; ctx., cortex; liv., liver; lys., cell lysate; med., culture medium).

In fig.7c, it is possible to appreciate a clear band approximately at 75kDa, in the lane where I loaded the proteins collected from the culture medium (black box). An analog signal was also present in the lanes containing proteins extracted from the cell lysate of the transfected HAS3 cells, whereas no signal was present in the culture medium and cell lysate of the non-transfected HAS3 cells. Moreover, the signal localized at 75kDa was not present in the lane where the proteins extracted from the cortex of adult mice have been loaded (2nd lane, ctx). There, a clear band was detectable at around 44kDa, which is the weight of the native cortical Hapln1 protein. The difference in molecular weight between the two signals highlights that Hapln1-mRuby2 was not only expressed intact, but also the fusion protein was likely secreted intact. To check that Hapln1-mRuby2 was secreted and not released after possible cell death, I decided to reveal in the culture medium the presence of the cytoplasmic β-tubulin. This protein must be absent in the culture medium, and indeed no signal is observed in the lane containing the proteins collected from the culture medium (fig.7d, right panel). The same result was also observed in the lane with 3μg of the proteins extracted from cell lysates, an amount of protein in the same range of that present in the culture medium. This experiment showed me that the protein Hapln1-mRuby2 was secreted in the culture medium but the lack of the β-tubulin signal from the protein cell lysate (3μg) do not allow me to definitively conclude that its presence in the cell medium is not due to simple dispersion after cell death. Furthermore, in the immunocytochemical experiment it was not clear whether the function of Hapln1 was maintained given the lack of Hapln1-mRuby2 localization in the pericellular compartment. Since the *in vitro* model used to validate the ubiquitous plasmid was an approximation of PNN complexity, we decided to continue the validation of Hapln1-mRuby2 directly *in vivo*.

4.3 The fluorescent reporter Hapln1-mRuby2 labels PNNs *in vivo*

The *in vitro* validation of the fusion protein Hapln1-mRuby2 demonstrated that the construct was expressed intact by the cells and likely also secreted in an intact form. To understand whether the function of the native Hapln1 was also retained after its fusion with the fluorophore mRuby2, I decided to test the fusion protein directly *in vivo* by packing the plasmid in a PHP.eB AAV. AAVs made with this particular capsid variant are able to cross the blood brain barrier, so different routes of administration can be performed. This feature

increases a lot the experimental flexibility of the PNN fluorescent reporter (Chan et al., 2017).

To test the ubiquitous AAV, I first injected 250nL of a 1,6 x 10^{10} vg/mL AAV solution in the left visual cortex of an adult mouse (P90) and waited 40 days. The native Hapln1 protein has a low turnover in the visual cortex of about 82 days, so 40 days seemed a good compromise for Hapln1-mRuby2 insertion in the already mature PNNs. As shown in the representative figure 8a, the expression of the fusion protein was indeed very high, an outcome not surprising due to the ubiquitous and strong nature of the CAG promoter. Interestingly, the signal was located in the extracellular space, meaning that the fusion protein Hapln1-mRuby2 was secreted *in vivo*. In the extracellular space it was also possible to observe some structures highly resembling PNNs. To verify that they were PNNs, I performed an immunohistochemical experiment using the WFA, the standard marker of PNNs, and an antibody against parvalbumin (anti-PV). As already mentioned in the Introduction of this thesis, most of the PNNs surround PV interneurons in the visual cortex, so performing this kind of experiment was the best option to validate the ubiquitous construct. As shown in fig.8b, there was a good co-localization between Hapln1-mRuby2 and the WFA around a PV interneuron, demonstrating that the fusion protein was able to tag PNNs. To be sure that the signal coming from these marked structures was specific and not due to the deposition of the mRuby2 fluorophore only, I performed another immunohistochemistry experiment using the antibody directed against the Hapln1 protein (fig.8c). The colocalization between Hapln1-mRuby2 and the antibody against Hapln1 demonstrated that Hapln1-mRuby2 was indeed secreted and retained in PNNs, meaning that also the function of the native Hapln1 protein was preserved.

Despite these significant results, it was possible to observe structures negative for the WFA staining (WFA^-) labeled by the construct (fig.8d). Although not all the PNNs are positive for the WFA (WFA^+), the high presence of Hapln1-mRuby2$^+$ and WFA^- structures encountered, made me hypothesize that they were possible off-targets. The function of the native Hapln1 link protein is to stabilize the interactions between the CSPGs and hyaluronan, leading to the proper aggregation and maturation of PNNs. The overexpression of Hapln1-mRuby2 could drive the aggregation of extracellular matrix components also in other cell types, resulting either in new WFA^- PNNs or in just pericellular matrix aggregates.

The most important aspect of the development of a PNN genetic fluorescent reporter was to establish whether it was possible to visualize PNNs *in vivo*. To understand that, I performed a two-photon imaging session (fig.8e). The signal observed from Hapln1-mRubty2 in the imaging session was intense and localized throughout the ECM, reflecting the observation made in the immunohistochemistry experiment. In particular, the contrast between the

tagged PNNs and the surrounding diffuse extracellular matrix was extremely low, resulting in an unreliable evaluation of what could be a PNNs or not.

The high amount of possible off-targets encountered combined with the low contrast between PNNs and the diffuse ECM observed in the imaging sessions lead me to find a possible solution to decrease these effects.

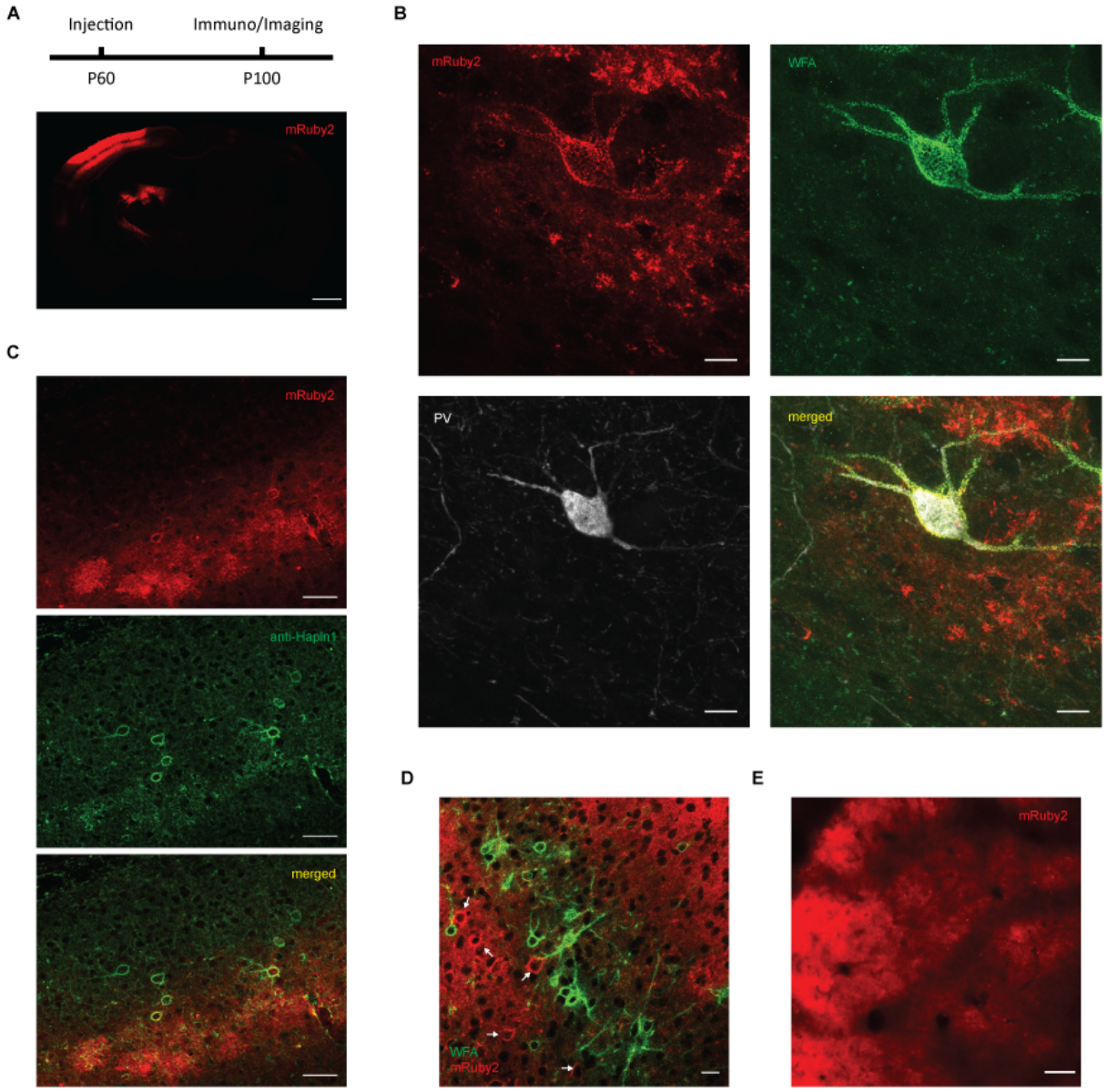

Fig.8. *In vivo* validation of Hapln1-mRuby2: (A) Top, representative diagram of the experimental protocol. At P60 animals have been injected in the primary visual cortex and imaging sessions and immunohistochemistry have been performed at P100. Bottom, representative image showing the expression of the Hapln1-mRuby2 in the injection site. Note that extensive expression was observed also in subcortical structures. Scale bar: 1mm **(B)** Colocalization between Hapln1-mRuby2 and the WFA around PV interneurons. Scale bar: 10µm. **(C)** Colocalization between Hapln1-mRuby2 and anti-Hapln1. Scale bar: 50µm. **(D)** Hapln1-mRuby2 also highlights WFA-negative structures suggesting the presence of possible off-targets (white arrows). Scale bar: 20µm. **(E)** Representative *in vivo* image of the expression of Hapln1-mRuby2. Note the strong signal and the low contrast between PNNs and the diffuse extracellular matrix. Scale bar: 50µm.

4.4 Limiting the expression of Hapln1-mRuby2 in neurons is sufficient to tag PNNs

A possible solution to decrease the off-targets and increase the contrast between PNNs and the diffuse ECM was to restrict the expression of Hapln1-mRuby2 only in PV interneurons. This is because PNNs extensively ensheath these neurons in the visual cortex and many PNN components are expressed by PV interneurons. Recently, it has been reported however that also astrocytes transcribe the hapln1 gene and the origin of the Hapln1 protein inserted in PNNs could be ascribed to both cellular populations (Devienne et al., 2021; Tasic et al., 2018). Therefore, to verify that limiting the expression of Hapln1-mRuby2 only in PV interneurons was sufficient to label PNNs, I decided to take an intermediate step and verify that excluding astrocytes was sufficient to label these ECM structures. To do that, I replaced the ubiquitous CAG promoter with the neuron-specific hSyn1 promoter and I verified the capability of the newly generated neuron-specific AAV to label PNNs (Kügler et al., 2003).
After 40 days from the injection in the visual cortex of adult mice (P90) of 250nL of a 2,32 x 10^{10} vg/mL neuron-specific AAV solution, I performed an immunohistochemistry experiment to verify the colocalization of Hapln1-mRuby2 and the WFA around PV interneurons. In fig.9a, it is possible to observe that the neuron-specific construct tags PNNs. Therefore, limiting the expression of Hapln1-mRuby2 only in the neuronal population is sufficient to label PNNs. However, the neuron-specific construct was likely expressed by both excitatory and inhibitory neurons. Indeed, the overexpression by either neuronal populations may cause the formation of the WFA^- structures as shown in fig.9b. It is possible that the excitatory transduced cells retained Hapln1-mRuby2 in their pericellular matrix, possibly inducing the aggregation of other extracellular components. Once established that limiting the expression of Hapln1-mRuby2 only in neurons was sufficient to have labelled PNNs, I decided to generate a new construct to be expressed only in PV interneurons.

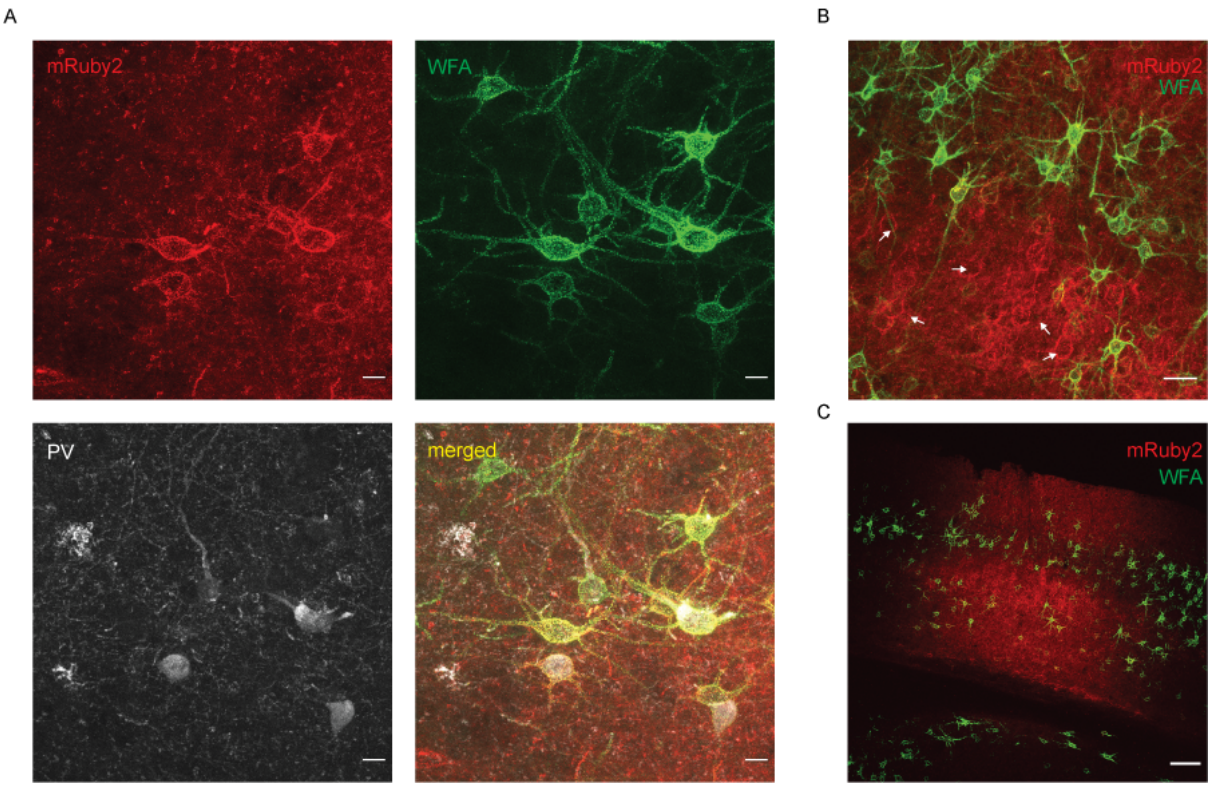

Fig.9. Neuron-specific expression of Hapln1-mRuby2: (A) Colocalization between Hapln1-mRuby2 and the WFA around PV interneurons. Scale bar: 20µm. **(B)** The neuron-specific expression of Hapln1-mRuby2 highlights possible off-targets (white arrows). Scale bar: 30µm. **(C)** Representative image showing the extensive expression of the neuron-specific construct in the injection site. Scale bar: 100µm.

4.5 *In vitro* and *in vivo* validation of the conditional Hapln1-mRuby2 construct

To restrict the expression of Hapln1-mRuby2 only to PV interneurons, I decided to generate a conditional construct to be expressed only in the presence of the Cre recombinase. Indeed several transgenic lines expressing the Cre-recombinase in specific neuronal populations are available to control the spatial expression of genes. In particular, I decided to use a transgenic mouse line expressing the Cre-recombinase only in PV interneurons (B6.129P2-Pvalbtm1(cre)Arbr/J strain mice). This enzyme can revert the orientation of a gene of interest when it is inserted between specific sequences.

A

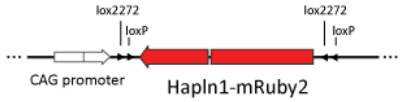
lox2272
loxP
lox2272
loxP
CAG promoter
Hapln1-mRuby2

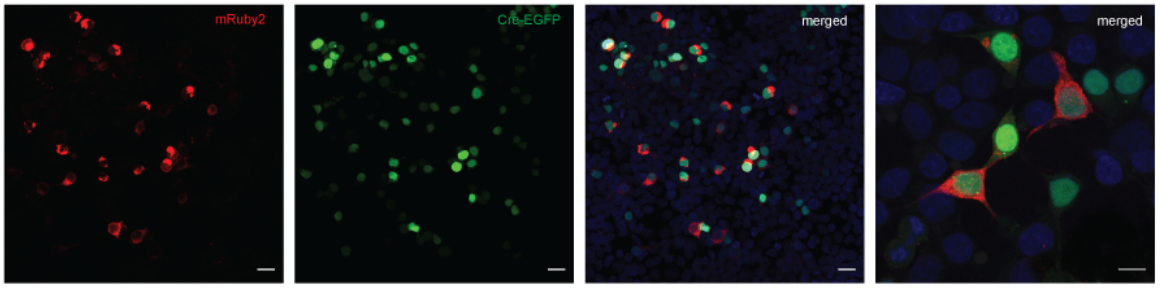
mRuby2
Cre-EGFP
merged
merged

B

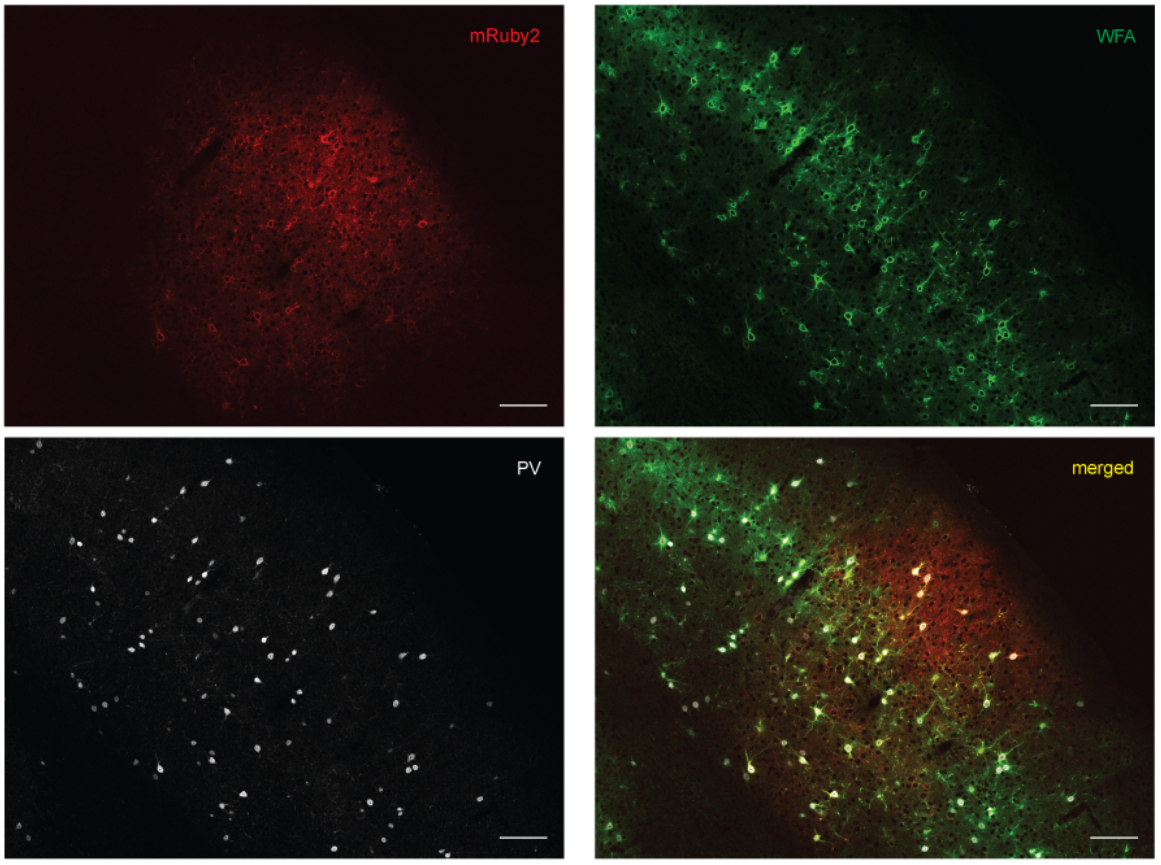
mRuby2
WFA
PV
merged

C

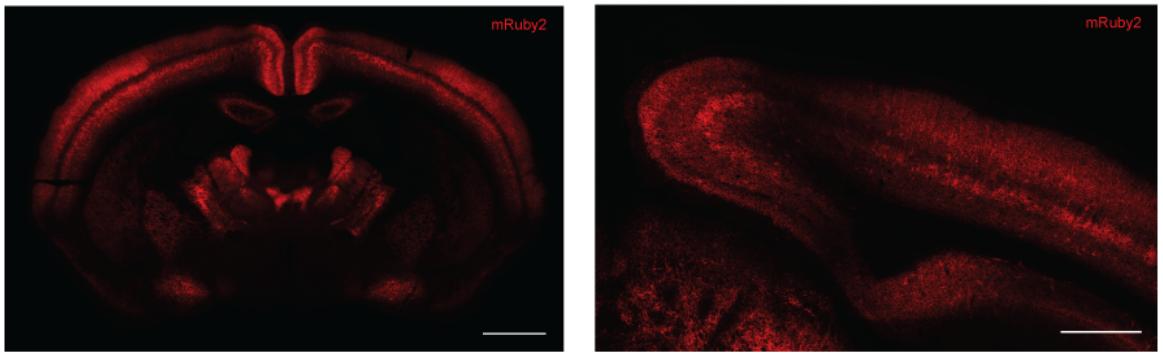
mRuby2
mRuby2

Fig.10. Validation of the conditional construct: (A) Top, graphic representation of the conditional construct. Bottom, *in vitro* validation of the conditional construct. Scale bar: 20 µm. Bottom right panel, representative image taken at higher magnification. Scale bar 10 µm. **(B)** Colocalization between Hapln1-mRuby2 and the WFA around PV interneurons. Scale bar: 100µm. **(C)** Retro orbital injection of the conditional AAV. Left, representative image showing the brain-wide expression of Hapln1-mRuby2. Scale bar 1mm. Right, representative image showing the expression of Hapln1-mRuby2 in the cortex. Scale bar 500µm.

The right combination of loxP and lox2272 recombination sequences promote the exchange of orientation of an open reading frame included in an inverted orientation in respect to the promoter. Only in the presence of this enzyme the gene of interest can be transcribed, and consequently the protein produced. To generate a conditional construct, I cloned the Hapln1-mRuby2 sequence in an inverted orientation in a conditional plasmid under the control of the strong CAG promoter to maximize its expression (fig.10a, top).

To validate *in vitro* the conditional construct I decided to transfect the HEK293T cell line. To understand if the conditional construct was indeed Cre-dependent, I performed a cotransfection with the conditional Hapln1-mRuby2 plasmid and a plasmid containing the Cre-recombinase fused to a GFP. Even without a detailed quantification, it was possible to observe that the expression of Hapln1-mRuby2 was present only in cells also expressing the nuclear-localized Cre-GFP (fig. 10a, bottom).

To validate the conditional construct *in vivo*, I injected the corresponding AAV into the left visual cortex of an adult transgenic mouse, expressing the Cre-recombinase in PV interneurons specifically (PV-Cre). The difference in the expression pattern in respect to the ubiquitous and the neuronal-specific constructs was highlighted by the evident decrease in the signal intensity (fig.10b). To be sure that the construct was expressed only in PV interneurons I also injected a WT animal with the conditional AAV, and as expected, the construct did not show any apparent expression (not shown). At first sight, the structures highlighted by the conditional construct were clearly visible, with a better contrast between PNN-like structures and the surrounding diffuse ECM in respect to the previous two AAV variants. I performed an immunohistochemistry experiment to demonstrate that those structures were WFA^+ PNNs (fig.10b). The extensive colocalization between Hapln1-mRuby2 and the WFA, revealed that limiting the expression of Hapln1-mRuby2 only in PV interneurons was sufficient to highlight PNNs.

To further validate the conditional AAV, I decided to inject it through another route of administration. The capsid variant PHP.eB can cross the blood-brain barrier (Chan et al., 2017). Accordingly, I injected the conditional AAV retro orbitally in P60 mice to understand its expression pattern. In fig.10c, it is possible to note the brain-wide Hapln1-mRuby2 expression and, interestingly, the good contrast between the labeled PNN-like structures and the diffuse ECM.

A

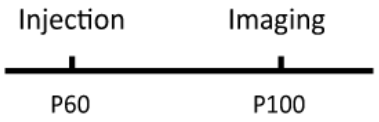
Injection
Imaging
P60
P100

B

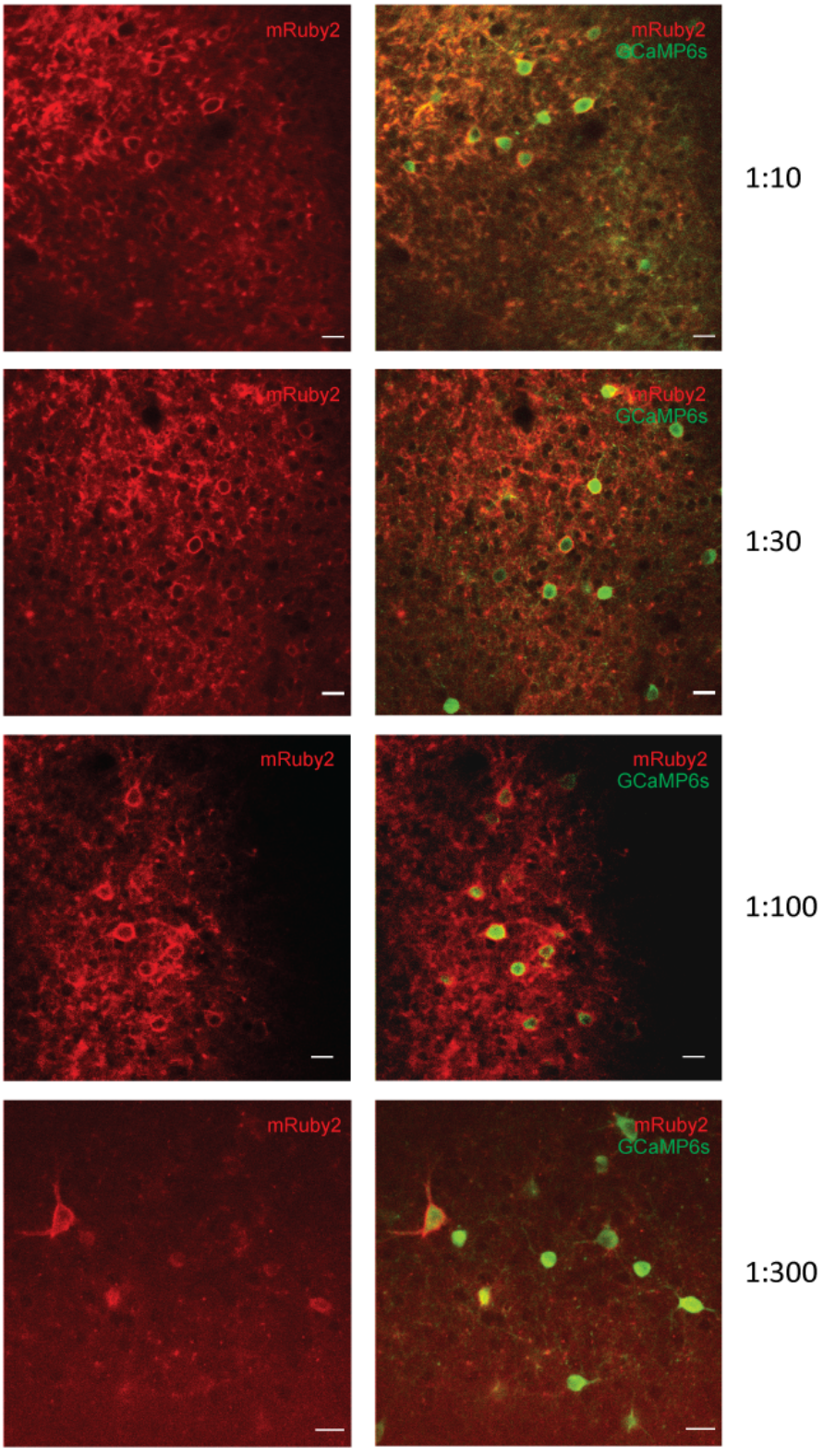
mRuby2
mRuby2
GCaMP6s
1:10
mRuby2
mRuby2
GCaMP6s
1:30
mRuby2
mRuby2
GCaMP6s
1:100
mRuby2
mRuby2
GCaMP6s
1:300

Fig.11. *In vivo* imaging of PNNs: (A) Top, schematic diagram of the experimental protocol. Injections have been performed at P60 and imaging sessions at P100. **(B)** Representative images of *in vivo* imaging sessions of PNNs highlighted by the conditional Hapln1-mRuby2 surrounding PV interneurons expressing the calcium indicator GCaMP6s. Imaging sessions have been performed in animals injected with different dilutions of the conditional AAV. Scale bar: 20μm.

The promising signal intensity and the increased contrast between PNNs and the diffuse ECM led me to further characterize the conditional AAV.

Firstly, I verified the possibility to visualize PNNs in *in vivo* imaging sessions using different dilutions of the conditional AAV. Moreover, performing simultaneous PNN and GCaMP6 imaging would have proved the feasibility in performing PNN-associated neurons functional imaging. Accordingly, I decided to co-inject four different dilutions of the conditional Hapln1-mRuby2 AAV with a conditional GCaMP6s AAV in the visual cortex of adult animals (P60) (fig.11a). In fig.11b, it is possible to observe PNNs highlighted by Hapln1-mRuby2 *in vivo* using the four different dilutions around PV interneurons expressing GCaMP6s. To my knowledge this is the first time that PNNs were visualized *in vivo* using a genetic approach.

These important results encouraged me to continue with conditional AAV characterization. In particular, understanding whether the overexpression of the conditional Hapln1-mRuby2 could cause an increase in PNN density and intensity was necessary. Moreover, evaluating the tagging efficiency of the conditional Hapln1-mRuby2 would have allowed me to understand the possible applications of tagging PNNs *in vivo* with this genetic methodology.

4.6 Characterization of the conditional AAV

To characterize the conditional AAV, I performed a single injection of the virus into the left primary visual cortex of mice. By comparing the treated cortex with the non-injected and untreated contralateral cortex, I intended to evaluate through an immunohistochemistry experiment possible changes in parameters that could have been altered following the overexpression of Hapln1-mRuby2 such as PNN density and WFA staining intensity. These possible alterations could have been dose dependent. Therefore, different dilutions have been injected. I decided to inject the 1:30, 1:100, and 1:300 dilutions since, in the in vivo imaging sessions, they provided the best contrast between PNNs and the diffuse ECM, allowing better *in vivo* visualization of these extracellular matrix structures. Moreover, the native Hapln1 has an extremely low turnover in the visual cortex (Fornasiero et al., 2018). Accordingly, the native Hapln1 could have limited the insertion of the exogenous

Hapln1-mRuby2 in mature PNNs but, likely, not in developing PNNs, possibly resulting in a different number of PNNs tagged by Hapln1-mRuby2. For this reason, I decided to perform the unilateral injection of the different AAV dilutions in P20 and P60 animals.

The first parameter that I analyzed was the efficiency of the conditional AAV to tag PNNs at the two different ages of injection. The mean percentage of WFA+ PNNs tagged by Hapln1-mRuby2 in the whole injection site oscillated between 15% and 40% in all experimental groups (fig.12a). In particular, the lowest percentage of colocalization has been observed for the experimental group in which the conditional AAV was injected at P60 and diluted 1:100. In contrast, the highest percentage has been observed in the experimental group in which the virus was injected at P20 with the dilution 1:300 (fig.12a). A significant difference has been observed between the two different ages with the dilutions 1:100 and 1:300. Interestingly, among the Hapln1-mRuby2+ PNNs, a high percentage were also WFA^+. In particular, in the P20 1:100 and 1:300 experimental groups, this percentage is around 85%, demonstrating the high specificity of Hapln1-mRuby2 in tagging WFA^+ PNNs (fig.12b). These data revealed that only a fraction of PNNs in the whole injection site have been labeled by Hapln1-mRuby2 but the labeling was highly specific for WFA^+ PNNs. Moreover, among the experimental groups, the animals of the 1:300 P20 group had the highest percentage of PNNs labelled.

In addition to evaluating the tagging efficiency of the conditional AAV, verifying a possible change in the density of WFA^+ PNNs and PV interneurons after the overexpression of Hapln1-mRuby2 was essential. Since I was interested in understanding whether the different dilutions would impact these parameters differently, I performed the analysis by dividing the experimental groups according to their age. In fig.12c, it is possible to observe an increase in WFA^+ PNNs mean density in the treated cortex compared to the contralateral untreated control cortex. Indeed, it is possible to notice a main effect of the treatment in animals injected at P20 and in animals injected at P60 independently from the AAV dilution. In addition, an increase in PV interneuron density in the treated cortex has been observed in some experimental groups at P60, in particular when the virus has been injected with the dilution 1:100 and 1:300 (fig.12d).

To understand whether the increase in PNNs density was due to an increase of PV interneurons overlapping with WFA^+ PNNs, I compared the percentage of WFA^+PV^+ interneurons in the treated and the contralateral control cortex. In fig.12e, it is possible to observe an increase in the percentage of PV interneurons surrounded by WFA^+PNNs with the only exception of the 1:100 P60 and 1:300 P60 groups. The increase in WFA^+PV^+ PNNs has been also suggested analyzing the percentage of WFA^+ PNNs overlapping with PV interneurons (fig.12f). Indeed, no significant difference was observed between the treated cortex and the control cortex.

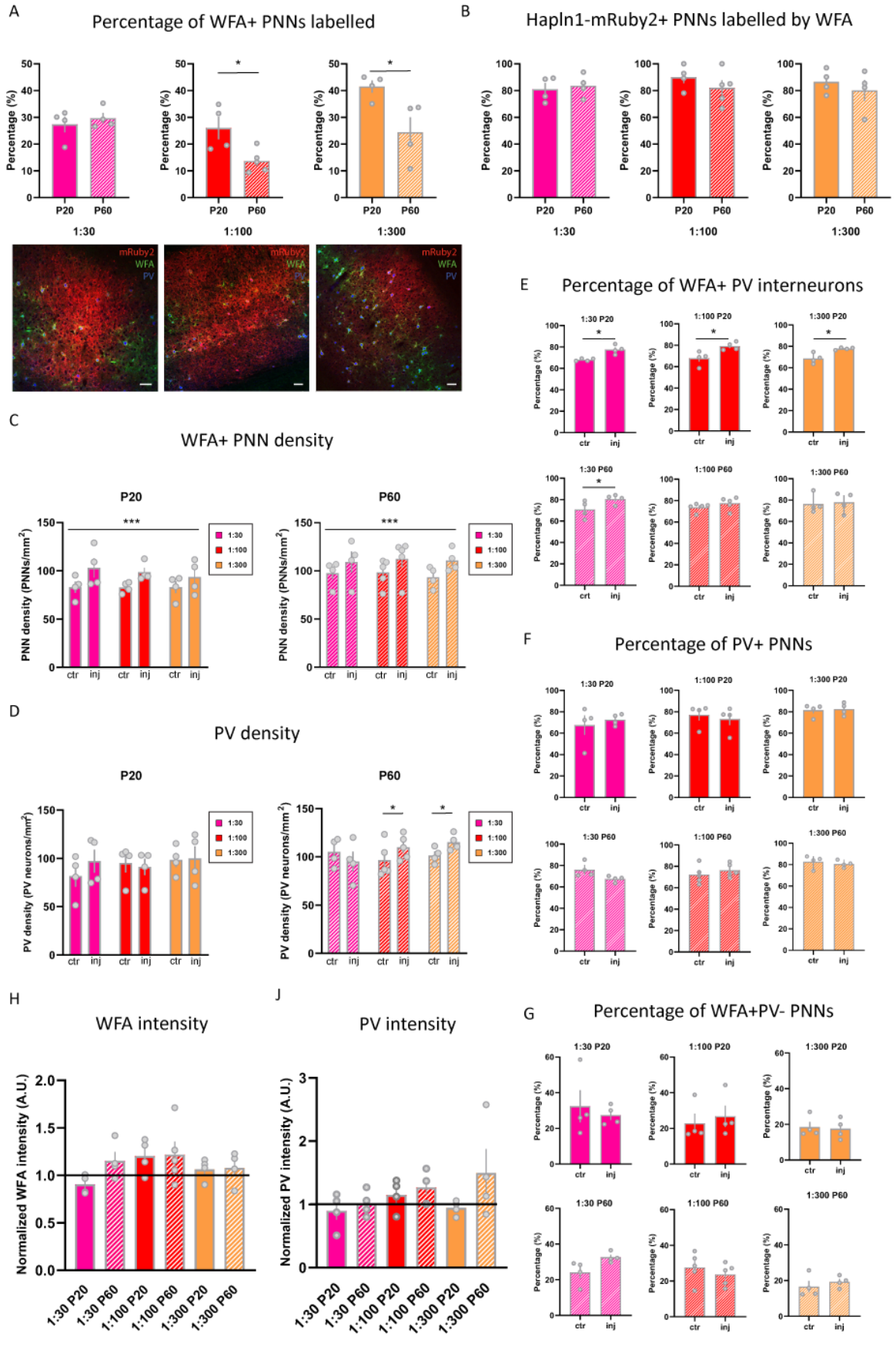
A
Percentage of WFA+ PNNs labelled
Percentage (%)
P20
P60
1:30
1:100
1:300
mRuby2
WFA
PV
B
Hapln1-mRuby2+ PNNs labelled by WFA
C
WFA+ PNN density
P20
P60
PNN density (PNNs/mm²)
***
1:30
1:100
1:300
ctr
inj
D
PV density
PV density (PV neurons/mm²)
E
Percentage of WFA+ PV interneurons
1:30 P20
1:100 P20
1:300 P20
1:30 P60
1:100 P60
1:300 P60
F
Percentage of PV+ PNNs
G
Percentage of WFA+PV- PNNs
H
WFA intensity
Normalized WFA intensity (A.U.)
J
PV intensity
Normalized PV intensity (A.U.)

Fig.12. Characterization of the conditional AAV: (A) Fig.12. Characterization of the conditional AAV: (A) Top, comparison of the percentage of WFA+ Hapln1-mRuby2+ PNNs over the total of WFA+ PNNs in the injection site between P20 and P60 injection time points using the dilution 1:30, 1:100, 1:300. Unpaired t-test P60 vs P20 for 1:30 (n=4), 1:100 (P20 n=4; P60 n=5), 1:300 (n=4). For 1:100 p=0.0233, 1:300 p=0.0293. Bottom, Representative images showing different expressions of Hapln1-mRuby2 according to the different dilutions. Note the low contrast between PNNs and the diffuse ECM in the higher dilutions with respect to the high contrast in the 1:300 condition. Scale bar: 50 µm. **(B)** Percentage of Hapln1-mRuby2+ WFA+ PNNs over the total of Hapln1-mRuby2+ PNNs. **(C)** Left**,** comparison of the WFA+ PNNs mean density between the non injected control cortex (ctr) and the treated cortex (inj) for the different conditional AAV dilutions injected at P20. 1:30 n= 4; 1:100 n = 4; 1:300 n=4; Two-way RM ANOVA treatment*dilution, main effect of the treatment $F(1,9) = 28.40$ $p = 0.0005$ (***). Right, comparison of the WFA+ PNNs mean density between the non injected control cortex (ctr) and the treated cortex (inj) for the different conditional AAV dilutions injected at P60. 1:30 n= 4; 1:100 n = 5; 1:300 n=4; Two-way RM ANOVA treatment*dilution, main effect of the treatment $F(1,10) = 21.78$ $p = 0.0009$ (***). **(D)** Left**,** comparison of PV interneurons mean density between the non injected control cortex (ctr) and the treated cortex (inj) for the different conditional AAV dilutions injected at P20. 1:30 n= 4; 1:100 n = 4; 1:300 n=4; Two-way RM ANOVA treatment*dilution, no significant differences. Right, comparison of PV interneurons mean density between the non injected control cortex (ctr) and the treated cortex (inj) for the different conditional AAV dilutions injected at P60. 1:30 n= 4; 1:100 n = 5; 1:300 n=4; Two-way RM ANOVA treatment*dilution, interaction $F(2,10) = 8.710$ $p = 0.0065$, post hoc Holm-Sidak adjusted p-values ctr vs inj 1:100 $t_{10} = 3.217$ $p = 0.0274$ (*); 1:300 $t_{10} = 2.951$ $p = 0.0429$ (*). **(E)** Comparison of the percentage of WFA+ PV interneurons over the total PV interneuron population between the control non injected cortex (crt) and the treated cortex (inj). Paired t-test inj. vs ctr. for 1:30 P20 (n=4), 1:100 P20 (n=4), 1:300 P20 (n=4), 1:30 P60 (n=4), 1:100 P60 (n=5), 1:300 P60 (n=4). For 1:30 P20 group, p=0.0119; for 1:30 P60 group p=0.0409, for 1:100 P20 group p=0.0382, for 1:300 P20 group p=0.0226. **(F)** Comparison of the percentage of WFA+ PV+ PNNs over the total of WFA+ PNNs between the control non injected cortex (crt) and the treated cortex (inj). Paired t-test inj. vs ctr. for r 1:30 P20 (n=4), 1:100 P20 (n=4), 1:300 P20 (n=4), 1:30 P60 (n=4), 1:100 P60 (n=5), 1:300 P60 (n=4), no significant differences. **(G)** Comparison of the percentage of WFA+ PV- PNNs over the total of WFA+ PNNs between the control non injected cortex (crt) and the treated cortex (inj). Paired t-test inj. vs ctr. for r 1:30 P20 (n=4), 1:100 P20 (n=4), 1:300 P20 (n=4), 1:30 P60 (n=4), 1:100 P60 (n=5), 1:300 P60 (n=4). no significant differences. **(H)** Normalized WFA mean staining intensity of the treated cortex to the contralateral uninjected control cortex for the groups 1:30 P20 (n=4), 1:30 P60 (n=4), 1:100 P20 (n=4), 1:100 P60 (n=5), 1:300 P20 (n=4), 1:300 P60 (n=4). One sample t-test, no significant differences for all groups. **(J)** Normalized PV mean staining intensity of the treated cortex to the contralateral uninjected control cortex for each animal for the groups 1:30 P20 (n=4), 1:30 P60 (n=4), 1:100 P20 (n=4), 1:100 P60 (n=5), 1:300 P20 (n=4), 1:300 P60 (n=4). One sample t-test, no significant differences for all groups. Data are expressed as mean ± SEM.

To better comprehend whether the observed increase of PNNs was specifically due only to the increase of WFA^+PV^+ PNNs or also to the increase of WFA^+PV^- PNNs, a further analysis has been conducted. As shown in fig.12g, the injection of the different dilutions of the conditional virus at the two different time points did not alter the percentage of WFA^+PV^- PNNs between the treated and the control cortex. These data show that the increase in PNN density observed after the viral injection is mainly due to the increase in the PNNs associated with PV interneurons.

The overexpression of Hapln1-mRuby2 could have altered another important parameter of PNNs, such as the WFA staining intensity. Since the native Hapln1 is essential in driving the proper maturation of PNNs, it is believed that Hapln1 has a CSPG aggregating nature *in vivo* (Carulli et al., 2010; Kwok et al., 2010). Accordingly, the overexpression of Hapln1-mRuby2 could have promoted the overall increase in PNN-CSPGs also in already existing PNNs,

likely increasing the WFA staining intensity. In fig.12h, it is possible to notice that no significant increase in the WFA mean staining intensity has been observed between the treated and the control cortex at both ages of injection.

Finally, I performed further analysis to understand if the overexpression of Hapln1-mRuby2 could have altered PV staining intensity. It has been reported that in the CA1 region of the hippocampus, the enzymatic degradation of the CSPGs led to a low PV state associated with an increased plastic condition (Donato et al., 2013). Accordingly, I considered controlling the average PV staining intensity due to the increased PNN density observed after the viral injection. The analysis revealed no change in the mean PV staining intensity between the treated and control cortex for all experimental groups (fig.12j). Although the analysis needs to be implemented, augmenting the statistical units to corroborate these results, the injection of the conditional AAV led to an overall increase in PNN density independently from the viral dilution injected. Interestingly, an increase in PV interneuron density has been found in animals injected at P60 with dilution 1:100 and 1:300. In contrast, no change between the injected cortex and the control cortex could be observed for WFA and PV mean staining intensity.

5. Discussion

Our knowledge about perineuronal nets (PNNs) and their essential functions in the CNS has been limited so far by the lack of proper tools to study these structures *in vivo*. During my PhD, I developed a genetic methodology allowing to visualize PNNs *in vivo*. The need to genetically label PNNs was due to their heterogeneity in terms of biochemical and molecular composition. Indeed, the sulfation pattern of PNNs varies in different brain regions, but also during development, and in pathological conditions (Enwright et al., 2016; Foscarin et al., 2017; Logsdon et al., 2022; Miyata et al., 2018; Sabbagh et al., 2018). Accordingly, markers recognizing specific GAG-CSPGs do not label all PNNs.

Accordingly, I used the antibody AB1031 recognizing the core protein of aggrecan to label PNNs *in vivo*. Unfortunately, the PNN-like structures labeled with this technique can be visible only for a short period of time, limiting the validity of this method for longitudinal studies. I observed similar results with the injection of WFA-fluorescein in a pilot experiment. The limited time period in which the PNN-like structures were visible with these markers could be due to the low quantity of the two different markers injected. Indeed, another study reported that PNNs can be observed *in vivo* for up to 2 months after the injection of WFA-fluorescein in the somatosensory cortex (Benbenishty et al., 2023). It is worth nothing that the total amount of WFA-fluorescein injected in this study is not entirely clear. According to the materials and methods section, 1 to 3 injections of 1.5ul each of a 0.7mg/mL WFA-fluorescein solution have been performed. Considering that I performed a single injection of 700nl of 0.2mg/mL WFA-fluorescein, Benbenishty and colleagues injected a quantity of WFA-fluorescein from 7.5 to 22.5 times higher. The high amount of WFA-fluorescein administered could have allowed the researchers to maintain an adequate pool of WFA-fluorescein bound to PNNs over time, preventing that removal processes take place.

It is also important to note that the WFA is a plant lectin; therefore, the injection of elevated amounts of WFA-fluorescein and its persistence for such a long time might induce a consistent immune response in the brain. Indeed, it has been reported that the administration of WFA in microglial cultures induces a proliferation of this population and an increase in the activity of extracellular matrix remodeling enzymes such as MMP9 (Liuzzi et al., 1999). Moreover, it has been reported that lesions in the spinal cord activate microglia, promote microglia-dependent PNN degradation, and alter PNN-associated neuron physiology (Tansley et al., 2022).

Thus, multiple injections of high amounts of WFA-fluorescein could extensively activate microglia, likely leading to a possible localized alteration of PNNs and an alteration of PNN-associated neuron physiology. Unfortunately, Benbenishty and colleagues did not perform a detailed PNN quantification comparing the injection site with a control condition.

The considerations about the potential immune response caused by the administration of high levels of exogenous molecules led me to discontinue the characterization of the AB1031 anti-aggrecan antibody as a tool to longitudinally visualize PNNs.

An alternative method to visualize PNNs *in vivo* is to genetically label these structures by making one of their components fluorescent. A possible approach could have been creating a transgenic mouse line making fluorescent one of the PNN components. This process would have been very expensive in terms of costs and time. Since a reliable in vitro model of PNNs is not available, developing a PNN fluorescent component would have required an *in vivo* validation making any potential modification needed very complex to be performed.

Another approach to genetically label PNNs is to deliver the PNN fluorescent component through viral vectors. In this framework, AAVs are extensively used for the application in brain circuits since they are poorly immunogenic, the viral genome remains mostly in an episomal form, they provide long-term expression in non-dividing cells, and capsid variants like the PHP.eB have been recently developed to cross the blood-brain barrier (Bessis et al., 2004; Chan et al., 2017; Haberman et al., 1998). This approach's inherent flexibility led to considering this technology to label PNNs genetically.

Among PNN components, the hapln1 gene is the ideal candidate to be conveyed by AAVs: indeed, the Hapln1 protein is critical in organizing PNNs (Carulli et al., 2010; Kwok et al., 2010) and, the Hapln1 coding sequence is small, fitting the limited genome capacity of AAVs. For these reasons, I developed a plasmid containing a Hapln1-mRuby2 fusion protein.

The proper expression, secretion capability and function of the fusion protein Hapln1-mRuby2 have been validated *in vitro* and *in vivo*. Indeed, I found that the fusion protein was expressed intact in the HAS3 cell line, as shown by the colocalization between the anti-Hapln1 and mRuby2. Moreover, I demonstrated the presence of Hapln1-mRuby2 in the culture medium of the same cell line, suggesting a correct secretion of the fusion protein. The secretion of Hapln1-mRuby2 in the intact form has been also verified *in vivo*. Moreover, I found that Hapln1-mRuby2 was inserted in PNNs, demonstrating the retention of the function of the native Hapln1 protein.

Despite these significant results, the extensive expression of Hapln1-mRuby2 led by the strong and ubiquitous CAG promoter also labeled WFA-negative extracellular structures. Although WFA-negative PNNs have been reported also in the visual cortex, the recurrence of these structures in my experimental conditions suggested they may be possible off-targets

(Miyata et al., 2018). The aggregation of Hapln1-mRuby2 around different neuronal populations other than PV interneurons (for instance excitatory neurons) might cause unpredictable effects. Indeed, Hapln1-mRuby2 might induce the aggregation of ECM components likely affecting neuron physiology. In addition, the extensive expression of Hapln1-mRuby2 driven by the strong and ubiquitous promoter CAG did not allow a proper visualization of PNNs *in vivo* due to the low contrast between PNNs and the surrounding diffuse extracellular matrix. Altogether, the presence of possible off-targets combined with the low contrast between PNNs and the diffuse ECM observed *in vivo* prompted me to find a way to restrict the expression of Hapln1-mRuby2 only in PV interneurons.

The native Hapln1 is expressed by neurons and astrocytes (Tasic et al., 2018). Hence, limiting the expression of Hapln1-mRuby2 in PV interneurons might be not sufficient to label PNNs *in vivo*. Accordingly, an intermediate step was to limit the expression of Hapln1-mRuby2 only in neurons using the synapsin promoter that is widely used to drive the expression of transgenes in neuronal cells (Kügler et al., 2003). Restricting Hapln1-mRuby2 expression only to the neuronal population was sufficient to tag PNNs. However, the still high expression of Hapln1-mRuby2 revealed several WFA-negative structures, highlighting possible off-targets similar to what I observed with the ubiquitous AAV. The likely expression of Hapln1-mRuby2 by all neuronal populations, including the excitatory one, could be responsible for the high number of the WFA-negative structures detected.

Thus, I developed a conditional version of the construct to limit the expression of Hapln1-mRuby2 in PV interneurons. By injecting the conditional AAV in the visual cortex of PV-Cre mice, PNNs can be visualized *in vivo*. To my knowledge, this is the first time that genetically-labeled PNNs have been observed *in vivo*. Moreover, the simultaneous visualization of the calcium sensor GCaMP6s provides the feasibility of the combined visualization of PNNs and recording of PV interneurons activity *in vivo* in the same imaging session.

Using multiple AAV dilutions allowed me to distinguish between PNNs and the diffuse ECM during the imaging sessions, even though the higher was the contrast, the higher was the dilution. Indeed, lower dilutions such as 1:30 and 1:100 still displayed a remarkable expression of Hapln1-mRuby2 that made sometimes difficult to recognize Hapln1-mRuby2^{+} PNNs during the quantification process. Indeed, the highest percentage of colocalization could be observed in the most diluted condition (1:300) with the injection performed at P20. Although the number of animals needs to be increased, the same dilution injected at P60 revealed a drastic reduction in the percentage of labeled PNNs. The same observation can be made for the animals injected with the dilution 1:100 at P60 with respect to 1:100 P20 animals. One possible explanation could be the less insertion capacity of Hapln1-mRuby in already mature PNNs. Indeed, the native Hapln1 could compete with Hapln1-mRuby2 for the

binding sites resulting in a lower number of PNNs labeled by Hapln1-mRuby2. Another possibility could be the role of the ECM in limiting viral infections at low titers. A looser and less structured matrix, such as that present in the young brain could facilitate viral infection, while mature PNNs may act as a barrier for AAV infection. Indeed, it has been demonstrated that the enzymatic degradation of PNNs improves lentiviral transduction efficiency, suggesting that the same effect could be present also for AAVs (Wanisch et al., 2013). Moreover, transduction efficiency may be different near the injection site or far from it. Therefore, a detailed analysis of the degree of colocalization between Hapln1-mRuby2$^+$ and WFA$^+$ PNNs relative to the distance from the injection site needs to be performed in order to highlight spatial differences in the percentage of PNNs labeled by the construct.

Interestingly, most of the PNNs tagged by the fusion protein are also positive for the WFA. The mean value in the experimental groups is around 80%, underlining the high specificity of Hapln1-mRuby2 in labeling PNNs, at least in the visual cortex. Indeed, the most abundant class of PNNs are WFA$^+$ in the visual cortex (Miyata et al., 2018). In contrast, the remaining fraction of PNNs tagged by the construct could belong to the WFA$^-$ PNN class. Further experiments should be conducted to verify this hypothesis and establish whether the WFA$^-$ structures labeled by Hapln1-mRuby2 are actually PNNs.

The injection of the conditional AAV led to a relatively small increase in PNN density. This increase was independent from the AAV dilution and the age of injection. It has been previously reported that lesions in the CNS induce an increase in CSPGs in the surrounding area (Bradbury et al., 2002; Morgenstern et al., 2002). Since the contralateral cortex has not been treated in the present experimental conditions, an additional control must be performed injecting a control virus to better determine whether the increase of PNN density is due to the overexpression of Hapln1-mRuby2 or to an increase in the expression of CSPGs caused by cortical lesion and viral infection. However, I hypothesize that the trend towards an increase of PNN density is most likely associated with the overexpression of the Hapln1-mRuby2 fusion protein. Indeed, it has been reported that Hapln1 induces CSPG aggregation in the pericellular matrix of HAS3 cells (Kwok et al., 2010). Similarly, PV interneurons naturally lacking PNNs could be driven to form *de novo* WFA$^+$ PNNs by expressing Hapln1-mRuby2. In fact, an increased percentage of PV interneurons surrounded by PNNs can be observed in the injected cortex in almost all the experimental groups. It is important to note that in my experimental condition forty days have passed from the injection of the conditional AAV to the evaluation of the effects of the expression of Link-mRuby2. Waiting such a long period could cause an accumulation of Hapln1-mRuby2 and to the *de novo* formation of PNNs. Restricting such a period could be essential in finding a time window in which my reporter does not cause these alterations. Moreover, the

extensive expression of my reporter promoted by the CAG promoter could contribute to the observed effects.

Indeed, an increase in PNN number has also been observed in the CA1 region of the hippocampus after the overexpression of Hapln1 guided by the activity of the promoter EF1a, similar in strength to the CAG promoter (Qin et al., 2010; Shi et al., 2019). Although the viral titer injected by Shi and colleagues is not reported, it is possible that the AAV titer injected could be higher from the one I used, especially considering the dilutions 1:100 or 1:300. Interestingly, Shi and colleagues observed an overall increase in the WFA intensity after the overexpression of Hapln1. In contrast, I reported no increase in this parameter. It is possible that the Hapln1-mRuby2 overexpression in my experimental condition likely does not alter the amount of CSPGs recognized by the WFA in the already present PNNs. Augmenting the statistical units will provide a better comprehension of the effects of Hapln1-mRuby2 overexpression on WFA intensity. The absence of increased WFA staining intensity compared to the outcome observed in Shi and colleague's work could suggest the presence of a threshold for the induction of CSPG aggregation in PNNs. It is possible to speculate that this threshold may also be present for the *de novo* induction of PNNs, suggesting that a reduction of the expression of Hapln1-mRuby2 could be a possible solution to avoid the formation of new PNNs. Indeed, changing the promoter regulating the expression of Hapln1-mRuby2 could be a promising strategy. Accordingly, it has been reported that the injection at P40 of an AAV expressing Hapln1 under the control of the neuron-specific synapsin promoter does not alter PNN density in the CA1 of the hippocampus (Ramsaran et al., 2023). Although it is impossible to compare Shi and colleagues and Ramsaran and colleague's experimental conditions, the different strength of the promoter might be fundamental in generating such different outcomes.

A similar threshold could also be present for parvalbumin expression. In the previous literature, it has been reported that the enzymatic removal of CSPGs in the CA1 region of the hippocampus leads to a decrease in PV expression and to a more plastic state of the circuit (Donato et al., 2013). The results of Donato and colleagues suggest that PNNs may regulate the expression of PV. Therefore, the overall increase in PNN around PV interneurons could lead to changes in PV expression towards higher values. My data showed no change in PV mean staining intensity between the injected and the control cortex but revealed an increase in PV interneuron density in animals injected at P60 with the dilutions 1:100 and 1:300. It is possible that in adult animals, the formation of new PNNs could cause opposite effects to their enzymatic degradation, shifting the PV expression to higher values and, therefore, allowing the identification of previously very low expressing PV interneurons.

In summary, by developing the fusion protein Hapln1-mRuby2, PNNs have been genetically labeled and visualized *in vivo* for the first time. Indeed, by limiting the expression of the PNN fluorescent reporter Hapln1-mRuby2 only in PV interneurons, a sufficient contrast has been obtained between PNNs and the surrounding diffuse ECM for the *in vivo* imaging of these extracellular matrix structures. The direct injection of the conditional AAV in the visual cortex led to very specific labeling of WFA^+ PNNs. However, only a fraction has been labeled in the whole injection site. In particular, the experimental condition 1:300 P20 provided the highest labeling. Further analysis will reveal the spatial tagging efficiency of Hapln1-mRuby2, likely more pronounced near the injection site and less far from it. The injection of the conditional AAV led to an increase in PNN density in the treated cortex compared to the control condition, irrespective of the viral titer injected. The increase in PNN density, independently from the viral titer injected, could be explained by the strength of the promoter regulating the expression of Hapln1-mRuby2. Further reducing Hapln1-mRuby2 expression may be a promising strategy to label PNNs *in vivo* without altering their density.

6. Conclusion and future perspective

I demonstrated the possibility to genetically label PNNs and perform *in vivo* imaging sessions of these extracellular matrix structures along with neuronal activity reporters. The development of the fusion protein Hapln1-mRuby2 successfully retained the function of the native Hapln1 protein. This important finding will likely allow the genetic labeling of PNNs *in vivo* through more optimized AAVs.

Developing a second generation genetic fluorescent reporter for PNN visualization *in vivo* will require careful evaluation of many important parameters. In particular, the viral titer could be a critical aspect. Indeed, a very high titer could transduce more PV interneurons enabling to tag more PNNs. Still, higher transduction could prominently alter PNNs density by inducing the expression of Hapln1-mRuby2 in more PV interneurons naturally lacking PNNs. If a threshold for the new formation of PNNs exists, decreasing the expression of Hapln1-mRuby2 might be essential. For this purpose, new alternative genetic regulatory elements can be involved to optimize the expression cassette of Hapln1-mRuby2.

For instance, it has been reported that short variants of the CAG promoter or the mouse phosphoglycerate kinase promoter (mPGK) drive a lower gene expression with respect to the full CAG promoter (Nieuwenhuis et al., 2021; Qin et al., 2010). Replacing the strong

CAG promoter with these weaker promoters could be a valid solution to limit the expression of Hapln1-mRuby2. Moreover, the expression of Hapln1 under the control of the synapsin promoter do not alter adult PNN density of the CA1 region of the hippocampus in contrast to what has been observed overexpressing Hapln1 utilizing the ubiquitous and strong promoter Ef1a (Ramsaran et al., 2023; Shi et al., 2019). Another possibility is to replace the CAG promoter with the endogenous promoter of the hapln1 gene. In principle, this region could be essential in the fine regulation of the native hapln1 gene. A detailed characterization of this regulatory sequence, however, is essential before the possible application to my construct.

In addition to cis-regulatory sequences such as promoters, many enhancers have been used in AAV technology to regulate gene expression in specific neuronal populations. Indeed, several enhancers have been used to limit the expression of genes in PV interneurons (Mich et al., 2021). However, it has still to be discovered whether one of these enhancers can limit the expression of genes only in PNN-associated neurons.

Other interesting regulatory sequences are the 3'UTRs of mRNAs. These sequences are responsible for gene expression post-transcriptional control. Indeed, they contain miRNA target sequences recently engineered for AAV technology. Indeed, the miRNA target sequences cloned into the AAV expression cassette promoted both limited gene expression and localized expression in specific cell subpopulations (Hordeaux et al., 2020; Keaveney et al., 2018). The right combination of these regulatory elements could be the key to labeling genetically PNNs through the AAV technology without inducing any alterations in important PNN metrics such as PNN density.

Interestingly, where the synapsin promoter drives the expression of Hapln1 as in Ramsaran et colleagues's work, the overexpression of Hapln1 fails to elicit modifications in PNN density, and no alterations have been observed during engram formation and episodic-like memory precision (Ramsaran et al., 2023). It is evident that the effects of Hapln1 overexpression should be assessed on a case-by-case basis, considering the region of the brain in which the overexpression occurs and the specific function under investigation. For example, in the visual cortex, even in the absence of the increase of PNN density, it should be demonstrated that the overexpression of Hapln1 does not modify the processing of visual stimuli. Indeed, Faini and colleagues have shown that the enzymatic disruption of PNNs changes the gain of visual processing (Faini et al., 2018). Therefore, it is possible to speculate that the overexpression of a PNN component such as Hapln1 might induce some alterations. Record the activity of PV interneurons in response to a visual stimulus characterized by increasing contrast after the injection of the virus might be a possible experiment to verify the absence of any alterations for this specific function in the visual cortex.

Developing an optimized genetic tool for the *in vivo* visualization of PNNs would allow for investigating many elusive aspects regarding these structures and their functions. In particular, understanding why some neurons develop a PNN while others do not is one of the most fascinating questions in the field. For example, most PNNs are associated with PV interneurons in the cortex. Conversely, in the CA2 region of the hippocampus, PNNs are associated with excitatory pyramidal neurons, emphasizing potential divergent roles for PNNs in these distinct brain areas (Carstens et al., 2016). The intrinsic flexibility of the conditionality of the genetic tool I developed could be fundamental in allowing the study of these possible differences.

Furthermore, this tool could allow the study of possible differences in the subpopulations of PV interneurons in the cortex. According to Lupori and colleagues, approximately half of the PV interneurons in the entire cortex are surrounded by PNNs, while the remaining half are not (Lupori et al., 2023). This fraction changes between cortical areas, with primary sensory areas having more pronounced PNN expression than associative ones. Their study also reveals a strong correlation between PNNs and PV expression. Elevated levels of PV have previously been linked to reduced plasticity, which is aligned with their association with PNNs (Donato et al., 2013). The most prominent PNN expression in primary sensory areas could be associated with a lower plastic capability with respect to other regions, such as associative cortices. This aspect could be addressed by studying PNNs and their associated neurons *in vivo*. Moreover, the co-presence of the two subpopulations of PV interneurons in the same area may be essential in giving the right balance between stability and plasticity to circuits and, thus, in sustaining their correct functioning. This speculation arises from the evidence that links neurodevelopmental disorders to aberrant plasticity, resulting, for instance, in dysfunctional sensory processing and altered PNN organization and maturation. Hence, the *in vivo* study of PNN-associated neurons and their network would be essential for both physiological and pathological perspectives.

In conclusion, the development of the fusion protein Hapln1-mRuby2 successfully retained the function of the native Hapln1 protein. This important finding paves the way for developing a transgenic mouse line expressing fluorescent PNNs. By replacing a native allele with the hapln1-mRuby2 gene developed here, it might be possible to study PNN *in vivo*, likely without inducing any alterations. Developing a transgenic line with visible PNNs will likely provide many important answers regarding the many elusive functions of PNNs.

7. Bibliography

Agetsuma, M., Hamm, J. P., Tao, K., Fujisawa, S., & Yuste, R. (2018). Parvalbumin-Positive Interneurons Regulate Neuronal Ensembles in Visual Cortex. *Cerebral Cortex* , *28*(5), 1831–1845.

Amilhon, B., Huh, C. Y. L., Manseau, F., Ducharme, G., Nichol, H., Adamantidis, A., & Williams, S. (2015). Parvalbumin Interneurons of Hippocampus Tune Population Activity at Theta Frequency. *Neuron*, *86*(5), 1277–1289.

Andrioli, A., Alonso-Nanclares, L., Arellano, J. I., & DeFelipe, J. (2007). Quantitative analysis of parvalbumin-immunoreactive cells in the human epileptic hippocampus. In *Neuroscience* (Vol. 149, Issue 1, pp. 131–143). https://doi.org/10.1016/j.neuroscience.2007.07.029

Araque, A., Parpura, V., Sanzgiri, R. P., & Haydon, P. G. (1999). Tripartite synapses: glia, the unacknowledged partner. *Trends in Neurosciences*, *22*(5), 208–215.

Arranz, A. M., Perkins, K. L., Irie, F., Lewis, D. P., Hrabe, J., Xiao, F., Itano, N., Kimata, K., Hrabetova, S., & Yamaguchi, Y. (2014). Hyaluronan deficiency due to Has3 knock-out causes altered neuronal activity and seizures via reduction in brain extracellular space. *The Journal of Neuroscience: The Official Journal of the Society for Neuroscience*, *34*(18), 6164–6176.

Aspberg, A., Miura, R., Bourdoulous, S., Shimonaka, M., Heinegård, D., Schachner, M., Ruoslahti, E., & Yamaguchi, Y. (1997). The C-type lectin domains of lecticans, a family of aggregating chondroitin sulfate proteoglycans, bind tenascin-R by protein– protein interactions independent of carbohydrate moiety. In *Proceedings of the National Academy of Sciences* (Vol. 94, Issue 19, pp. 10116–10121).

https://doi.org/10.1073/pnas.94.19.10116

Atallah, B. V., Bruns, W., Carandini, M., & Scanziani, M. (2012). Parvalbumin-expressing interneurons linearly transform cortical responses to visual stimuli. *Neuron*, *73*(1), 159–170.

Avermann, M., Tomm, C., Mateo, C., Gerstner, W., & Petersen, C. C. H. (2012). Microcircuits of excitatory and inhibitory neurons in layer 2/3 of mouse barrel cortex. *Journal of Neurophysiology*, *107*(11), 3116–3134.

Balmer, T. S. (2016). Perineuronal Nets Enhance the Excitability of Fast-Spiking Neurons. *eNeuro*, *3*(4). https://doi.org/10.1523/ENEURO.0112-16.2016

Banerjee, S. B., Gutzeit, V. A., Baman, J., Aoued, H. S., Doshi, N. K., Liu, R. C., & Ressler, K. J. (2017). Perineuronal Nets in the Adult Sensory Cortex Are Necessary for Fear Learning. *Neuron*, *95*(1), 169–179.e3.

Bartos, M., Vida, I., & Jonas, P. (2007). Synaptic mechanisms of synchronized gamma oscillations in inhibitory interneuron networks. *Nature Reviews. Neuroscience*, *8*(1), 45–56.

Bekku, Y., Saito, M., Moser, M., Fuchigami, M., Maehara, A., Nakayama, M., Kusachi, S., Ninomiya, Y., & Oohashi, T. (2012). Bral2 is indispensable for the proper localization of brevican and the structural integrity of the perineuronal net in the brainstem and cerebellum. *The Journal of Comparative Neurology*, *520*(8), 1721–1736.

Bekku, Y., Vargová, L., Goto, Y., Vorísek, I., Dmytrenko, L., Narasaki, M., Ohtsuka, A., Fässler, R., Ninomiya, Y., Syková, E., & Oohashi, T. (2010). Bral1: its role in diffusion barrier formation and conduction velocity in the CNS. *The Journal of Neuroscience: The Official Journal of the Society for Neuroscience*, *30*(8), 3113–3123.

Benbenishty, A., Peled-Hajaj, S., Krishnaswamy, V. R., Har-Gil, H., Havusha-Laufer, S., Ruggiero, A., Slutsky, I., Blinder, P., & Sagi, I. (2023). Longitudinal imaging of perineuronal nets. *Neurophotonics*, *10*(1), 015008.

Berardi, N., Pizzorusso, T., & Maffei, L. (2000). Critical periods during sensory development. *Current Opinion in Neurobiology*, *10*(1), 138–145.

Bessis, N., GarciaCozar, F. J., & Boissier, M.-C. (2004). Immune responses to gene therapy vectors: influence on vector function and effector mechanisms. *Gene Therapy*, *11 Suppl 1*, S10–S17.

Beurdeley, M., Spatazza, J., Lee, H. H. C., Sugiyama, S., Bernard, C., Di Nardo, A. A., Hensch, T. K., & Prochiantz, A. (2012). Otx2 binding to perineuronal nets persistently regulates plasticity in the mature visual cortex. *The Journal of Neuroscience: The Official Journal of the Society for Neuroscience*, *32*(27), 9429–9437.

Bitanihirwe, B. K. Y., & Woo, T.-U. W. (2014). Perineuronal nets and schizophrenia: the importance of neuronal coatings. *Neuroscience and Biobehavioral Reviews*, *45*, 85–99.

Boggio, E. M., Ehlert, E. M., Lupori, L., Moloney, E. B., De Winter, F., Vander Kooi, C. W., Baroncelli, L., Mecollari, V., Blits, B., Fawcett, J. W., Verhaagen, J., & Pizzorusso, T. (2019). Inhibition of Semaphorin3A Promotes Ocular Dominance Plasticity in the Adult Rat Visual Cortex. *Molecular Neurobiology*, *56*(9), 5987–5997.

Bradbury, E. J., Moon, L. D. F., Popat, R. J., King, V. R., Bennett, G. S., Patel, P. N., Fawcett, J. W., & McMahon, S. B. (2002). Chondroitinase ABC promotes functional recovery after spinal cord injury. *Nature*, *416*(6881), 636–640.

Brückner, G., Brauer, K., Härtig, W., Wolff, J. R., Rickmann, M. J., Derouiche, A., Delpech, B., Girard, N., Oertel, W. H., & Reichenbach, A. (1993). Perineuronal nets provide a polyanionic, glia-associated form of microenvironment around certain neurons in many parts of the rat brain. In *Glia* (Vol. 8, Issue 3, pp. 183–200). https://doi.org/10.1002/glia.440080306

Brückner, G., Hausen, D., Härtig, W., Drlicek, M., Arendt, T., & Brauer, K. (1999). Cortical areas abundant in extracellular matrix chondroitin sulphate proteoglycans are less affected by cytoskeletal changes in Alzheimer's disease. *Neuroscience*, *92*(3), 791–805.

Br�ckner, G., Grosche, J., Schmidt, S., H�rtig, W., Margolis, R. U., Delpech, B., Seidenbecher, C. I., Czaniera, R., & Schachner, M. (2000). Postnatal development of perineuronal nets in wild-type mice and in a mutant deficient in tenascin-R. In *The Journal of Comparative Neurology* (Vol. 428, Issue 4, pp. 616–629).

https://doi.org/10.1002/1096-9861(20001225)428:4<616::aid-cne3>3.0.co;2-k

Cabungcal, J.-H., Counotte, D. S., Lewis, E. M., Tejeda, H. A., Piantadosi, P., Pollock, C., Calhoon, G. G., Sullivan, E. M., Presgraves, E., Kil, J., Elliot Hong, L., Cuenod, M., Do, K. Q., & O'Donnell, P. (2014). Juvenile Antioxidant Treatment Prevents Adult Deficits in a Developmental Model of Schizophrenia. In *Neuron* (Vol. 83, Issue 5, pp. 1073–1084). https://doi.org/10.1016/j.neuron.2014.07.028

Cabungcal, J.-H., Steullet, P., Morishita, H., Kraftsik, R., Cuenod, M., Hensch, T. K., & Do, K. Q. (2013). Perineuronal nets protect fast-spiking interneurons against oxidative stress. *Proceedings of the National Academy of Sciences of the United States of America*, *110*(22), 9130–9135.

Caillard, O., Moreno, H., Schwaller, B., Llano, I., Celio, M. R., & Marty, A. (2000). Role of the calcium-binding protein parvalbumin in short-term synaptic plasticity. *Proceedings of the National Academy of Sciences of the United States of America*, *97*(24), 13372–13377.

Calof, A. L., & Reichardt, L. F. (1985). Response of purified chick motoneurons to myotube conditioned medium: laminin is essential for the substratum-binding, neurite outgrowth-promoting activity. *Neuroscience Letters*, *59*(2), 183–189.

Carceller, H., Guirado, R., Ripolles-Campos, E., Teruel-Marti, V., & Nacher, J. (2020). Perineuronal Nets Regulate the Inhibitory Perisomatic Input onto Parvalbumin Interneurons and γ Activity in the Prefrontal Cortex. *The Journal of Neuroscience: The Official Journal of the Society for Neuroscience*, *40*(26), 5008–5018.

Cardin, J. A., Carlén, M., Meletis, K., Knoblich, U., Zhang, F., Deisseroth, K., Tsai, L.-H., & Moore, C. I. (2009). Driving fast-spiking cells induces gamma rhythm and controls sensory responses. *Nature*, *459*(7247), 663–667.

Carstens, K. E., Lustberg, D. J., Shaughnessy, E. K., McCann, K. E., Alexander, G. M., & Dudek, S. M. (2021). Perineuronal net degradation rescues CA2 plasticity in a mouse model of Rett syndrome. *The Journal of Clinical Investigation*, *131*(16). https://doi.org/10.1172/JCI137221

Carstens, K. E., Phillips, M. L., Pozzo-Miller, L., Weinberg, R. J., & Dudek, S. M. (2016).

Perineuronal Nets Suppress Plasticity of Excitatory Synapses on CA2 Pyramidal Neurons. *The Journal of Neuroscience: The Official Journal of the Society for Neuroscience*, *36*(23), 6312–6320.

Carter, B. C., & Bean, B. P. (2009). Sodium entry during action potentials of mammalian neurons: incomplete inactivation and reduced metabolic efficiency in fast-spiking neurons. *Neuron*, *64*(6), 898–909.

Carulli, D., Broersen, R., de Winter, F., Muir, E. M., Mešković, M., de Waal, M., de Vries, S., Boele, H.-J., Canto, C. B., De Zeeuw, C. I., & Verhaagen, J. (2020). Cerebellar plasticity and associative memories are controlled by perineuronal nets. *Proceedings of the National Academy of Sciences of the United States of America*, *117*(12), 6855–6865.

Carulli, D., Pizzorusso, T., Kwok, J. C. F., Putignano, E., Poli, A., Forostyak, S., Andrews, M. R., Deepa, S. S., Glant, T. T., & Fawcett, J. W. (2010). Animals lacking link protein have attenuated perineuronal nets and persistent plasticity. *Brain: A Journal of Neurology*, *133*(Pt 8), 2331–2347.

Carulli, D., Rhodes, K. E., Brown, D. J., Bonnert, T. P., Pollack, S. J., Oliver, K., Strata, P., & Fawcett, J. W. (2006). Composition of perineuronal nets in the adult rat cerebellum and the cellular origin of their components. *The Journal of Comparative Neurology*, *494*(4), 559–577.

Carulli, D., & Verhaagen, J. (2021). An Extracellular Perspective on CNS Maturation: Perineuronal Nets and the Control of Plasticity. *International Journal of Molecular Sciences*, *22*(5). https://doi.org/10.3390/ijms22052434

Celio, M. R. (1986). Parvalbumin in most gamma-aminobutyric acid-containing neurons of the rat cerebral cortex. *Science*, *231*(4741), 995–997.

Celio, M. R., Spreafico, R., De Biasi, S., & Vitellaro-Zuccarello, L. (1998). Perineuronal nets: past and present. *Trends in Neurosciences*, *21*(12), 510–515.

Chan, K. Y., Jang, M. J., Yoo, B. B., Greenbaum, A., Ravi, N., Wu, W.-L., Sánchez-Guardado, L., Lois, C., Mazmanian, S. K., Deverman, B. E., & Gradinaru, V. (2017). Engineered AAVs for efficient noninvasive gene delivery to the central and

peripheral nervous systems. *Nature Neuroscience*, *20*(8), 1172–1179.

Cheah, M., Andrews, M. R., Chew, D. J., Moloney, E. B., Verhaagen, J., Fässler, R., & Fawcett, J. W. (2016). Expression of an Activated Integrin Promotes Long-Distance Sensory Axon Regeneration in the Spinal Cord. *The Journal of Neuroscience: The Official Journal of the Society for Neuroscience*, *36*(27), 7283–7297.

Chelini, G., Pantazopoulos, H., Durning, P., & Berretta, S. (2018). The tetrapartite synapse: a key concept in the pathophysiology of schizophrenia. *European Psychiatry: The Journal of the Association of European Psychiatrists*, *50*, 60–69.

Chen, Z.-L., Haegeli, V., Yu, H., & Strickland, S. (2009). Cortical deficiency of laminin gamma1 impairs the AKT/GSK-3beta signaling pathway and leads to defects in neurite outgrowth and neuronal migration. *Developmental Biology*, *327*(1), 158–168.

Christensen, A. C., Lensjø, K. K., Lepperød, M. E., Dragly, S.-A., Sutterud, H., Blackstad, J. S., Fyhn, M., & Hafting, T. (2021). Perineuronal nets stabilize the grid cell network. *Nature Communications*, *12*(1), 253.

Chu, P., Abraham, R., Budhu, K., Khan, U., De Marco Garcia, N., & Brumberg, J. C. (2018). The Impact of Perineuronal Net Digestion Using Chondroitinase ABC on the Intrinsic Physiology of Cortical Neurons. *Neuroscience*, *388*, 23–35.

Ciampi, L., Carrara, F., Totaro, V., Mazziotti, R., Lupori, L., Santiago, C., Amato, G., Pizzorusso, T., & Gennaro, C. (2022). Learning to count biological structures with raters' uncertainty. *Medical Image Analysis*, *80*, 102500.

Cinalli, D. A., Jr, Cohen, S. J., Guthrie, K., & Stackman, R. W., Jr. (2020). Object Recognition Memory: Distinct Yet Complementary Roles of the Mouse CA1 and Perirhinal Cortex. *Frontiers in Molecular Neuroscience*, *13*, 527543.

Dauth, S., Grevesse, T., Pantazopoulos, H., Campbell, P. H., Maoz, B. M., Berretta, S., & Parker, K. K. (2016). Extracellular matrix protein expression is brain region dependent. *The Journal of Comparative Neurology*, *524*(7), 1309–1336.

Day, A. J., & Prestwich, G. D. (2002). Hyaluronan-binding proteins: tying up the giant. *The Journal of Biological Chemistry*, *277*(7), 4585–4588.

Deák, F., Mátés, L., Krysan, K., Liu, Z., Szabó, P. E., Mann, J. R., Beier, D. R., & Kiss, I. (1999). Characterization and chromosome location of the mouse link protein gene (Crtl1). *Cytogenetics and Cell Genetics*, *87*(1-2), 75–79.

Deepa, S. S., Carulli, D., Galtrey, C., Rhodes, K., Fukuda, J., Mikami, T., Sugahara, K., & Fawcett, J. W. (2006). Composition of perineuronal net extracellular matrix in rat brain: a different disaccharide composition for the net-associated proteoglycans. *The Journal of Biological Chemistry*, *281*(26), 17789–17800.

DeFelipe, J., & González-Albo, M. C. (1998). Chandelier cell axons are immunoreactive for GAT-1 in the human neocortex. *Neuroreport*, *9*(3), 467–470.

Descalzo, V. F., Nowak, L. G., Brumberg, J. C., McCormick, D. A., & Sanchez-Vives, M. V. (2005). Slow adaptation in fast-spiking neurons of visual cortex. *Journal of Neurophysiology*, *93*(2), 1111–1118.

Devienne, G., Picaud, S., Cohen, I., Piquet, J., Tricoire, L., Testa, D., Di Nardo, A. A., Rossier, J., Cauli, B., & Lambolez, B. (2021). Regulation of perineuronal nets in the adult cortex by the activity of the cortical network. *The Journal of Neuroscience: The Official Journal of the Society for Neuroscience*. https://doi.org/10.1523/JNEUROSCI.0434-21.2021

Dick, G., Tan, C. L., Alves, J. N., Ehlert, E. M. E., Miller, G. M., Hsieh-Wilson, L. C., Sugahara, K., Oosterhof, A., van Kuppevelt, T. H., Verhaagen, J., Fawcett, J. W., & Kwok, J. C. F. (2013). Semaphorin 3A binds to the perineuronal nets via chondroitin sulfate type E motifs in rodent brains. *The Journal of Biological Chemistry*, *288*(38), 27384–27395.

Di Cristo, G., Wu, C., Chattopadhyaya, B., Ango, F., Knott, G., Welker, E., Svoboda, K., & Huang, Z. J. (2004). Subcellular domain-restricted GABAergic innervation in primary visual cortex in the absence of sensory and thalamic inputs. *Nature Neuroscience*, *7*(11), 1184–1186.

Dingess, P. M., Harkness, J. H., Slaker, M., Zhang, Z., Wulff, S. S., Sorg, B. A., & Brown, T. E. (2018). Consumption of a High-Fat Diet Alters Perineuronal Nets in the Prefrontal

Cortex. *Neural Plasticity*, *2018*, 2108373.

Dityatev, A., & Rusakov, D. A. (2011). Molecular signals of plasticity at the tetrapartite synapse. *Current Opinion in Neurobiology*, *21*(2), 353–359.

Do, K. Q., Trabesinger, A. H., Kirsten-Krüger, M., Lauer, C. J., Dydak, U., Hell, D., Holsboer, F., Boesiger, P., & Cuénod, M. (2000). Schizophrenia: glutathione deficit in cerebrospinal fluid and prefrontal cortex in vivo. *The European Journal of Neuroscience*, *12*(10), 3721–3728.

Domínguez, S., Rey, C. C., Therreau, L., Fanton, A., Massotte, D., Verret, L., Piskorowski, R. A., & Chevaleyre, V. (2019). Maturation of PNN and ErbB4 Signaling in Area CA2 during Adolescence Underlies the Emergence of PV Interneuron Plasticity and Social Memory. In *Cell Reports* (Vol. 29, Issue 5, pp. 1099–1112.e4). https://doi.org/10.1016/j.celrep.2019.09.044

Donato, F., Rompani, S. B., & Caroni, P. (2013). Parvalbumin-expressing basket-cell network plasticity induced by experience regulates adult learning. *Nature*, *504*(7479), 272–276.

Drago, J., Nurcombe, V., & Bartlett, P. F. (1991). Laminin through its long arm E8 fragment promotes the proliferation and differentiation of murine neuroepithelial cells in vitro. *Experimental Cell Research*, *192*(1), 256–265.

Drexel, M., Preidt, A. P., Kirchmair, E., & Sperk, G. (2011). Parvalbumin interneurons and calretinin fibers arising from the thalamic nucleus reuniens degenerate in the subiculum after kainic acid-induced seizures. *Neuroscience*, *189*(1-2), 316–329.

Duan, Y., & Giger, R. J. (2010). A New Role for RPTPσ in Spinal Cord Injury: Signaling Chondroitin Sulfate Proteoglycan Inhibition. In *Science Signaling* (Vol. 3, Issue 110). https://doi.org/10.1126/scisignal.3110pe6

Du, J., Zhang, L., Weiser, M., Rudy, B., & McBain, C. J. (1996). Developmental expression and functional characterization of the potassium-channel subunit Kv3.1b in parvalbumin-containing interneurons of the rat hippocampus. *The Journal of Neuroscience: The Official Journal of the Society for Neuroscience*, *16*(2), 506–518.

Durand, S., Patrizi, A., Quast, K. B., Hachigian, L., Pavlyuk, R., Saxena, A., Carninci, P.,

Hensch, T. K., & Fagiolini, M. (2012). NMDA receptor regulation prevents regression of visual cortical function in the absence of Mecp2. *Neuron*, *76*(6), 1078–1090.

Enwright, J. F., Sanapala, S., Foglio, A., Berry, R., Fish, K. N., & Lewis, D. A. (2016). Reduced Labeling of Parvalbumin Neurons and Perineuronal Nets in the Dorsolateral Prefrontal Cortex of Subjects with Schizophrenia. *Neuropsychopharmacology: Official Publication of the American College of Neuropsychopharmacology*, *41*(9), 2206–2214.

Fagiolini, M., Fritschy, J.-M., Löw, K., Möhler, H., Rudolph, U., & Hensch, T. K. (2004). Specific GABAA circuits for visual cortical plasticity. *Science*, *303*(5664), 1681–1683.

Fagiolini, M., & Hensch, T. K. (2000). Inhibitory threshold for critical-period activation in primary visual cortex. *Nature*, *404*(6774), 183–186.

Faini, G., Aguirre, A., Landi, S., Lamers, D., Pizzorusso, T., Ratto, G. M., Deleuze, C., & Bacci, A. (2018). Perineuronal nets control visual input via thalamic recruitment of cortical PV interneurons. *eLife*, *7*. https://doi.org/10.7554/eLife.41520

Faltz, L. L., Caputo, C. B., Kimura, J. H., Schrode, J., & Hascall, V. C. (1979). Structure of the complex between hyaluronic acid, the hyaluronic acid-binding region, and the link protein of proteoglycan aggregates from the swarm rat chondrosarcoma. *The Journal of Biological Chemistry*, *254*(4), 1381–1387.

Favuzzi, E., Marques-Smith, A., Deogracias, R., Winterflood, C. M., Sánchez-Aguilera, A., Mantoan, L., Maeso, P., Fernandes, C., Ewers, H., & Rico, B. (2017). Activity-Dependent Gating of Parvalbumin Interneuron Function by the Perineuronal Net Protein Brevican. *Neuron*, *95*(3), 639–655.e10.

Fawcett, J. W., & Kwok, J. C. F. (2022). Proteoglycan Sulphation in the Function of the Mature Central Nervous System. *Frontiers in Integrative Neuroscience*, *16*, 895493.

Flanagan, L. A., Rebaza, L. M., Derzic, S., Schwartz, P. H., & Monuki, E. S. (2006). Regulation of human neural precursor cells by laminin and integrins. *Journal of Neuroscience Research*, *83*(5), 845–856.

Flatow, J., Buckley, P., & Miller, B. J. (2013). Meta-Analysis of Oxidative Stress in Schizophrenia. In *Biological Psychiatry* (Vol. 74, Issue 6, pp. 400–409).

https://doi.org/10.1016/j.biopsych.2013.03.018

Fornasiero, E. F., Mandad, S., Wildhagen, H., Alevra, M., Rammner, B., Keihani, S., Opazo, F., Urban, I., Ischebeck, T., Sakib, M. S., Fard, M. K., Kirli, K., Centeno, T. P., Vidal, R. O., Rahman, R.-U., Benito, E., Fischer, A., Dennerlein, S., Rehling, P., … Rizzoli, S. O. (2018). Precisely measured protein lifetimes in the mouse brain reveal differences across tissues and subcellular fractions. *Nature Communications*, *9*(1), 4230.

Foscarin, S., Ponchione, D., Pajaj, E., Leto, K., Gawlak, M., Wilczynski, G. M., Rossi, F., & Carulli, D. (2011). Experience-dependent plasticity and modulation of growth regulatory molecules at central synapses. *PloS One*, *6*(1), e16666.

Foscarin, S., Raha-Chowdhury, R., Fawcett, J. W., & Kwok, J. C. F. (2017). Brain ageing changes proteoglycan sulfation, rendering perineuronal nets more inhibitory. *Aging*, *9*(6), 1607–1622.

Frischknecht, R., Heine, M., Perrais, D., Seidenbecher, C. I., Choquet, D., & Gundelfinger, E. D. (2009). Brain extracellular matrix affects AMPA receptor lateral mobility and short-term synaptic plasticity. *Nature Neuroscience*, *12*(7), 897–904.

Galarreta, M., & Hestrin, S. (1999). A network of fast-spiking cells in the neocortex connected by electrical synapses. *Nature*, *402*(6757), 72–75.

Galarreta, M., & Hestrin, S. (2002). Electrical and chemical synapses among parvalbumin fast-spiking GABAergic interneurons in adult mouse neocortex. *Proceedings of the National Academy of Sciences of the United States of America*, *99*(19), 12438–12443.

Galtrey, C. M., Kwok, J. C. F., Carulli, D., Rhodes, K. E., & Fawcett, J. W. (2008). Distribution and synthesis of extracellular matrix proteoglycans, hyaluronan, link proteins and tenascin-R in the rat spinal cord. *The European Journal of Neuroscience*, *27*(6), 1373–1390.

Gama, C. I., Tully, S. E., Sotogaku, N., Clark, P. M., Rawat, M., Vaidehi, N., Goddard, W. A., 3rd, Nishi, A., & Hsieh-Wilson, L. C. (2006). Sulfation patterns of glycosaminoglycans encode molecular recognition and activity. *Nature Chemical Biology*, *2*(9), 467–473.

Gandal, M. J., Edgar, J. C., Klook, K., & Siegel, S. J. (2012). Gamma synchrony: towards a

translational biomarker for the treatment-resistant symptoms of schizophrenia. *Neuropharmacology*, *62*(3), 1504–1518.

Gogolla, N., Caroni, P., Lüthi, A., & Herry, C. (2009). Perineuronal nets protect fear memories from erasure. *Science*, *325*(5945), 1258–1261.

Gordon, J. A., & Stryker, M. P. (1996). Experience-dependent plasticity of binocular responses in the primary visual cortex of the mouse. *The Journal of Neuroscience: The Official Journal of the Society for Neuroscience*, *16*(10), 3274–3286.

Griffiths, S., Scott, H., Glover, C., Bienemann, A., Ghorbel, M. T., Uney, J., Brown, M. W., Warburton, E. C., & Bashir, Z. I. (2008). Expression of long-term depression underlies visual recognition memory. *Neuron*, *58*(2), 186–194.

Grumet, M., Friedlander, D. R., & Sakurai, T. (1996). Functions of brain chondroitin sulfate proteoglycans during developments: interactions with adhesion molecules. *Perspectives on Developmental Neurobiology*, *3*(4), 319–330.

Gulyás, A. I., Megías, M., Emri, Z., & Freund, T. F. (1999). Total Number and Ratio of Excitatory and Inhibitory Synapses Converging onto Single Interneurons of Different Types in the CA1 Area of the Rat Hippocampus. In *The Journal of Neuroscience* (Vol. 19, Issue 22, pp. 10082–10097). https://doi.org/10.1523/jneurosci.19-22-10082.1999

Haberman, R. P., McCown, T. J., & Samulski, R. J. (1998). Inducible long-term gene expression in brain with adeno-associated virus gene transfer. *Gene Therapy*, *5*(12), 1604–1611.

Hagberg, B. (2002). Clinical manifestations and stages of Rett syndrome. *Mental Retardation and Developmental Disabilities Research Reviews*, *8*(2), 61–65.

Hagerman, R. J., & Hagerman, P. J. (2008). Testing for fragile X gene mutations throughout the life span. *JAMA: The Journal of the American Medical Association*, *300*(20), 2419–2421.

Hagihara, K., Miura, R., Kosaki, R., Berglund, E., Ranscht, B., & Yamaguchi, Y. (1999). Immunohistochemical evidence for the brevican-tenascin-R interaction: colocalization in perineuronal nets suggests a physiological role for the interaction in the adult rat brain.

The Journal of Comparative Neurology, *410*(2), 256–264.

Härtig, W., Brauer, K., Bigl, V., & Brückner, G. (1994). Chondroitin sulfate proteoglycan-immunoreactivity of lectin-labeled perineuronal nets around parvalbumin-containing neurons. *Brain Research*, *635*(1-2), 307–311.

Härtig, W., Brauer, K., & Brückner, G. (1992). Wisteria floribunda agglutinin-labelled nets surround parvalbumin-containing neurons. *Neuroreport*, *3*(10), 869–872.

Heinegård, D., & Hascall, V. C. (1974). Aggregation of cartilage proteoglycans. 3. Characteristics of the proteins isolated from trypsin digests of aggregates. *The Journal of Biological Chemistry*, *249*(13), 4250–4256.

He, L.-J., Liu, N., Cheng, T.-L., Chen, X.-J., Li, Y.-D., Shu, Y.-S., Qiu, Z.-L., & Zhang, X.-H. (2014). Conditional deletion of Mecp2 in parvalbumin-expressing GABAergic cells results in the absence of critical period plasticity. *Nature Communications*, *5*, 5036.

Hensch, T. K. (2005). Critical period plasticity in local cortical circuits. *Nature Reviews. Neuroscience*, *6*(11), 877–888.

Hensch, T. K., Fagiolini, M., Mataga, N., Stryker, M. P., Baekkeskov, S., & Kash, S. F. (1998). Local GABA circuit control of experience-dependent plasticity in developing visual cortex. *Science*, *282*(5393), 1504–1508.

Hippenmeyer, S., Vrieseling, E., Sigrist, M., Portmann, T., Laengle, C., Ladle, D. R., & Arber, S. (2005). A developmental switch in the response of DRG neurons to ETS transcription factor signaling. *PLoS Biology*, *3*(5), e159.

Hirakawa, S., Oohashi, T., Su, W. D., Yoshioka, H., Murakami, T., Arata, J., & Ninomiya, Y. (2000). The brain link protein-1 (BRAL1): cDNA cloning, genomic structure, and characterization as a novel link protein expressed in adult brain. *Biochemical and Biophysical Research Communications*, *276*(3), 982–989.

Hitti, F. L., & Siegelbaum, S. A. (2014). The hippocampal CA2 region is essential for social memory. *Nature*, *508*(7494), 88–92.

Hordeaux, J., Buza, E. L., Jeffrey, B., Song, C., Jahan, T., Yuan, Y., Zhu, Y., Bell, P., Li, M., Chichester, J. A., Calcedo, R., & Wilson, J. M. (2020). MicroRNA-mediated inhibition of

transgene expression reduces dorsal root ganglion toxicity by AAV vectors in primates. *Science Translational Medicine*, *12*(569). https://doi.org/10.1126/scitranslmed.aba9188

Hou, X., Yoshioka, N., Tsukano, H., Sakai, A., Miyata, S., Watanabe, Y., Yanagawa, Y., Sakimura, K., Takeuchi, K., Kitagawa, H., Hensch, T. K., Shibuki, K., Igarashi, M., & Sugiyama, S. (2017). Chondroitin Sulfate Is Required for Onset and Offset of Critical Period Plasticity in Visual Cortex. *Scientific Reports*, *7*(1), 12646.

Hubel, D. H., & Wiesel, T. N. (1970). The period of susceptibility to the physiological effects of unilateral eye closure in kittens. In *The Journal of Physiology* (Vol. 206, Issue 2, pp. 419–436). https://doi.org/10.1113/jphysiol.1970.sp009022

Hu, H., Gan, J., & Jonas, P. (2014). Interneurons. Fast-spiking, parvalbumin^{+} GABAergic interneurons: from cellular design to microcircuit function. *Science*, *345*(6196), 1255263.

Hu, H., & Jonas, P. (2014). A supercritical density of Na(+) channels ensures fast signaling in GABAergic interneuron axons. *Nature Neuroscience*, *17*(5), 686–693.

Huynh, M. B., Ouidja, M. O., Chantepie, S., Carpentier, G., Maïza, A., Zhang, G., Vilares, J., Raisman-Vozari, R., & Papy-Garcia, D. (2019). Glycosaminoglycans from Alzheimer's disease hippocampus have altered capacities to bind and regulate growth factors activities and to bind tau. *PloS One*, *14*(1), e0209573.

Hylin, M. J., Orsi, S. A., Moore, A. N., & Dash, P. K. (2013). Disruption of the perineuronal net in the hippocampus or medial prefrontal cortex impairs fear conditioning. In *Learning & Memory* (Vol. 20, Issue 5, pp. 267–273). https://doi.org/10.1101/lm.030197.112

Irvine, S. F., & Kwok, J. C. F. (2018). Perineuronal Nets in Spinal Motoneurones: Chondroitin Sulphate Proteoglycan around Alpha Motoneurones. *International Journal of Molecular Sciences*, *19*(4). https://doi.org/10.3390/ijms19041172

Isaacson, J. S., & Scanziani, M. (2011). How Inhibition Shapes Cortical Activity. In *Neuron* (Vol. 72, Issue 2, pp. 231–243). https://doi.org/10.1016/j.neuron.2011.09.027

Itano, N., & Kimata, K. (2002). Mammalian Hyaluronan Synthases. In *IUBMB Life (International Union of Biochemistry and Molecular Biology: Life)* (Vol. 54, Issue 4, pp. 195–199). https://doi.org/10.1080/15216540214929

Ito-Ishida, A., Ure, K., Chen, H., Swann, J. W., & Zoghbi, H. Y. (2015). Loss of MeCP2 in Parvalbumin-and Somatostatin-Expressing Neurons in Mice Leads to Distinct Rett Syndrome-like Phenotypes. *Neuron*, *88*(4), 651–658.

Jumper, J., Evans, R., Pritzel, A., Green, T., Figurnov, M., Ronneberger, O., Tunyasuvunakool, K., Bates, R., Žídek, A., Potapenko, A., Bridgland, A., Meyer, C., Kohl, S. A. A., Ballard, A. J., Cowie, A., Romera-Paredes, B., Nikolov, S., Jain, R., Adler, J., … Hassabis, D. (2021). Highly accurate protein structure prediction with AlphaFold. *Nature*, *596*(7873), 583–589.

Kaar, S. J., Angelescu, I., Marques, T. R., & Howes, O. D. (2019). Pre-frontal parvalbumin interneurons in schizophrenia: a meta-analysis of post-mortem studies. *Journal of Neural Transmission* , *126*(12), 1637–1651.

Kadam, S. D., Sullivan, B. J., Goyal, A., Blue, M. E., & Smith-Hicks, C. (2019). Rett Syndrome and CDKL5 Deficiency Disorder: From Bench to Clinic. *International Journal of Molecular Sciences*, *20*(20). https://doi.org/10.3390/ijms20205098

Kann, O., Papageorgiou, I. E., & Draguhn, A. (2014). Highly energized inhibitory interneurons are a central element for information processing in cortical networks. *Journal of Cerebral Blood Flow and Metabolism: Official Journal of the International Society of Cerebral Blood Flow and Metabolism*, *34*(8), 1270–1282.

Kawaguchi, Y., Katsumaru, H., Kosaka, T., Heizmann, C. W., & Hama, K. (1987). Fast spiking cells in rat hippocampus (CA1 region) contain the calcium-binding protein parvalbumin. *Brain Research*, *416*(2), 369–374.

Kawaguchi, Y., & Kubota, Y. (1993). Correlation of physiological subgroupings of nonpyramidal cells with parvalbumin- and calbindinD28k-immunoreactive neurons in layer V of rat frontal cortex. In *Journal of Neurophysiology* (Vol. 70, Issue 1, pp. 387–396). https://doi.org/10.1152/jn.1993.70.1.387

Keaveney, M. K., Tseng, H.-A., Ta, T. L., Gritton, H. J., Man, H.-Y., & Han, X. (2018). A MicroRNA-Based Gene-Targeting Tool for Virally Labeling Interneurons in the Rodent Cortex. *Cell Reports*, *24*(2), 294–303.

Khoo, G. H., Lin, Y.-T., Tsai, T.-C., & Hsu, K.-S. (2019). Perineuronal Nets Restrict the Induction of Long-Term Depression in the Mouse Hippocampal CA1 Region. *Molecular Neurobiology*, *56*(9), 6436–6450.

Khoshkhoo, S., Vogt, D., & Sohal, V. S. (2017). Dynamic, Cell-Type-Specific Roles for GABAergic Interneurons in a Mouse Model of Optogenetically Inducible Seizures. In *Neuron* (Vol. 93, Issue 2, pp. 291–298). https://doi.org/10.1016/j.neuron.2016.11.043

Klausberger, T., & Somogyi, P. (2008). Neuronal diversity and temporal dynamics: the unity of hippocampal circuit operations. *Science*, *321*(5885), 53–57.

Kohnke, S., Buller, S., Nuzzaci, D., Ridley, K., Lam, B., Pivonkova, H., Bentsen, M. A., Alonge, K. M., Zhao, C., Tadross, J., Holmqvist, S., Shimizu, T., Hathaway, H., Li, H., Macklin, W., Schwartz, M. W., Richardson, W. D., Yeo, G. S. H., Franklin, R. J. M., … Blouet, C. (2021). Nutritional regulation of oligodendrocyte differentiation regulates perineuronal net remodeling in the median eminence. *Cell Reports*, *36*(2), 109362.

Kosaka, T., & Heizmann, C. W. (1989). Selective staining of a population of parvalbumin-containing GABAergic neurons in the rat cerebral cortex by lectins with specific affinity for terminal N-acetylgalactosamine. *Brain Research*, *483*(1), 158–163.

Krishnan, K., Wang, B.-S., Lu, J., Wang, L., Maffei, A., Cang, J., & Huang, Z. J. (2015). MeCP2 regulates the timing of critical period plasticity that shapes functional connectivity in primary visual cortex. *Proceedings of the National Academy of Sciences of the United States of America*, *112*(34), E4782–E4791.

Kügler, S., Kilic, E., & Bähr, M. (2003). Human synapsin 1 gene promoter confers highly neuron-specific long-term transgene expression from an adenoviral vector in the adult rat brain depending on the transduced area. *Gene Therapy*, *10*(4), 337–347.

Kuhlman, S. J., Tring, E., & Trachtenberg, J. T. (2011). Fast-spiking interneurons have an initial orientation bias that is lost with vision. *Nature Neuroscience*, *14*(9), 1121–1123.

Kwok, J. C. F., Carulli, D., & Fawcett, J. W. (2010). In vitro modeling of perineuronal nets: hyaluronan synthase and link protein are necessary for their formation and integrity. *Journal of Neurochemistry*, *114*(5), 1447–1459.

Kwok, J. C. F., Dick, G., Wang, D., & Fawcett, J. W. (2011). Extracellular matrix and perineuronal nets in CNS repair. *Developmental Neurobiology*, *71*(11), 1073–1089.

Lalo, U., Koh, W., Lee, C. J., & Pankratov, Y. (2021). The tripartite glutamatergic synapse. *Neuropharmacology*, *199*, 108758.

Lander, C., Kind, P., Maleski, M., & Hockfield, S. (1997). A family of activity-dependent neuronal cell-surface chondroitin sulfate proteoglycans in cat visual cortex. *The Journal of Neuroscience: The Official Journal of the Society for Neuroscience*, *17*(6), 1928–1939.

Lehmann, K., & Löwel, S. (2008). Age-dependent ocular dominance plasticity in adult mice. *PloS One*, *3*(9), e3120.

Lensjø, K. K., Christensen, A. C., Tennøe, S., Fyhn, M., & Hafting, T. (2017). Differential Expression and Cell-Type Specificity of Perineuronal Nets in Hippocampus, Medial Entorhinal Cortex, and Visual Cortex Examined in the Rat and Mouse. In *eneuro* (Vol. 4, Issue 3, pp. ENEURO.0379–16.2017). https://doi.org/10.1523/eneuro.0379-16.2017

Lensjø, K. K., Lepperød, M. E., Dick, G., Hafting, T., & Fyhn, M. (2017). Removal of Perineuronal Nets Unlocks Juvenile Plasticity Through Network Mechanisms of Decreased Inhibition and Increased Gamma Activity. *The Journal of Neuroscience: The Official Journal of the Society for Neuroscience*, *37*(5), 1269–1283.

Lesnikova, A., Casarotto, P. C., Fred, S. M., Voipio, M., Winkel, F., Steinzeig, A., Antila, H., Umemori, J., Biojone, C., & Castrén, E. (n.d.). *Chondroitinase and antidepressants promote plasticity by releasing TRKB from dephosphorylating control of PTPσ in parvalbumin neurons*. https://doi.org/10.1101/2020.08.13.249615

Lin, R., Rosahl, T. W., Whiting, P. J., Fawcett, J. W., & Kwok, J. C. F. (2011). 6-Sulphated chondroitins have a positive influence on axonal regeneration. *PloS One*, *6*(7), e21499.

Liu, Y., Ouyang, P., Zheng, Y., Mi, L., Zhao, J., Ning, Y., & Guo, W. (2021). A Selective Review of the Excitatory-Inhibitory Imbalance in Schizophrenia: Underlying Biology, Genetics, Microcircuits, and Symptoms. *Frontiers in Cell and Developmental Biology*, *9*, 664535.

Liuzzi, G. M., Santacroce, M. P., Peumans, W. J., Van Damme, E. J., Dubois, B., Opdenakker, G., & Riccio, P. (1999). Regulation of gelatinases in microglia and astrocyte cell cultures by plant lectins. *Glia*, *27*(1), 53–61.

Li, Y., Li, Z.-X., Jin, T., Wang, Z.-Y., & Zhao, P. (2017). Tau Pathology Promotes the Reorganization of the Extracellular Matrix and Inhibits the Formation of Perineuronal Nets by Regulating the Expression and the Distribution of Hyaluronic Acid Synthases. *Journal of Alzheimer's Disease: JAD*, *57*(2), 395–409.

Logsdon, A. F., Francis, K. L., Richardson, N. E., Hu, S. J., Faber, C. L., Phan, B. A., Nguyen, V., Setthavongsack, N., Banks, W. A., Woltjer, R. L., Keene, C. D., Latimer, C. S., Schwartz, M. W., Scarlett, J. M., & Alonge, K. M. (2022). Decoding perineuronal net glycan sulfation patterns in the Alzheimer's disease brain. *Alzheimer's & Dementia: The Journal of the Alzheimer's Association*, *18*(5), 942–954.

Long, K. R., & Huttner, W. B. (2019). How the extracellular matrix shapes neural development. *Open Biology*, *9*(1), 180216.

Lovelace, J. W., Wen, T. H., Reinhard, S., Hsu, M. S., Sidhu, H., Ethell, I. M., Binder, D. K., & Razak, K. A. (2016). Matrix metalloproteinase-9 deletion rescues auditory evoked potential habituation deficit in a mouse model of Fragile X Syndrome. In *Neurobiology of Disease* (Vol. 89, pp. 126–135). https://doi.org/10.1016/j.nbd.2016.02.002

Lundell, A., Olin, A. I., Mörgelin, M., al-Karadaghi, S., Aspberg, A., & Logan, D. T. (2004). Structural Basis for Interactions between Tenascins and Lectican C-Type Lectin Domains. In *Structure* (Vol. 12, Issue 8, pp. 1495–1506). https://doi.org/10.1016/j.str.2004.05.021

Lupori, L., Totaro, V., Cornuti, S., Ciampi, L., Carrara, F., Grilli, E., Viglione, A., Tozzi, F., Putignano, E., Mazziotti, R., Amato, G., Gennaro, C., Tognini, P., & Pizzorusso, T. (2023). A comprehensive atlas of perineuronal net distribution and colocalization with parvalbumin in the adult mouse brain. *Cell Reports*, *42*(7), 112788.

Markram, H., Toledo-Rodriguez, M., Wang, Y., Gupta, A., Silberberg, G., & Wu, C. (2004). Interneurons of the neocortical inhibitory system. In *Nature Reviews Neuroscience* (Vol.

5, Issue 10, pp. 793–807). https://doi.org/10.1038/nrn1519

Matthews, R. T., Kelly, G. M., Zerillo, C. A., Gray, G., Tiemeyer, M., & Hockfield, S. (2002). Aggrecan Glycoforms Contribute to the Molecular Heterogeneity of Perineuronal Nets. In *The Journal of Neuroscience* (Vol. 22, Issue 17, pp. 7536–7547). https://doi.org/10.1523/jneurosci.22-17-07536.2002

Mauney, S. A., Athanas, K. M., Pantazopoulos, H., Shaskan, N., Passeri, E., Berretta, S., & Woo, T.-U. W. (2013). Developmental pattern of perineuronal nets in the human prefrontal cortex and their deficit in schizophrenia. *Biological Psychiatry*, *74*(6), 427–435.

Ma, W.-P., Liu, B.-H., Li, Y.-T., Huang, Z. J., Zhang, L. I., & Tao, H. W. (2010). Visual representations by cortical somatostatin inhibitory neurons--selective but with weak and delayed responses. *The Journal of Neuroscience: The Official Journal of the Society for Neuroscience*, *30*(43), 14371–14379.

Ma, W., Tavakoli, T., Derby, E., Serebryakova, Y., Rao, M. S., & Mattson, M. P. (2008). Cell-extracellular matrix interactions regulate neural differentiation of human embryonic stem cells. *BMC Developmental Biology*, *8*, 90.

Mazziotti, R., Lupori, L., Sagona, G., Gennaro, M., Della Sala, G., Putignano, E., & Pizzorusso, T. (2017). Searching for biomarkers of CDKL5 disorder: early-onset visual impairment in CDKL5 mutant mice. *Human Molecular Genetics*, *26*(12), 2290–2298.

McRae, P. A., Rocco, M. M., Kelly, G., Brumberg, J. C., & Matthews, R. T. (2007). Sensory deprivation alters aggrecan and perineuronal net expression in the mouse barrel cortex. *The Journal of Neuroscience: The Official Journal of the Society for Neuroscience*, *27*(20), 5405–5413.

Mich, J. K., Graybuck, L. T., Hess, E. E., Mahoney, J. T., Kojima, Y., Ding, Y., Somasundaram, S., Miller, J. A., Kalmbach, B. E., Radaelli, C., Gore, B. B., Weed, N., Omstead, V., Bishaw, Y., Shapovalova, N. V., Martinez, R. A., Fong, O., Yao, S., Mortrud, M., … Levi, B. P. (2021). Functional enhancer elements drive subclass-selective expression from mouse to primate neocortex. *Cell Reports*, *34*(13),

108754.

Mirzadeh, Z., Alonge, K. M., Cabrales, E., Herranz-Pérez, V., Scarlett, J. M., Brown, J. M., Hassouna, R., Matsen, M. E., Nguyen, H. T., Garcia-Verdugo, J. M., Zeltser, L. M., & Schwartz, M. W. (2019). Perineuronal Net Formation during the Critical Period for Neuronal Maturation in the Hypothalamic Arcuate Nucleus. *Nature Metabolism*, *1*(2), 212–221.

Miyata, S., Komatsu, Y., Yoshimura, Y., Taya, C., & Kitagawa, H. (2012). Persistent cortical plasticity by upregulation of chondroitin 6-sulfation. *Nature Neuroscience*, *15*(3), 414–422, S1–S2.

Miyata, S., Nadanaka, S., Igarashi, M., & Kitagawa, H. (2018). Structural Variation of Chondroitin Sulfate Chains Contributes to the Molecular Heterogeneity of Perineuronal Nets. *Frontiers in Integrative Neuroscience*, *12*, 3.

Miyata, S., Nishimura, Y., & Nakashima, T. (2007). Perineuronal nets protect against amyloid beta-protein neurotoxicity in cultured cortical neurons. *Brain Research*, *1150*, 200–206.

Moon, L. D., Asher, R. A., Rhodes, K. E., & Fawcett, J. W. (2001). Regeneration of CNS axons back to their target following treatment of adult rat brain with chondroitinase ABC. *Nature Neuroscience*, *4*(5), 465–466.

Morawski, M., Brückner, G., Jäger, C., Seeger, G., & Arendt, T. (2010). Neurons associated with aggrecan-based perineuronal nets are protected against tau pathology in subcortical regions in Alzheimer's disease. *Neuroscience*, *169*(3), 1347–1363.

Morawski, M., Dityatev, A., Hartlage-Rübsamen, M., Blosa, M., Holzer, M., Flach, K., Pavlica, S., Dityateva, G., Grosche, J., Brückner, G., & Schachner, M. (2014). Tenascin-R promotes assembly of the extracellular matrix of perineuronal nets via clustering of aggrecan. *Philosophical Transactions of the Royal Society of London. Series B, Biological Sciences*, *369*(1654), 20140046.

Morawski, M., Reinert, T., Meyer-Klaucke, W., Wagner, F. E., Tröger, W., Reinert, A., Jäger, C., Brückner, G., & Arendt, T. (2015). Ion exchanger in the brain: Quantitative analysis of perineuronally fixed anionic binding sites suggests diffusion barriers with ion sorting

properties. *Scientific Reports*, *5*, 16471.

Morgenstern, D. A., Asher, R. A., & Fawcett, J. W. (2002). Chondroitin sulphate proteoglycans in the CNS injury response. *Progress in Brain Research*, *137*, 313–332.

Morikawa, S., Ikegaya, Y., Narita, M., & Tamura, H. (2017). Activation of perineuronal net-expressing excitatory neurons during associative memory encoding and retrieval. *Scientific Reports*, *7*, 46024.

Moser, E. I., Kropff, E., & Moser, M.-B. (2008). Place cells, grid cells, and the brain's spatial representation system. *Annual Review of Neuroscience*, *31*, 69–89.

Moser, E. I., Roudi, Y., Witter, M. P., Kentros, C., Bonhoeffer, T., & Moser, M.-B. (2014). Grid cells and cortical representation. *Nature Reviews. Neuroscience*, *15*(7), 466–481.

Moser, M.-B., Rowland, D. C., & Moser, E. I. (2015). Place cells, grid cells, and memory. *Cold Spring Harbor Perspectives in Biology*, *7*(2), a021808.

Nadanaka, S., Miyata, S., Yaqiang, B., Tamura, J.-I., Habuchi, O., & Kitagawa, H. (2020). Reconsideration of the Semaphorin-3A Binding Motif Found in Chondroitin Sulfate Using -Knockout Mice. *Biomolecules*, *10*(11). https://doi.org/10.3390/biom10111499

Niell, C. M., & Scanziani, M. (2021). How Cortical Circuits Implement Cortical Computations: Mouse Visual Cortex as a Model. *Annual Review of Neuroscience*, *44*, 517–546.

Niell, C. M., & Stryker, M. P. (2008). Highly selective receptive fields in mouse visual cortex. *The Journal of Neuroscience: The Official Journal of the Society for Neuroscience*, *28*(30), 7520–7536.

Nieuwenhuis, B., Haenzi, B., Hilton, S., Carnicer-Lombarte, A., Hobo, B., Verhaagen, J., & Fawcett, J. W. (2021). Optimization of adeno-associated viral vector-mediated transduction of the corticospinal tract: comparison of four promoters. *Gene Therapy*, *28*(1-2), 56–74.

Okhotin, V. E., & Kalinichenko, S. G. (2002). The histophysiology of neocortical basket cells. *Neuroscience and Behavioral Physiology*, *32*(5), 455–470.

Oohashi, T., Edamatsu, M., Bekku, Y., & Carulli, D. (2015). The hyaluronan and proteoglycan link proteins: Organizers of the brain extracellular matrix and key molecules for neuronal

function and plasticity. *Experimental Neurology*, *274*(Pt B), 134–144.

Oohashi, T., Hirakawa, S., Bekku, Y., Rauch, U., Zimmermann, D. R., Su, W.-D., Ohtsuka, A., Murakami, T., & Ninomiya, Y. (2002). Bral1, a brain-specific link protein, colocalizing with the versican V2 isoform at the nodes of Ranvier in developing and adult mouse central nervous systems. *Molecular and Cellular Neurosciences*, *19*(1), 43–57.

Pala, A., & Petersen, C. C. H. (2015). In vivo measurement of cell-type-specific synaptic connectivity and synaptic transmission in layer 2/3 mouse barrel cortex. *Neuron*, *85*(1), 68–75.

Pantazopoulos, H., Gisabella, B., Rexrode, L., Benefield, D., Yildiz, E., Seltzer, P., Valeri, J., Chelini, G., Reich, A., Ardelt, M., & Berretta, S. (2020). Circadian Rhythms of Perineuronal Net Composition. *eNeuro*, *7*(4). https://doi.org/10.1523/ENEURO.0034-19.2020

Pantazopoulos, H., Woo, T.-U. W., Lim, M. P., Lange, N., & Berretta, S. (2010). Extracellular matrix-glial abnormalities in the amygdala and entorhinal cortex of subjects diagnosed with schizophrenia. *Archives of General Psychiatry*, *67*(2), 155–166.

Patrizi, A., Awad, P. N., Chattopadhyaya, B., Li, C., Di Cristo, G., & Fagiolini, M. (2020). Accelerated Hyper-Maturation of Parvalbumin Circuits in the Absence of MeCP2. *Cerebral Cortex* , *30*(1), 256–268.

Petilla Interneuron Nomenclature Group, Ascoli, G. A., Alonso-Nanclares, L., Anderson, S. A., Barrionuevo, G., Benavides-Piccione, R., Burkhalter, A., Buzsáki, G., Cauli, B., Defelipe, J., Fairén, A., Feldmeyer, D., Fishell, G., Fregnac, Y., Freund, T. F., Gardner, D., Gardner, E. P., Goldberg, J. H., Helmstaedter, M., … Yuste, R. (2008). Petilla terminology: nomenclature of features of GABAergic interneurons of the cerebral cortex. *Nature Reviews. Neuroscience*, *9*(7), 557–568.

Pizzo, R., Gurgone, A., Castroflorio, E., Amendola, E., Gross, C., Sassoè-Pognetto, M., & Giustetto, M. (2016). Lack of Cdkl5 Disrupts the Organization of Excitatory and Inhibitory Synapses and Parvalbumin Interneurons in the Primary Visual Cortex. *Frontiers in Cellular Neuroscience*, *10*, 261.

Pizzorusso, T., Medini, P., Berardi, N., Chierzi, S., Fawcett, J. W., & Maffei, L. (2002). Reactivation of ocular dominance plasticity in the adult visual cortex. *Science*, *298*(5596), 1248–1251.

Pouille, F., & Scanziani, M. (2001). Enforcement of temporal fidelity in pyramidal cells by somatic feed-forward inhibition. *Science*, *293*(5532), 1159–1163.

Protic, D. D., Aishworiya, R., Salcedo-Arellano, M. J., Tang, S. J., Milisavljevic, J., Mitrovic, F., Hagerman, R. J., & Budimirovic, D. B. (2022). Fragile X Syndrome: From Molecular Aspect to Clinical Treatment. *International Journal of Molecular Sciences*, *23*(4). https://doi.org/10.3390/ijms23041935

Qin, J. Y., Zhang, L., Clift, K. L., Hulur, I., Xiang, A. P., Ren, B.-Z., & Lahn, B. T. (2010). Systematic comparison of constitutive promoters and the doxycycline-inducible promoter. *PloS One*, *5*(5), e10611.

Ramsaran, A. I., Wang, Y., Golbabaei, A., Aleshin, S., de Snoo, M. L., Yeung, B.-R. A., Rashid, A. J., Awasthi, A., Lau, J., Tran, L. M., Ko, S. Y., Abegg, A., Duan, L. C., McKenzie, C., Gallucci, J., Ahmed, M., Kaushik, R., Dityatev, A., Josselyn, S. A., & Frankland, P. W. (2023). A shift in the mechanisms controlling hippocampal engram formation during brain maturation. *Science*, *380*(6644), 543–551.

Ranson, A., Cheetham, C. E. J., Fox, K., & Sengpiel, F. (2012). Homeostatic plasticity mechanisms are required for juvenile, but not adult, ocular dominance plasticity. In *Proceedings of the National Academy of Sciences* (Vol. 109, Issue 4, pp. 1311–1316). https://doi.org/10.1073/pnas.1112204109

Reichelt, A. C., Lemieux, C. A., Princz-Lebel, O., Singh, A., Bussey, T. J., & Saksida, L. M. (2021). Age-dependent and region-specific alteration of parvalbumin neurons, perineuronal nets and microglia in the mouse prefrontal cortex and hippocampus following obesogenic diet consumption. *Scientific Reports*, *11*(1), 5593.

Riga, D., Kramvis, I., Koskinen, M. K., van Bokhoven, P., van der Harst, J. E., Heistek, T. S., Jaap Timmerman, A., van Nierop, P., van der Schors, R. C., Pieneman, A. W., de Weger, A., van Mourik, Y., Schoffelmeer, A. N. M., Mansvelder, H. D., Meredith, R. M.,

Hoogendijk, W. J. G., Smit, A. B., & Spijker, S. (2017). Hippocampal extracellular matrix alterations contribute to cognitive impairment associated with a chronic depressive-like state in rats. *Science Translational Medicine*, *9*(421). https://doi.org/10.1126/scitranslmed.aai8753

Righes Marafiga, J., Vendramin Pasquetti, M., & Calcagnotto, M. E. (2021). GABAergic interneurons in epilepsy: More than a simple change in inhibition. *Epilepsy & Behavior: E&B*, *121*(Pt B), 106935.

Rolls, A., Shechter, R., & Schwartz, M. (2009). The bright side of the glial scar in CNS repair. *Nature Reviews. Neuroscience*, *10*(3), 235–241.

Romberg, C., Yang, S., Melani, R., Andrews, M. R., Horner, A. E., Spillantini, M. G., Bussey, T. J., Fawcett, J. W., Pizzorusso, T., & Saksida, L. M. (2013). Depletion of perineuronal nets enhances recognition memory and long-term depression in the perirhinal cortex. *The Journal of Neuroscience: The Official Journal of the Society for Neuroscience*, *33*(16), 7057–7065.

Rose, T., Jaepel, J., Hübener, M., & Bonhoeffer, T. (2016). Cell-specific restoration of stimulus preference after monocular deprivation in the visual cortex. *Science*, *352*(6291), 1319–1322.

Rowlands, D., Lensjø, K. K., Dinh, T., Yang, S., Andrews, M. R., Hafting, T., Fyhn, M., Fawcett, J. W., & Dick, G. (2018). Aggrecan Directs Extracellular Matrix-Mediated Neuronal Plasticity. *The Journal of Neuroscience: The Official Journal of the Society for Neuroscience*, *38*(47), 10102–10113.

Rubenstein, J. L. R., & Merzenich, M. M. (2003). Model of autism: increased ratio of excitation/inhibition in key neural systems. In *Genes, Brain and Behavior* (Vol. 2, Issue 5, pp. 255–267). https://doi.org/10.1034/j.1601-183x.2003.00037.x

Rudy, B., & McBain, C. J. (2001). Kv3 channels: voltage-gated K+ channels designed for high-frequency repetitive firing. *Trends in Neurosciences*, *24*(9), 517–526.

Sabbagh, U., Monavarfeshani, A., Su, K., Zabet-Moghadam, M., Cole, J., Carnival, E., Su, J., Mirzaei, M., Gupta, V., Salekdeh, G. H., & Fox, M. A. (2018). Distribution and

development of molecularly distinct perineuronal nets in visual thalamus. *Journal of Neurochemistry*, *147*(5), 626–646.

Sale, A., Maya Vetencourt, J. F., Medini, P., Cenni, M. C., Baroncelli, L., De Pasquale, R., & Maffei, L. (2007). Environmental enrichment in adulthood promotes amblyopia recovery through a reduction of intracortical inhibition. *Nature Neuroscience*, *10*(6), 679–681.

Sato, M., & Stryker, M. P. (2008). Distinctive features of adult ocular dominance plasticity. *The Journal of Neuroscience: The Official Journal of the Society for Neuroscience*, *28*(41), 10278–10286.

Scarlett, J. M., Hu, S. J., & Alonge, K. M. (2022). The “Loss” of Perineuronal Nets in Alzheimer’s Disease: Missing or Hiding in Plain Sight? In *Frontiers in Integrative Neuroscience* (Vol. 16). https://doi.org/10.3389/fnint.2022.896400

Shen, H. H. (2018). Core Concept: Perineuronal nets gain prominence for their role in learning, memory, and plasticity. *Proceedings of the National Academy of Sciences of the United States of America*, *115*(40), 9813–9815.

Shen, Y., Tenney, A. P., Busch, S. A., Horn, K. P., Cuascut, F. X., Liu, K., He, Z., Silver, J., & Flanagan, J. G. (2009). PTPsigma is a receptor for chondroitin sulfate proteoglycan, an inhibitor of neural regeneration. *Science*, *326*(5952), 592–596.

Shi, W., Wei, X., Wang, X., Du, S., Liu, W., Song, J., & Wang, Y. (2019). Perineuronal nets protect long-term memory by limiting activity-dependent inhibition from parvalbumin interneurons. *Proceedings of the National Academy of Sciences of the United States of America*, *116*(52), 27063–27073.

Sigal, Y. M., Bae, H., Bogart, L. J., Hensch, T. K., & Zhuang, X. (2019). Structural maturation of cortical perineuronal nets and their perforating synapses revealed by superresolution imaging. *Proceedings of the National Academy of Sciences of the United States of America*, *116*(14), 7071–7076.

Sirko, S., von Holst, A., Wizenmann, A., Götz, M., & Faissner, A. (2007). Chondroitin sulfate glycosaminoglycans control proliferation, radial glia cell differentiation and neurogenesis in neural stem/progenitor cells. *Development* , *134*(15), 2727–2738.

Sohal, V. S., & Rubenstein, J. L. R. (2019). Excitation-inhibition balance as a framework for investigating mechanisms in neuropsychiatric disorders. *Molecular Psychiatry*, *24*(9), 1248–1257.

Sohal, V. S., Zhang, F., Yizhar, O., & Deisseroth, K. (2009). Parvalbumin neurons and gamma rhythms enhance cortical circuit performance. *Nature*, *459*(7247), 698–702.

Sommeijer, J.-P., & Levelt, C. N. (2012). Synaptotagmin-2 is a reliable marker for parvalbumin positive inhibitory boutons in the mouse visual cortex. *PloS One*, *7*(4), e35323.

Spatazza, J., Lee, H. H. C., Di Nardo, A. A., Tibaldi, L., Joliot, A., Hensch, T. K., & Prochiantz, A. (2013). Choroid-plexus-derived Otx2 homeoprotein constrains adult cortical plasticity. *Cell Reports*, *3*(6), 1815–1823.

Spicer, A. P., Joo, A., & Bowling, R. A. (2003). A Hyaluronan Binding Link Protein Gene Family Whose Members Are Physically Linked Adjacent to Chrondroitin Sulfate Proteoglycan Core Protein Genes. In *Journal of Biological Chemistry* (Vol. 278, Issue 23, pp. 21083–21091). https://doi.org/10.1074/jbc.m213100200

Spicer, A. P., & Tien, J. Y. L. (2004). Hyaluronan and morphogenesis. *Birth Defects Research. Part C, Embryo Today: Reviews*, *72*(1), 89–108.

Stenzel, D., Wilsch-Bräuninger, M., Wong, F. K., Heuer, H., & Huttner, W. B. (2014). Integrin αvβ3 and thyroid hormones promote expansion of progenitors in embryonic neocortex. *Development* , *141*(4), 795–806.

Sugiyama, S., Di Nardo, A. A., Aizawa, S., Matsuo, I., Volovitch, M., Prochiantz, A., & Hensch, T. K. (2008). Experience-dependent transfer of Otx2 homeoprotein into the visual cortex activates postnatal plasticity. *Cell*, *134*(3), 508–520.

Suttkus, A., Rohn, S., Jäger, C., Arendt, T., & Morawski, M. (2012). Neuroprotection against iron-induced cell death by perineuronal nets - an in vivo analysis of oxidative stress. *American Journal of Neurodegenerative Disease*, *1*(2), 122–129.

Suttkus, A., Rohn, S., Weigel, S., Glöckner, P., Arendt, T., & Morawski, M. (2014). Aggrecan, link protein and tenascin-R are essential components of the perineuronal net to protect

neurons against iron-induced oxidative stress. *Cell Death & Disease*, *5*, e1119.

Syková, E., & Nicholson, C. (2008). Diffusion in brain extracellular space. *Physiological Reviews*, *88*(4), 1277–1340.

Takeuchi, T., Duszkiewicz, A. J., & Morris, R. G. M. (2014). The synaptic plasticity and memory hypothesis: encoding, storage and persistence. *Philosophical Transactions of the Royal Society of London. Series B, Biological Sciences*, *369*(1633), 20130288.

Tansley, S., Gu, N., Guzmán, A. U., Cai, W., Wong, C., Lister, K. C., Muñoz-Pino, E., Yousefpour, N., Roome, R. B., Heal, J., Wu, N., Castonguay, A., Lean, G., Muir, E. M., Kania, A., Prager-Khoutorsky, M., Zhang, J., Gkogkas, C. G., Fawcett, J. W., … Khoutorsky, A. (2022). Microglia-mediated degradation of perineuronal nets promotes pain. *Science*, *377*(6601), 80–86.

Tasic, B., Yao, Z., Graybuck, L. T., Smith, K. A., Nguyen, T. N., Bertagnolli, D., Goldy, J., Garren, E., Economo, M. N., Viswanathan, S., Penn, O., Bakken, T., Menon, V., Miller, J., Fong, O., Hirokawa, K. E., Lathia, K., Rimorin, C., Tieu, M., … Zeng, H. (2018). Shared and distinct transcriptomic cell types across neocortical areas. *Nature*, *563*(7729), 72–78.

Tewari, B. P., Chaunsali, L., Campbell, S. L., Patel, D. C., Goode, A. E., & Sontheimer, H. (2018). Perineuronal nets decrease membrane capacitance of peritumoral fast spiking interneurons in a model of epilepsy. *Nature Communications*, *9*(1), 4724.

Thompson, E. H., Lensjø, K. K., Wigestrand, M. B., Malthe-Sørenssen, A., Hafting, T., & Fyhn, M. (2018). Removal of perineuronal nets disrupts recall of a remote fear memory. *Proceedings of the National Academy of Sciences of the United States of America*, *115*(3), 607–612.

Tien, J. Y. L., & Spicer, A. P. (2005). Three vertebrate hyaluronan synthases are expressed during mouse development in distinct spatial and temporal patterns. *Developmental Dynamics: An Official Publication of the American Association of Anatomists*, *233*(1), 130–141.

Tsien, R. Y. (2013). Very long-term memories may be stored in the pattern of holes in the

perineuronal net. *Proceedings of the National Academy of Sciences of the United States of America*, *110*(30), 12456–12461.

Ueno, H., Fujii, K., Suemitsu, S., Murakami, S., Kitamura, N., Wani, K., Aoki, S., Okamoto, M., Ishihara, T., & Takao, K. (2018). Expression of aggrecan components in perineuronal nets in the mouse cerebral cortex. *IBRO Reports*, *4*, 22–37.

Ueno, H., Suemitsu, S., Okamoto, M., Matsumoto, Y., & Ishihara, T. (2017). Sensory experience-dependent formation of perineuronal nets and expression of Cat-315 immunoreactive components in the mouse somatosensory cortex. *Neuroscience*, *355*, 161–174.

Ueno, H., Takao, K., Suemitsu, S., Murakami, S., Kitamura, N., Wani, K., Okamoto, M., Aoki, S., & Ishihara, T. (2018). Age-dependent and region-specific alteration of parvalbumin neurons and perineuronal nets in the mouse cerebral cortex. *Neurochemistry International*, *112*, 59–70.

Villard, L. (2013). Faculty Opinions recommendation of The CDKL5 disorder is an independent clinical entity associated with early-onset encephalopathy. In *Faculty Opinions – Post-Publication Peer Review of the Biomedical Literature*. https://doi.org/10.3410/f.717979602.793471373

Von Frijtag, J. C., Reijmers, L. G., Van der Harst, J. E., Leus, I. E., Van den Bos, R., & Spruijt, B. M. (2000). Defeat followed by individual housing results in long-term impaired reward- and cognition-related behaviours in rats. *Behavioural Brain Research*, *117*(1-2), 137–146.

Vo, T., Carulli, D., Ehlert, E. M. E., Kwok, J. C. F., Dick, G., Mecollari, V., Moloney, E. B., Neufeld, G., de Winter, F., Fawcett, J. W., & Verhaagen, J. (2013). The chemorepulsive axon guidance protein semaphorin3A is a constituent of perineuronal nets in the adult rodent brain. *Molecular and Cellular Neurosciences*, *56*, 186–200.

Wang, H., Katagiri, Y., McCann, T. E., Unsworth, E., Goldsmith, P., Yu, Z.-X., Tan, F., Santiago, L., Mills, E. M., Wang, Y., Symes, A. J., & Geller, H. M. (2008). Chondroitin-4-sulfation negatively regulates axonal guidance and growth. *Journal of Cell*

Science, *121*(Pt 18), 3083–3091.

Wang, Y., Zhang, P., & Wyskiel, D. R. (2016). Chandelier Cells in Functional and Dysfunctional Neural Circuits. *Frontiers in Neural Circuits*, *10*, 33.

Wanisch, K., Kovac, S., & Schorge, S. (2013). Tackling obstacles for gene therapy targeting neurons: disrupting perineural nets with hyaluronidase improves transduction. *PloS One*, *8*(1), e53269.

Weber, P., Bartsch, U., Rasband, M. N., Czaniera, R., Lang, Y., Bluethmann, H., Margolis, R. U., Levinson, S. R., Shrager, P., Montag, D., & Schachner, M. (1999). Mice deficient for tenascin-R display alterations of the extracellular matrix and decreased axonal conduction velocities in the CNS. *The Journal of Neuroscience: The Official Journal of the Society for Neuroscience*, *19*(11), 4245–4262.

Wen, T. H., Afroz, S., Reinhard, S. M., Palacios, A. R., Tapia, K., Binder, D. K., Razak, K. A., & Ethell, I. M. (2018). Genetic Reduction of Matrix Metalloproteinase-9 Promotes Formation of Perineuronal Nets Around Parvalbumin-Expressing Interneurons and Normalizes Auditory Cortex Responses in Developing Fmr1 Knock-Out Mice. *Cerebral Cortex* , *28*(11), 3951–3964.

Wen, T. H., Binder, D. K., Ethell, I. M., & Razak, K. A. (2018). The Perineuronal “Safety” Net? Perineuronal Net Abnormalities in Neurological Disorders. *Frontiers in Molecular Neuroscience*, *11*, 270.

Wiesel, T. N., & Hubel, D. H. (1963). EFFECTS OF VISUAL DEPRIVATION ON MORPHOLOGY AND PHYSIOLOGY OF CELLS IN THE CAT’S LATERAL GENICULATE BODY. In *Journal of Neurophysiology* (Vol. 26, Issue 6, pp. 978–993). https://doi.org/10.1152/jn.1963.26.6.978

Wilczynski, G. M., Konopacki, F. A., Wilczek, E., Lasiecka, Z., Gorlewicz, A., Michaluk, P., Wawrzyniak, M., Malinowska, M., Okulski, P., Kolodziej, L. R., Konopka, W., Duniec, K., Mioduszewska, B., Nikolaev, E., Walczak, A., Owczarek, D., Gorecki, D. C., Zuschratter, W., Ottersen, O. P., & Kaczmarek, L. (2008). Important role of matrix metalloproteinase 9 in epileptogenesis. In *Journal of Cell Biology* (Vol. 180, Issue 5, pp. 1021–1035).

https://doi.org/10.1083/jcb.200708213

Wingert, J. C., & Sorg, B. A. (2021). Impact of Perineuronal Nets on Electrophysiology of Parvalbumin Interneurons, Principal Neurons, and Brain Oscillations: A Review. *Frontiers in Synaptic Neuroscience*, *13*, 673210.

Woo, T.-U. W., Spencer, K., & McCarley, R. W. (2010). Gamma Oscillation Deficits and the Onset and Early Progression of Schizophrenia. In *Harvard Review of Psychiatry* (Vol. 18, Issue 3, pp. 173–189). https://doi.org/10.3109/10673221003747609

Yasuhara, O., Akiyama, H., McGeer, E. G., & McGeer, P. L. (1994). Immunohistochemical localization of hyaluronic acid in rat and human brain. *Brain Research*, *635*(1-2), 269–282.

Yazaki-Sugiyama, Y., Kang, S., Câteau, H., Fukai, T., & Hensch, T. K. (2009). Bidirectional plasticity in fast-spiking GABA circuits by visual experience. *Nature*, *462*(7270), 218–221.

Ye, Q., & Miao, Q.-L. (2013). Experience-dependent development of perineuronal nets and chondroitin sulfate proteoglycan receptors in mouse visual cortex. *Matrix Biology: Journal of the International Society for Matrix Biology*, *32*(6), 352–363.

Yizhar, O., Fenno, L. E., Prigge, M., Schneider, F., Davidson, T. J., O'Shea, D. J., Sohal, V. S., Goshen, I., Finkelstein, J., Paz, J. T., Stehfest, K., Fudim, R., Ramakrishnan, C., Huguenard, J. R., Hegemann, P., & Deisseroth, K. (2011). Neocortical excitation/inhibition balance in information processing and social dysfunction. *Nature*, *477*(7363), 171–178.

Zhang, N., Yan, Z., Liu, H., Yu, M., He, Y., Liu, H., Liang, C., Tu, L., Wang, L., Yin, N., Han, J., Scarcelli, N., Yang, Y., Wang, C., Zeng, T., Chen, L.-L., & Xu, Y. (2021). Hypothalamic Perineuronal Nets Are Regulated by Sex and Dietary Interventions. *Frontiers in Physiology*, *12*, 714104.

Zimmermann, D. R., & Dours-Zimmermann, M. T. (2008). Extracellular matrix of the central nervous system: from neglect to challenge. *Histochemistry and Cell Biology*, *130*(4), 635–653.

8. Appendix

During my PhD I was also involved in projects focused on the study of the Creatine Transporter Deficiency disorder (CTD), a metabolic and neurodevelopmental disorder caused by the lack of functionality of the gene slc6a8, encoding the solute carrier family 6-member 8 protein or creatine transporter (CrT). The expression of CrT is heterogeneous in the brain, suggesting that cellular populations may be differentially affected by the lack of creatine supply. Among the neuronal populations characterized by a high metabolic profile are PV interneurons which also expressed abundant CrT. Accordingly, PV interneurons could be crucial in the pathogenesis of CTD. Below is a published article showing PV interneurons' crucial role in CTD.

8.1 Cell-specific vulnerability to metabolic failure: the crucial role of parvalbumin expressing neurons in Creatine Transporter Deficiency

8.1.1 Introduction

Creatine Transporter Deficiency (CTD) is an X-linked metabolic disorder causing cerebral creatine (Cr) deficit, intellectual disability, psycho-motor impairment, autistic-like behavior, and epilepsy. CTD etiology has been related to multiple mutations in the solute carrier family 6-member 8 (*Slc6a8*) gene encoding the protein responsible for cellular Cr uptake [1,2].
Animal models either lacking the *Slc6a8* gene or engineered to express an allele with a point mutation found in patients, largely reproduce the endophenotype of the human condition [3-8]. The availability of these transgenic lines of rodents allowed the scientific community to take initial steps towards dissecting the pathological determinants of CTD[8]. Loss-of-function of *Slc6a8* does not result in overt alterations of brain structure and neuronal density, but rather induces a subtle reorganization of cerebral circuits and cellular metabolic processes [3,5,7,8-15]. However, a clear picture of the key cellular players involved in the development and progression of CTD is still missing. This represents a major issue, because

a better knowledge of the causative mechanisms is crucial to identify novel druggable targets of translational value for a disease that is still untreatable [8].

Different cell types in the brain have distinctive metabolic profiles [16], resulting in a highly diversified energy demand in neuronal and glial populations [17]. Neurons consume 75-80% of the energy produced [18,19] and might be particularly susceptible to the decreased ATP availability observed in CTD [9]. Intriguingly, the analysis of Slc6a8 RNA and protein levels revealed that its expression presents a significant heterogeneity across brain circuits [20-22], with a prominent expression in fast-spiking, parvalbumin-expressing (PV^+) interneurons and oligodendrocytes [22,23]. Thus, we hypothesized that the perturbation of energy supply due to Cr deficiency might have a multiform impact on the different brain cell populations. To test this possibility, we used a multi-level approach, ranging from RNA sequencing to patch-clamp recordings, behavioral assessment, optical imaging and EEG to explore cell-specific consequences of *Slc6a8* deletion.

We found that a defective supply of Cr affects the transcriptome of excitatory and inhibitory neurons, and oligodendrocytes, inducing a morphological and functional rearrangement of neural circuits. In this framework, we focused on the high-energy-requiring PV^+ GABAergic interneurons, demonstrating that this cellular population crucially contributes to the pathogenesis of CTD and might represent a suitable target for therapeutic intervention.

8.1.2 Materials and Methods

Animals

We employed male mice hemizygous for the deletion of exons 5-7 in the *Slc6a8* gene (KO; $CrT^{-/y}$) and their wild-type (WT; $CrT^{+/y}$) littermates [4]. To target patch-clamp recordings to PV^+ interneurons, we injected an AAV pCAG-FLEX-EGFP-WPRE vector (Addgene viral prep #51502-AAV9) in the lateral ventricles of newborn $CrT^{+/y}$ and $CrT^{-/y}$ mice expressing Cre recombinase under the parvalbumin (PV) promoter (PV::$CrT^{+/y}$ and PV::$CrT^{-/y}$, respectively). Finally, we generated a conditional mouse line carrying the floxed *Slc6a8* and PV-Cre alleles (PV::$CrTfl^{+/y}$ and PV::$CrTfl^{-/y}$) to study the effects of cell-specific *Slc6a8* deletion. Mice carrying the deleted/floxed *Slc6a8* allele were on pure C57Bl/6J background; mice with the PV-Cre allele were from the B6.129P2-Pvalbtm1(cre)Arbr/J strain (JAX stock #017320). Mutant and wild-type animals for each group were invariably selected from the same litters, with a minimum of three litters for each experiment. All experiments were authorized by the Italian Ministry of Health (#1052/2020-PR). Data collection and analysis were performed

blind to experimental conditions. See Supplementary Information file for a more detailed description of methods.

Bulk RNA sequencing (bulk RNA-seq)

Total RNA was extracted from the cerebral cortices of 3 $CrT^{+/y}$ and 4 $CrT^{-/y}$ animals (postnatal day 100, PND100) using the Qiagen RNeasy Midi Kit (Qiagen Inc.). RNA libraries were constructed using the Universal Plus mRNA-Seq kit (Tecan Genomics) and sequenced on paired-end 150 bp mode on NovaSeq 6000 (Illumina) at the Istituto di Genomica Applicata (IGA). The resulting sequencing data for each library were post-processed to obtain FastQ files, then demultiplexed using Bcl2Fastq 2.20 version of the Illumina pipeline. FastQ files can be accessed at the GEO repository (GSE218797). Transcriptomic data were run through Limma [24], to determine differentially expressed genes (DEGs, adjusted p-value < 0.1). Gene Ontology (GO) analysis was performed using the ShinyGO tool [25]. To search for interaction networks of corresponding proteins, we used the STRING database [26]. Validation of top DEGs was performed with quantitative PCR (qPCR).

Single-nucleus RNA sequencing (snRNA-seq)

Nuclei were acutely purified from the cerebral cortex of 2 $CrT^{+/y}$ and 2 $CrT^{-/y}$ animals PND100 as described previously, with minor modifications [27]. The whole cortex of the right cerebral hemisphere was manually dissected for each mouse. Tissue dissection was performed with extreme caution to avoid cross contamination with underlying brain tissue. For every sample, 15000 nuclei were loaded into a Chromium Single Cell A Chip (10x Genomics) and processed following the manufacturer's instructions. Single-nuclei RNA-seq libraries were prepared using the Chromium Single Cell 3' Library & Gel Bead kit v2 and i7 Multiplex kit (10x Genomics). Pooled libraries were then loaded on a HiSeq2500 instrument (Illumina) and sequenced to obtain 75 bp paired-end reads. snRNA-seq data can be accessed at the GEO repository (GSE216766). Sequenced samples were processed using the Cell Ranger (v.3.1.0) pipeline (10x Genomics). Downstream analyses were performed using the R package Seurat (v3.1.4). To explore the heterogeneity of the cortex, we identified 7 major cell populations. DEGs between the two groups were identified using the Wilcoxon Rank Sum test and Bonferroni correction (adjusted p-value < 0.1). GO analysis for each differentially expressed gene list was performed as described above. The overlap between snRNA-seq and bulk RNA-seq data was assessed using a Fisher Exact Test.

Electrophysiology

Brain slices containing the prefrontal cortex were prepared from PND30-P40 animals as described [28]. A subset of experiments was performed on visually identified pyramidal cells of layer II/III from $CrT^{+/y}$ and $CrT^{-/y}$ mice. Recordings from PV^{+} interneurons of cortical layers II/III and V were obtained by targeting GFP positive cells in PV::$CrT^{+/y}$ and PV::$CrT^{-/y}$ animals injected with the AAV pCAG-FLEX-EGFP-WPRE vector. Patch pipettes (2.5–4.5 MΩ resistance) were made from borosilicate glass capillaries (World Precision Instruments) using a P-97 puller (Sutter Instruments) and filled with a potassium gluconate-based solution. Whole-cell recordings were acquired using a Multiclamp 700A controlled by Clampex 11.2 via a Digidata 1550B amplifier (Molecular Devices). Clampfit 10.7 software was used for analysis. Differences between the groups were assessed with either a two-tailed t-test or two-way ANOVA (Graphpad Prism 9.4.1).

Immunohistochemistry

Coronal brain sections (45 mm) were processed for immunohistochemistry (Parvalbumin, 1:1000, catalog #195004, Synaptic System). To quantify the density of PV^{+} cells and synaptic puncta in the cerebral cortex we used a Zeiss microscope (Carl Zeiss). Differences between the two groups were assessed with a two-tailed t-test (Graphpad Prism 9.4.1).

Y maze

PV::$CrTfl^{+/y}$ and PV::$CrTfl^{-/y}$ mice (PND180) were allowed to explore a Y-shaped maze for a single trial of 8 min. Trials were video-recorded (Noldus Ethovision XT) for offline analysis. A triad was defined as a set of three consecutive arm entries, with each entry being into a different arm of the maze (e.g., A-B-C). The alternation percentage was calculated by dividing the number of triads by the number of possible alternations [5]. A two-tailed t-test revealed the difference between the two groups.

Open field and object recognition test

PV::CrTfl$^{+/y}$ and PV::CrTfl$^{-/y}$ mice were allowed to explore a squared arena for a single trial of 10 min (day 1, open field). An area corresponding to the center of the arena was defined to assess emotional behavior. Total movements of animals and the time spent in the center area were automatically computed by Noldus Ethovision. For the object recognition test (ORT), two identical objects were placed in diagonally opposite corners of the same arena, approximately 15 cm from the walls, and mice were allowed 10 min to explore them (day 2, familiarization phase). The testing phase was performed 24h after the familiarization phase (day 3). One of the familiar objects was replaced with a new one and mice were allowed to explore the two objects for 5 min. A discrimination index was computed as DI = (T_{new} - T_{old})/(T_{new} + T_{old}), where T_{new} is the time spent exploring the new object, and T_{old} is the time spent exploring the old one [5]. A two-tailed t-test was used to reveal the differences between the two groups.

Intrinsic optical signal (IOS) imaging

Surgery and imaging sessions were performed as described [29], starting at least two days after the Y maze. A metal ring was affixed over the binocular visual cortex and used to secure the animal under the objective. Images were visualized using a custom-made setup based on a Leica macroscope (Leica Z6 APO coupled with a Leica PanApo 2.0X; Leica Microsystems) and red-light LED illumination (630 nm). Visual stimuli were sinusoidal wave gratings (0.03 c/deg, 20 cd/m2, 90%, 4 Hz), generated using Matlab Psychtoolbox. A two-tailed t-test assessed differences between groups.

EEG recordings

A two-channel head mount was implanted on the skull of mice, at least two days after IOS imaging. EEG was recorded using a preamplifier connected to a data acquisition system and Sirenia Software 1.7.9 (Pinnacle Technology). We evaluated spontaneous (baseline) cortical activity for 24h, before assessing the effects of kainic acid (KA; intraperitoneal injection, 10 mg/kg). To quantify seizure episodes, we used Sirenia Seizure Pro 1.8.4 [29]. A two-tailed t-test and χ^2 test were used to assess differences between groups.

Stereotaxic injections of zolpidem

Zolpidem (100 mM) was injected at 3 sites surrounding the binocular visual cortex. A two-tailed t-test and two-way repeated measures ANOVA followed by post-hoc Holm–Sidak test were used to assess the effect of zolpidem treatment on cortical activity.

8.1.3 Results

Creatine deficiency affects brain expression of genes related to metabolism and synaptic signaling

To investigate how gene expression is altered in conditions of Cr depletion, we performed bulk RNA-seq from the cerebral cortex of adult $CrT^{+/y}$ and $CrT^{-/y}$ animals. We found 957 genes which expression was regulated by Cr, with 500 genes upregulated and 457 genes downregulated (Fig. 1a; Additional file 2: Table S1). As expected, *Slc6a8* was significantly downregulated in the cortex of $CrT^{-/y}$ mutant mice. These results were confirmed by qPCR (Additional file 3: Table S2). GO analysis for biological process revealed that the transcription of many genes involved in the cellular response to stress, protein translation and energy metabolism were upregulated (Fig. 1b; Additional file 4: Table S3), with ribosomes and mitochondria being the most enriched compartments in cellular component analysis (Fig. 1c; Additional file 5: Table S4). Accordingly, a search for corresponding protein-protein interaction (PPI) networks indicated that these genes were significantly connected in biological clusters related to the ribosomal function and the mitochondrial respiratory chain (Additional file 1: Fig. S1; Additional file 6: Table S5). In contrast, the list of downregulated genes was enriched for items implicated in the regulation of protein folding and synaptic signaling (Fig. 1d; Additional file 4: Table S3), and their transcription was primarily localized in the endoplasmic reticulum (ER) and postsynaptic compartment (Fig. 1e; Additional file 5: Table S4). PPI analysis identified the chaperone complex as the most represented cluster (Additional file 1: Fig. S2; Additional file 6: Table S5).

We then used snRNA-seq to generate a comprehensive map of the most affected cell types in the brain of $CrT^{-/y}$ mice. Supervised clustering analysis using canonical marker genes classified nuclei into seven major populations representing the main cell types: excitatory neurons, inhibitory neurons, astrocytes, oligodendrocytes (ODCs), oligodendrocyte precursors cells (OPCs), microglia, and vascular/endothelial cells (Fig. 2a,b; Additional file 1: Fig. S3d; Additional file 7: Table S6). Importantly, the *Slc6a8* gene was significantly downregulated in $CrT^{-/y}$ mutant mice (Additional file 1: Fig. S3e,f). Integrative analysis did not detect any compositional differences between the datasets (Fig. 2a-d; Additional file 8: Table S7), indicating that Cr deficiency does not cause major changes in the proportion of specific cell populations.

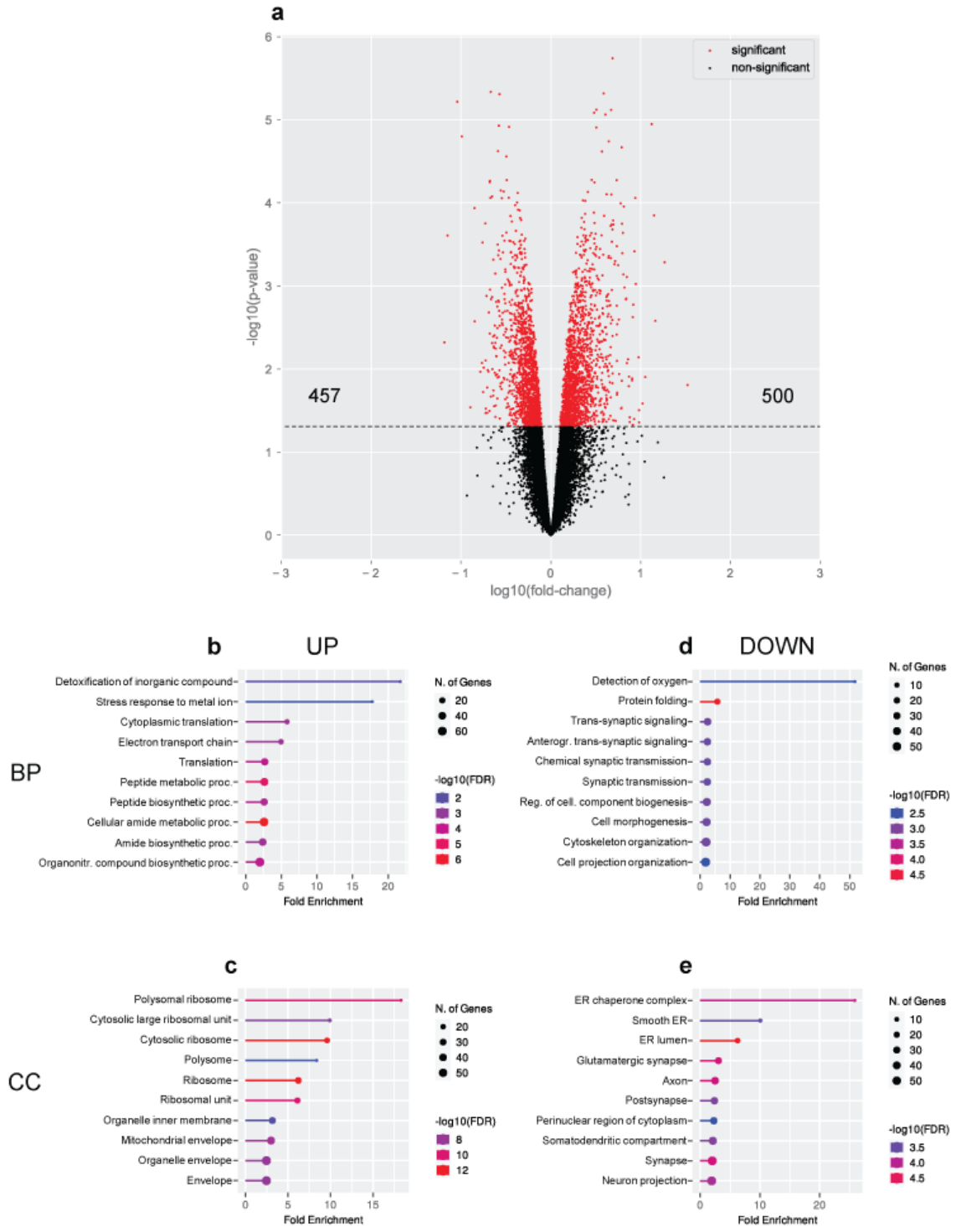

Fig. 1 Differentially expressed genes (DEGs) in the cerebral cortex of CrT$^{-/y}$ mice. a) Volcano plot of the DEGs in the bulk RNA-seq data sets from CrT$^{+/y}$ (n=3) and CrT$^{-/y}$ (n=4) animals. Red points mark the significantly up- or downregulated genes in the CrT$^{-/y}$ cerebral cortex ($p < 0.1$). **b,d)** Fold enrichment of top-level overrepresented GO terms for biological process (BP) highlighting metabolic pathways in the set of upregulated genes (b) and synaptic pathways in the set of downregulated genes (d). **c,e)** Fold enrichment of top-level overrepresented GO terms for cellular component (CC) highlighting ribosomes and mitochondria in the set of upregulated genes (c), and ER and synapses in the set of downregulated genes (e). Calculated by ShinyGO 0.76.3, FDR < 0.05.

Creatine deficiency affects the transcriptome of excitatory neurons, inhibitory cells and oligodendrocytes

We then used snRNA-seq to generate a comprehensive map of the most affected cell types in the brain of $CrT^{-/y}$ mice. Supervised clustering analysis using canonical marker genes classified nuclei into seven major populations representing the main cell types: excitatory neurons, inhibitory neurons, astrocytes, oligodendrocytes (ODCs), oligodendrocyte precursors cells (OPCs), microglia, and vascular/endothelial cells (Fig. 2a,b; Additional file 1: Fig. S3d; Additional file 7: Table S6). Importantly, the *Slc6a8* gene was significantly downregulated in $CrT^{-/y}$ mutant mice (Additional file 1: Fig. S3e,f). Integrative analysis did not detect any compositional differences between the datasets (Fig. 2a-d; Additional file 8: Table S7), indicating that Cr deficiency does not cause major changes in the proportion of specific cell populations.

Differential gene expression analysis revealed that 1146 genes were dynamically regulated across the genotypes in the cerebral cortex: while we failed to detect any differentially regulated genes (DEGs) in astrocytes and endothelial cells, we found significant changes in the transcriptome of excitatory (1029 genes: 271 upregulated and 758 downregulated) and inhibitory neurons (114 genes: 74 upregulated and 40 downregulated), oligodendrocytes (118 genes: 61 upregulated and 57 downregulated) and their precursors (OPCs, 2 genes: 1 upregulated and 1 downregulated), and microglial cells (23 genes: 19 upregulated and 4 downregulated; Fig. 2e, Additional file 9: Table S8). These data suggest that CTD affects multiple cell types, with neurons and oligodendrocytes being the most impacted populations. The validity of snRNA-seq was also strengthened by the following observations: i) a significant overlap was present between the DEGs in excitatory neurons, the most represented cell type in single nucleus profiling, and those identified with bulk RNA-seq (Additional file 1: Fig. S4a); ii) a significant correlation of the fold change was detected using snRNA-seq and bulk RNA-seq for DEGs common to the two lists (Additional file 1: Fig. S4b).

GO analysis revealed that genes associated with synaptic assembly, neurotransmission and circuit development were enriched for dynamic expression across the genotypes in both excitatory (Fig. 3a,b; Additional file 1: Fig. S5a,b) and inhibitory neurons (Fig. 3c,d; Additional file 1: Fig. S5c,d; Additional file 10: Table S9; Additional file 11: Table S10), suggesting that neurological symptoms of CTD might primarily stem from subtle defects of subcellular compartments such as dendrites, axons or synapses. While the alteration of these functional modules was bidirectional in excitatory neurons (Fig. 3a,b), overrepresentation of synaptic pathways was specific to the upregulated genes of inhibitory neurons. In contrast, this population was characterized by reduced levels of metabolic and proteostatic genes (Fig. 3d; Additional file 10: Table S9; Additional file 11: Table S10). To get

more specific insight into synaptic transcripts, we analyzed the lists of neuronal DEGs using SynGO, a curated database of proteins involved in synaptic functions and plasticity [30]. A significant overrepresentation of genes encoding for pre- and postsynaptic proteins was present in both excitatory (181/1029) and inhibitory neurons (34/114; Fig. 3e,f). Interestingly, the upregulation of synaptic-related items was also detected in oligodendrocytes and microglia (Fig. 4; Additional file 10: Table S9; Additional file 11: Table S10). Moreover, a decreased expression of genes involved in myelination processes was observed in CrT$^{-/y}$ oligodendrocytes (Fig. 4b; Additional file 10: Table S9; Additional file 11: Table S10). These data suggest that a subtle reorganization of brain circuits underlies the pathogenesis of CTD.

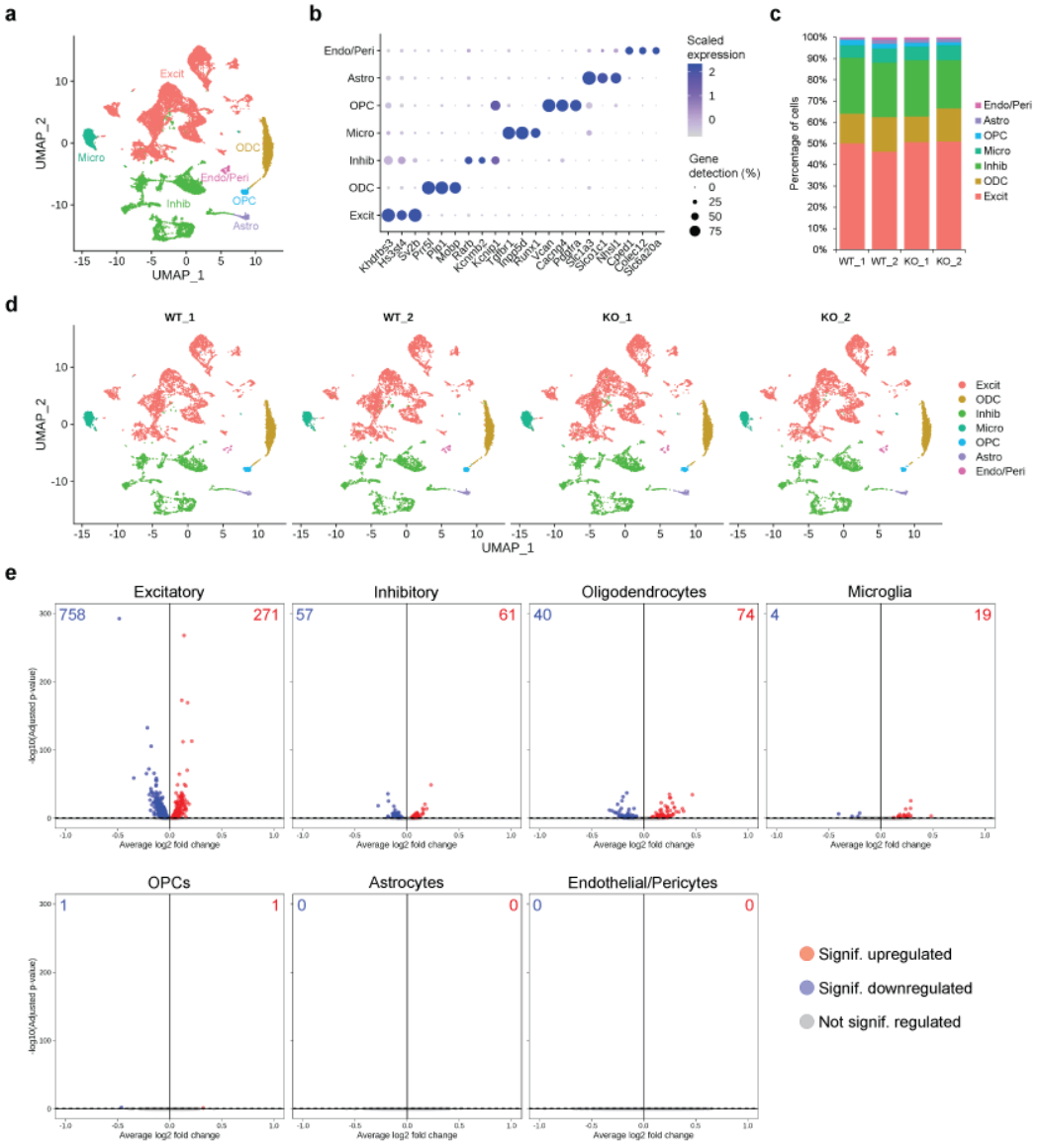

figure legend below

Fig. 2 snRNA-seq analysis of the cerebral cortex of CrT$^{+/y}$ (WT) and CrT$^{-/y}$ (KO) animals. a) UMAP plot showing the populations identified in the snRNA-seq dataset of CrT$^{+/y}$ (n=2) and CrT$^{-/y}$ (n=2) animals. **b)** Dot plot showing expression levels and gene detection of markers for the 7 major populations identified. **c)** Bar graphs showing comparable distribution of each cell population between replicates and genotypes. **d)** UMAP plot showing the populations identified in the snRNA-seq dataset of CrT$^{+/y}$ (n=2) and CrT$^{-/y}$ (n=2) animals by sample of origin. **e)** Volcano plots showing the DEGs for each major cell population. The up- and down-regulated genes are marked in red and blue, respectively and indicated at the top of each plot. Significant differences were detected in excitatory and inhibitory neurons, oligodendrocytes, and microglia, but not in astrocytes and vascular/endothelial cells (Wilcoxon Rank Sum test, adj p-value < 0.1).

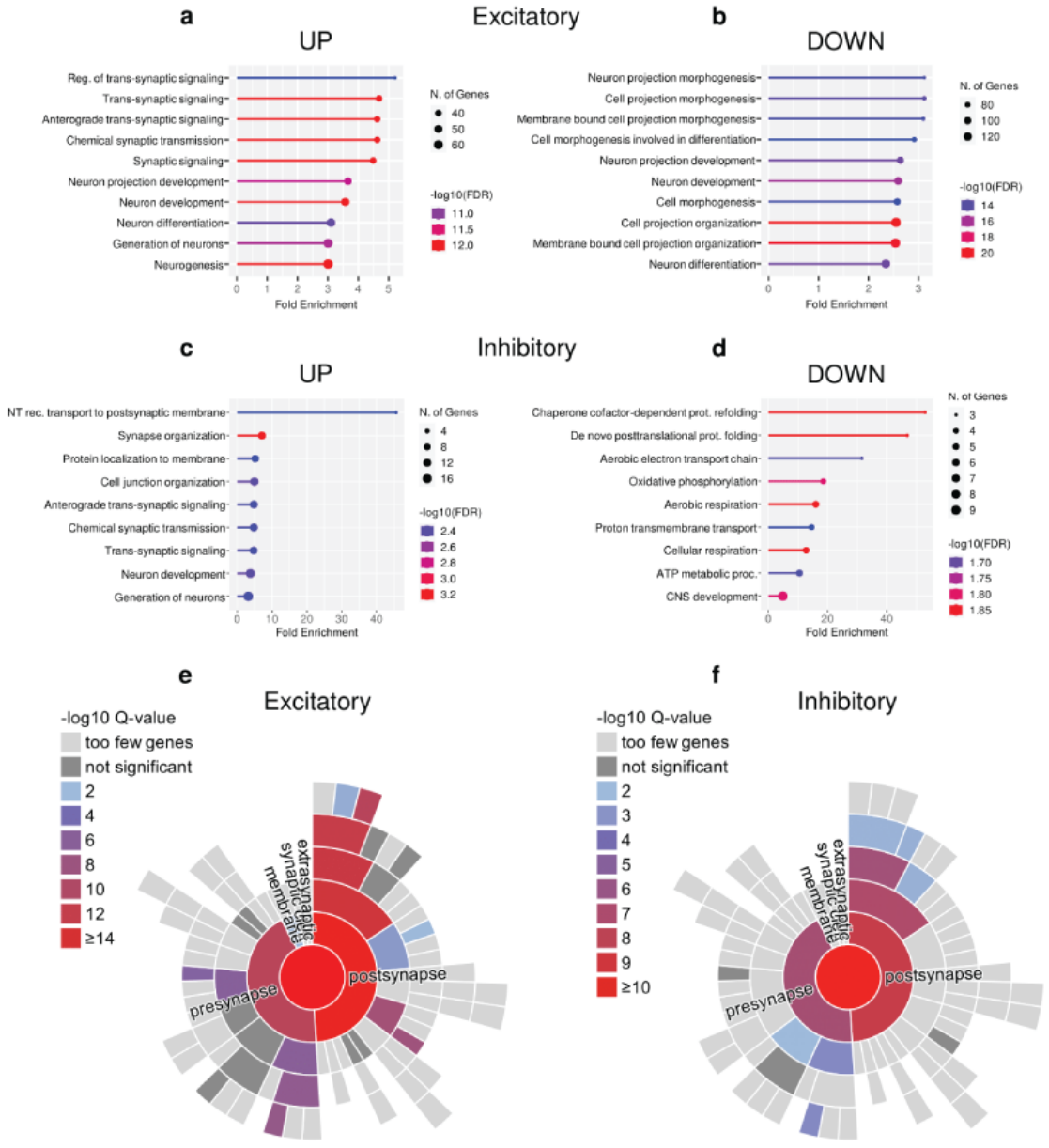

Fig. 3 Gene ontology (GO) analysis for biological process from the snRNA-seq data set showing enrichment in synaptic pathways in neuronal clusters. (a-d) Fold enrichment of top-level overrepresented GO terms in excitatory (a,b) and inhibitory (c,d) neurons. Calculated by ShinyGO 0.76.3, FDR < 0.05. **(e,f)** Hierarchical dendrograms of synaptic proteins corresponding to DEGs (SynGO database) showing significant enrichment by color code: (e) excitatory neurons (f) inhibitory neurons.

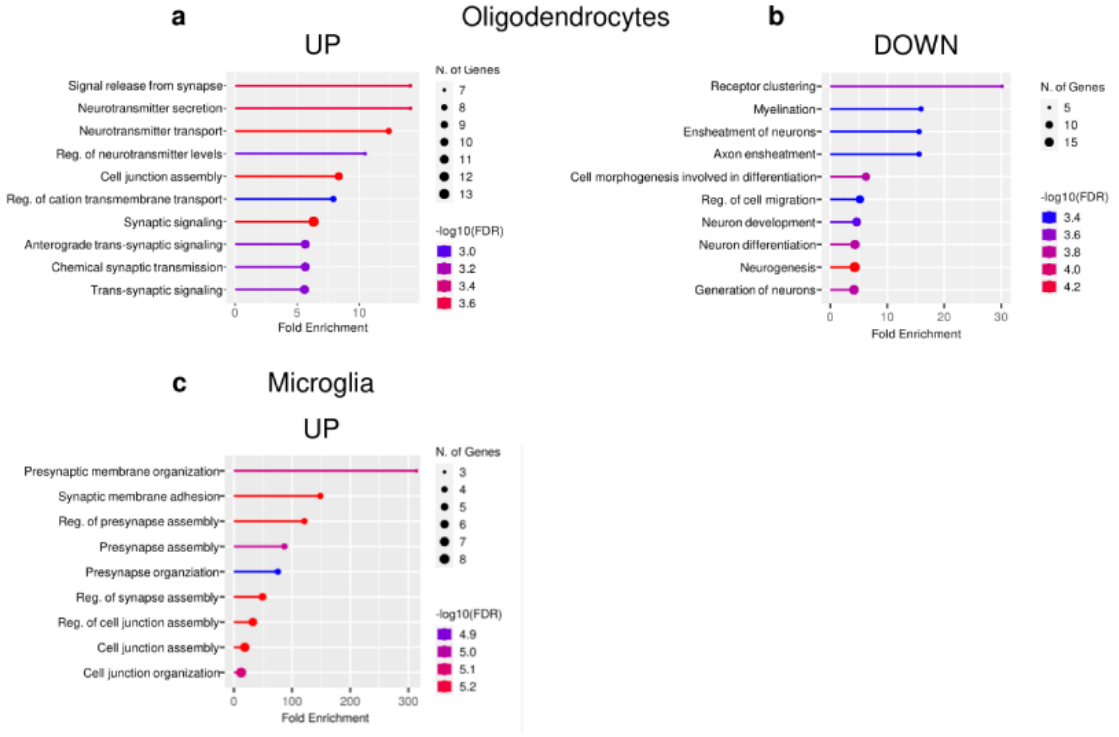

Fig. 4 GO analysis for biological process from the snRNA-seq data set showing enrichment in synaptic pathways in non-neuronal clusters. Fold enrichment of top-level overrepresented GO terms in oligodendrocytes **(a,b)** and microglia **(c)**. Calculated by ShinyGO 0.76.3, FDR < 0.05.

Opposite effects of Cr deficiency on the functional output of pyramidal and parvalbumin neurons

To investigate the functional consequences of *Slc6a8* deletion in specific neuronal populations, we first performed patch-clamp recordings in cortical pyramidal neurons. While we did not find any alterations in spontaneous synaptic activity (Fig. 5a; Additional file 1: Fig. S6a), we observed a significant increase in the firing frequency of pyramidal neurons in the cortex of $CrT^{-/y}$ animals (Fig. 5b; Additional file 1: Fig. S6b). Consistently, we also found a significant rise of membrane resistance and a reduction of rheobase (Fig. 5c; Additional file 1: Fig. S6c). In addition, the firing pattern of mutant neurons in response to stimuli of increasing intensity was consistently more sustained compared to that of wild-type cells (Fig. 5d; Additional file 1: Fig. S6d).

Since previous data indicated a specific alteration of the inhibitory phenotype in CTD, consisting in a decrease of the number of GABAergic, but not glutamatergic, synapses in the cerebral cortex of $CrT^{-/y}$ mice [5], we also analyzed the contribution of inhibitory cells to CTD pathogenesis. Inhibition in the brain is mediated by a rich variety of GABAergic interneurons

[31]. We focused on PV^+ interneurons because they play a central role in controlling the spike timing of principal cells [32], their typical fast-spiking activity is highly energy-demanding [33], and they show prominent expression of *Slc6a8* [23]. Patch-clamp recordings of cortical PV^+ interneurons showed a reduction of sodium and potassium voltage-gated currents (Fig. 6a; Additional file 1: Fig. S7a), a decline in firing frequency (Fig. 6b; Additional file 1: Fig. S7b), a reduced resistance to fatigue (Fig. 6c; Additional file 1: Fig. S7c), as well as an alteration of action potential amplitude, half-width and fast afterhyperpolarization (fAHP; Fig. 6d; Additional file 1: Fig. S7d) in $CrT^{-/y}$ neurons. To investigate whether PV^+ interneurons were also affected at the synaptic level, we used immunostaining for PV^+ synaptic puncta. We found that PV^+ synaptic density was decreased in the prefrontal cortex (PFC) and in the anterior cingulate cortex (ACC) of $CrT^{-/y}$ mice. A reduced number of PV^+ cells was also observed in the ACC (Fig. 6e). Overall, these data reveal a substantial impact of Cr deficiency on PV^+ interneurons, emerging at both the morphological and functional level.

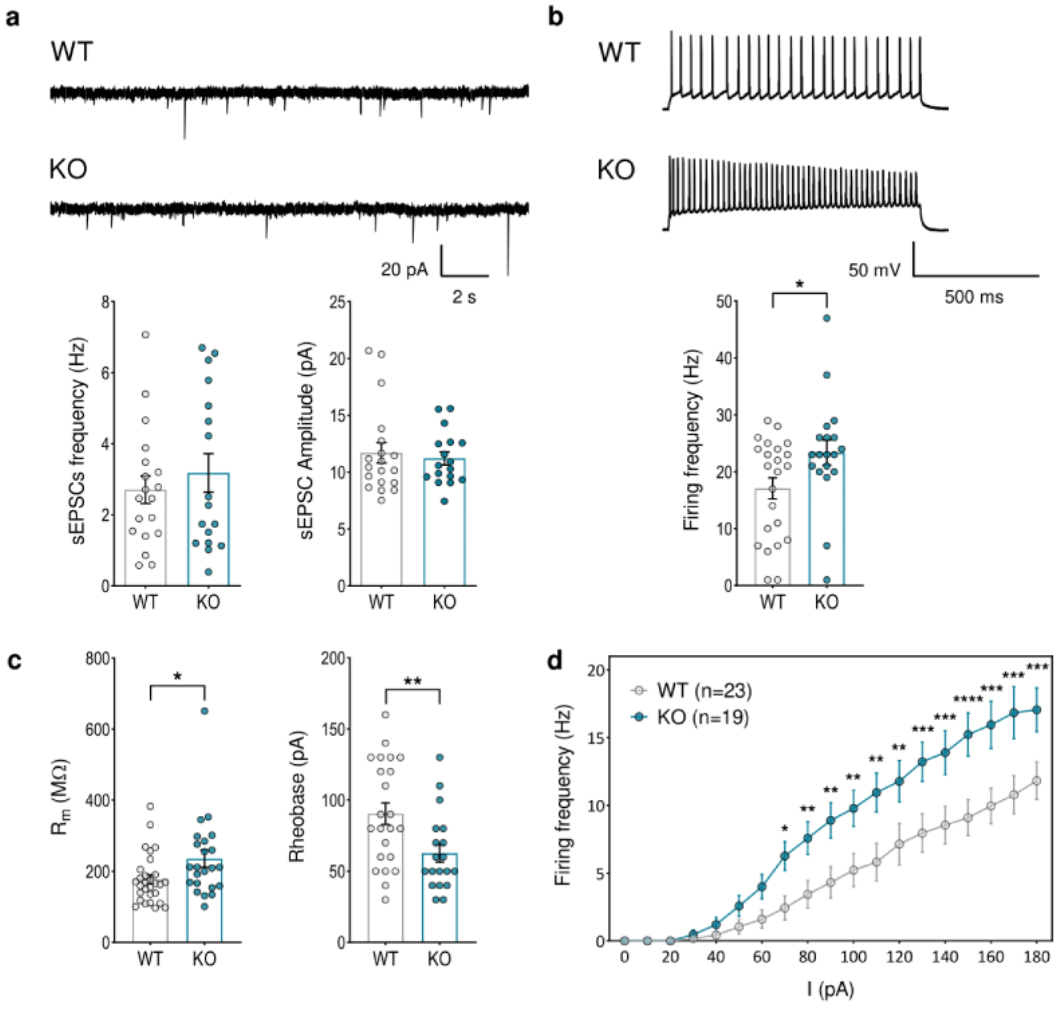

figure legend page below

Fig. 5 Electrophysiological characterization of layer II/III pyramidal neurons in the prefrontal cortex (PFC) of CrT$^{+/y}$ (WT) and CrT$^{-/y}$ (KO) mice. Recordings were obtained from 8 CrT$^{+/y}$ and 5 CrT$^{-/y}$ animals at PND35-40, dots represent individual cells. **a)** Representative traces (top) and quantification (bottom) of sEPSCs in pyramidal cells of CrT$^{+/y}$ and CrT$^{-/y}$ animals. No differences were found between the genotypes in frequency (t-test, p= 0.477, n= 19 cells for CrT$^{+/y}$ and 17 for CrT$^{-/y}$) and amplitude (Mann-Whitney test, p= 0.851, n= 19 cells for CrT$^{+/y}$ and 17 for CrT$^{-/y}$). **b)** Representative traces (top) and quantification (bottom) of firing frequency, showing an increased firing in CrT$^{-/y}$ pyramidal neurons (t-test, p <0.05, n= 23 cells for CrT$^{+/y}$ and 19 for CrT$^{-/y}$). **c)** CrT$^{-/y}$ pyramidal neurons display higher membrane resistance (left, Mann-Whitney test, p <0.05, , n= 29 cells for CrT$^{+/y}$ and 22 for CrT$^{-/y}$) and lower rheobase (right, t-test, p <0.05, , n= 23 cells for CrT$^{+/y}$ and 19 for CrT$^{-/y}$) compared to controls. **d)** Frequency vs. current plot showing persistently increased firing frequency in CrT$^{-/y}$ cells across a range of injected currents (Two-way RM ANOVA followed by Fisher's LSD test, n= 23 cells for CrT$^{+/y}$ and 19 for CrT$^{-/y}$). *p< 0.05, **p< 0.01, ***p<0.001, ****p<0.0001. Data are expressed as mean ± SEM.

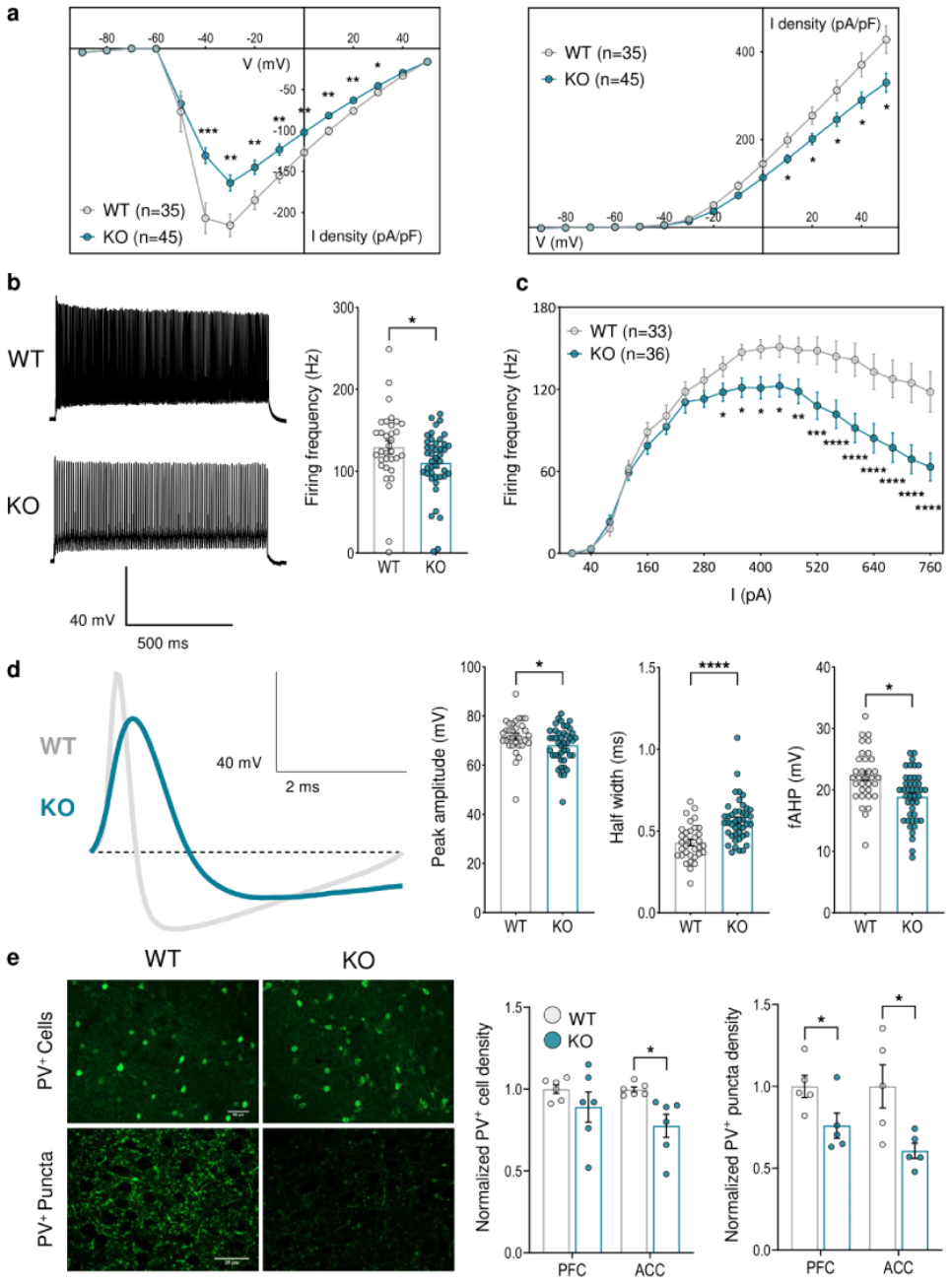

figure legend below

Fig. 6 Structural and functional characterization of PV^+ neurons in the PFC and anterior cingulate cortex (ACC) of $CrT^{+/y}$ (WT) and $CrT^{-/y}$ (KO) mice. a-d) Electrophysiological characterization of PV^+ neurons obtained from 5 $CrT^{+/y}$ and 8 $CrT^{-/y}$ animals, carrying the Cre-recombinase in *PV^+* cells ($PV::CrT^{+/y}$ and $PV::CrT^{-/y}$), injected with the AAV9 pCAG-FLEX-EGFP-WPRE vector; dots represent individual cells. a) Current-voltage relationships showing a decrease in peak Na^+ (left) and steady-state K^+ (right) current densities in $PV::CrT^{-/y}$ (KO) neurons with respect to WT controls (Two-way RM ANOVA followed by Fisher's LSD test, n= 35 cells for $PV::CrT^{+/y}$ and 45 for $PV::CrT^{-/y}$). b) Representative traces (left) and quantification (right), showing a decrease in firing frequency in $PV::CrT^{-/y}$ neurons (Mann-Whitney test, $p < 0.05$, n= 33 cells for $PV::CrT^{+/y}$ and 43 for $PV::CrT^{-/y}$). c) Frequency vs. current plot showing that $PV::CrT^{-/y}$ neurons persistently fire at lower frequency across a broad range of injected currents compared to controls (Two-way RM ANOVA followed by Fisher's LSD test, n= 33 cells for $PV::CrT^{+/y}$ and 36 for $PV::CrT^{-/y}$). d) Representative trace showing the typical profile of action potentials in the two groups (left) and quantification of action potential amplitude (left graph), half-width (central graph) and fAHP (right graph), indicating an alteration in all three parameters in $CrT^{-/y}$ neurons (Mann-Whitney test, $p < 0.05$ for peak amplitude and fAHP, $p<0.0001$ for half-width, n= 33 cells for $PV::CrT^{+/y}$ and 43 for $PV::CrT^{-/y}$). **e)** Representative images (left) and quantification of PV^+ cells (center) and puncta density (right) in the PFC and ACC of $CrT^{+/y}$ (n = 5) and $CrT^{-/y}$ animals (n = 6), showing a global reduction in PV^+ puncta and a decrease in PV^+ cells restricted to the ACC (t-test, $p < 0.05$ for all comparisons). Dots represent individual animals. *p< 0.05, **p< 0.01, ***p<0.001, ****p<0.0001. Data are expressed as mean ± SEM.

Neurological endophenotype of conditional mice carrying a specific deletion of *Slc6a8* in parvalbuminergic interneurons

In light of the marked impairment of PV^+ interneurons and synapses in the brain of $CrT^{-/y}$ mice, we asked whether the deletion of *Slc6a8* only in these cells might be sufficient to recapitulate the phenotype of the whole-body knockout animals. To this purpose, we generated a conditional mouse model carrying a floxed *Slc6a8* allele and expressing Cre recombinase under the PV promoter. The body weight of $PV::CrTfl^{-/y}$ mice was slightly lower than that measured for $PV::CrTfl^{+/y}$ littermates (Additional file 1: Fig. S8). Since we previously showed that the performance in the Y maze can accurately discriminate between mutant and wild-type animals in our whole-body model of CTD [29], we first used this behavioral task to evaluate the cognitive phenotype in the conditional model and we found a clear impairment of spontaneous alternation in $PV::CrTfl^{-/y}$ mice (Fig. 7a). We also detected a deterioration of object recognition memory: the discrimination index in the ORT at 24h, indeed, was significantly lower in conditional mutant mice compared to $PV::CrTfl^{+/y}$ littermates, indicating a reduced capacity to recall the familiar object (Fig. 7b). We then analyzed general activity and anxiety-related behavior of $PV::CrTfl^{-/y}$ and $PV::CrTfl^{+/y}$ animals in the open field arena used for cognitive assessment. We found no difference in the total distance moved (Fig. 7c) and velocity (Fig. 7d) among the two groups, indicating that the difference in cognitive capacities are not due to changes in the ability to cope with stress in challenging conditions. To verify whether the main neurophysiological alterations described in $CrT^{-/y}$ animals were also present in the conditional model, we measured visually-evoked hemodynamic responses using IOS, and the susceptibility to epilepsy in response to kainic acid challenge [29]. As

previously reported for whole-body CrT$^{-/y}$ mice [29], PV::CrTfl$^{-/y}$ animals showed a significant alteration in the amplitude of cortical response to visual stimulation (Fig. 7e,f) and a higher susceptibility to kainic acid challenge according to the Racine scale (Fig. 7g), with lower latency of epileptiform activity (Fig. 7h), and increased frequency, duration and severity of epileptic episodes (Fig. 7i-k).

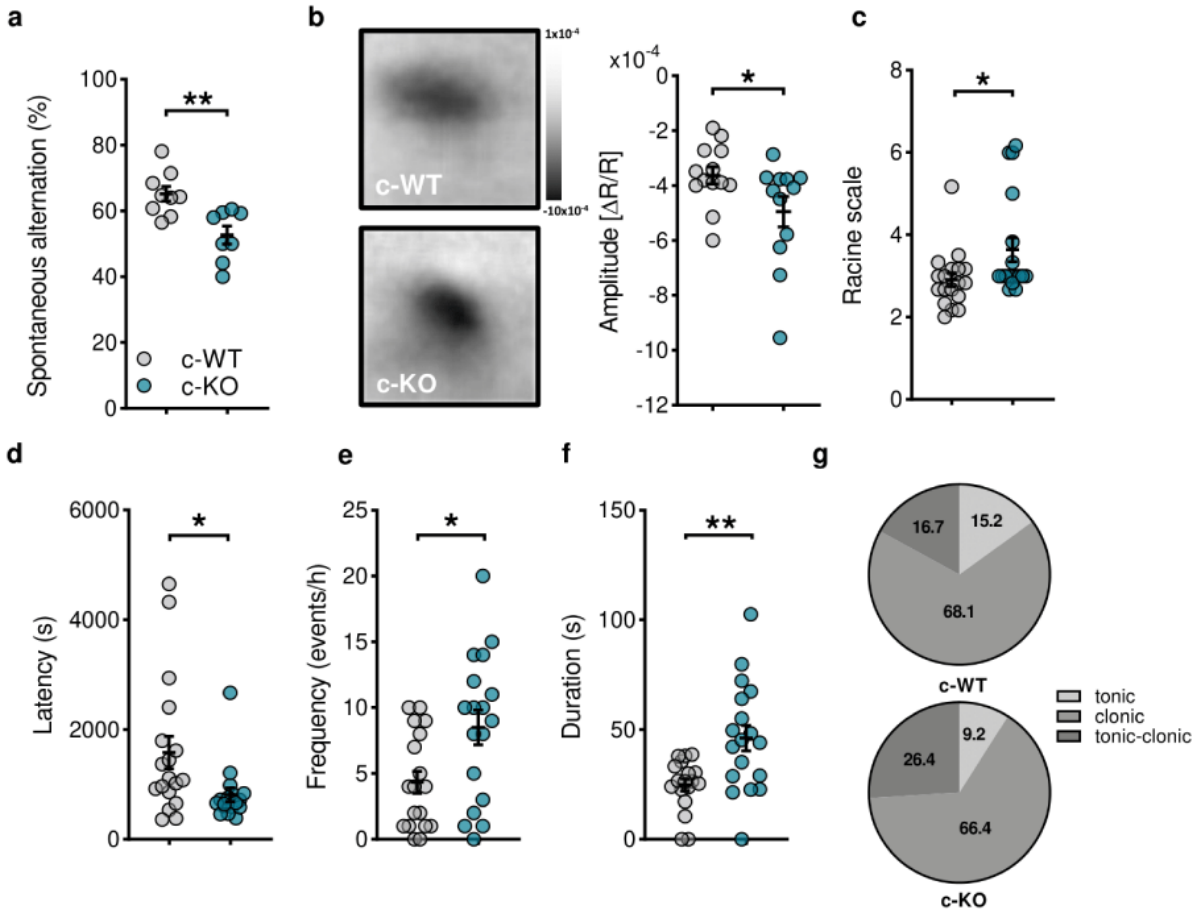

Fig. 7 Behavioral, physiological and EEG characterization of PV::CrTfl animals. a) Percentage of spontaneous alternation in the Y-maze test, showing a poorer performance in PV::CrTfl$^{-/y}$ (c-KO, n = 8) mice compared to PV::CrTfl$^{-/y}$ littermates (c-WT, n=9; t-test, $p < 0.01$). **b)** A significantly lower discrimination index was found in PV::CrTfl$^{-/y}$ mice with respect to PV::CrTfl$^{+/y}$ littermates (n = 5 for both groups; t-test $p < 0.01$). **c)** Total distance moved in the open field arena did not differ between PV::CrTfl$^{-/y}$ and PV::CrTfl$^{+/y}$ mice (n = 5 for both groups; Mann-Whitney test, $p = 0.69$). **d)** PV::CrTfl$^{-/y}$ and PV::CrTfl$^{+/y}$ animals spent a comparable amount of time in the center of the open field arena (t-test, $p = 0.824$). **e)** Representative images of IOS imaging in the visual cortex of PV::CrTfl$^{+/y}$ (top, n = 13) and PV::CrTfl$^{-/y}$ mice (bottom, n = 12). Dark areas represent active portions of brain tissue. The look-up-table is also shown. Scale bar: 1.8 mm. L, lateral; A, anterior. **f)** Quantification of IOS imaging showed an increased amplitude of the hemodynamic response in mutant animals (t-test: $p < 0.05$). **g)** Effect of kainic acid (KA) treatment at the behavioral level. Circles represent the maximum seizure rating score of individual mice over a period of 1 h after KA administration. PV::CrTfl$^{-/y}$ mice displayed a higher Racine score compared to wild-type littermates (n = 18 for both groups; t-test, $p < 0.05$). **h-k)** Severity of the epileptic phenotype in response to KA at the electrophysiological level.

PV::CrTfl$^{-/y}$ mice have a lower latency to the first seizure (h, t-test, $p < 0.05$), and increased frequency (i, t-test, $p < 0.05$) and duration (j, t-test, $p < 0.01$) of seizure events with respect to PV::CrTfl$^{+/y}$ animals. For PV::CrTfl$^{+/y}$ animals not presenting seizures during the 1 h of monitoring, the observation was extended until the occurrence of the first electrographical burst to provide a latency value. Circles represent single data values. Relative percentage of tonic, clonic and tonic–clonic seizures in PV::CrTfl$^{+/y}$ and PV::CrTfl$^{-/y}$ (k) indicates that seizure severity is more pronounced in PV::CrTfl$^{-/y}$ animals (c^2 test; $p < 0.001$). *p< 0.05, **p< 0.01, ns: not significant. Data are expressed as mean ± SEM.

Acute administration of zolpidem improves CTD phenotype

Finally, we tested whether pharmacological manipulation of the activity of PV$^+$ interneurons could rescue the CTD phenotype. Since it has been previously reported that $GABA_A$ receptors incorporating the a1 subunit are enriched at the postsynaptic level in PV$^+$ boutons [34], we used Zolpidem (Zolp), a specific agonist of a1-containing $GABA_A$ receptors, to activate synaptic targets of PV$^+$ interneurons [35,36], and we measured IOS signals in the visual cortex of CrT$^{-/y}$ animals before and after acute injection of Zolp or sterile PBS. We found that Zolp treatment significantly improved the amplitude of visually evoked IOS in CrT$^{-/y}$ mice, whereas no significant change was detected upon vehicle injection (Fig. 8b,c). Notably, IOS amplitude in Zolp-treated CrT$^{-/y}$ mice became comparable to that recorded in CrT$^{+/y}$ animals (Fig. 8b).

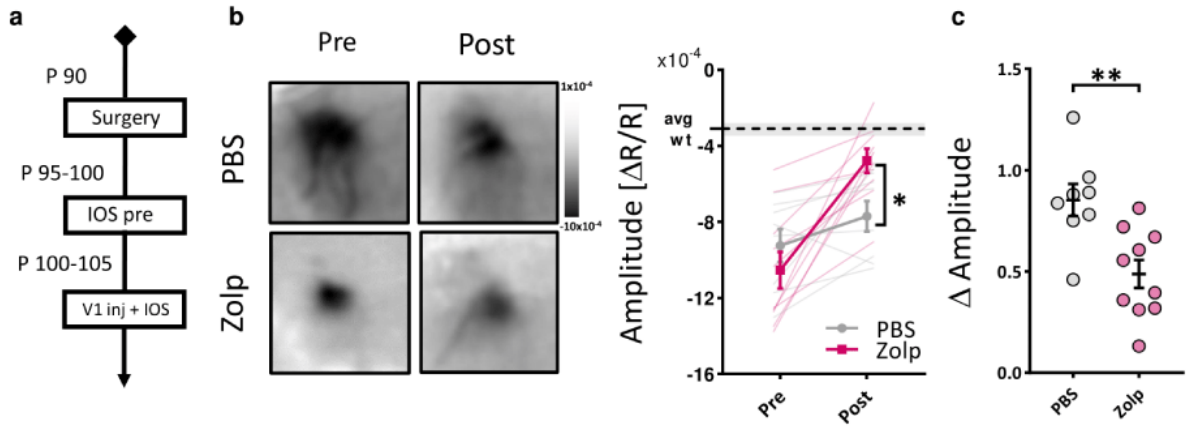

Fig. 8 Visual IOS responses after zolpidem administration. a) Experimental timeline. **b)** Representative images and **c)** quantification of IOS imaging in the visual cortex before and after zolpidem (n = 10, Zolp) or PBS injections, (n = 8) showing that Zolp treatment normalizes hemodynamic responses in CrT$^{-/y}$ mice (Two-way RM ANOVA, interaction time x treatment: p< 0.01, Sidak post-hoc multiple comparisons, $p < 0.05$ at post). Dashed line represents the average amplitude and grey area indicates the 95% confidence interval for WT mice, as previously measured [35]. The look-up-table is also shown. Scale bar: 1.8 mm. L, lateral; A, anterior. **c)** Delta of pre-post injection amplitude (t-test, $p < 0.01$). *p< 0.05, **p< 0.01. Data are expressed as mean ± SEM. Circles represent single data values.

8.1.4 Discussion

Loss-of-function mutations in the *Slc6a8* gene cause a plethora of neuropsychiatric symptoms that are well reproduced in rodent models of CTD, indicating that cellular Cr uptake is critical for proper brain function and behavior [1,8]. The Cr/phosphoCr system is a crucial hub for energy metabolism in every cell of the body, preserving ATP homeostasis and acting as an effective, mobilizable reservoir of high-energy phosphates generated in the mitochondrial compartment [37,38]. The molecular pathophysiology of CTD involves a severe disruption of metabolism [9,12,39], resulting in the compensatory upregulation of proteins implicated in energy homeostasis and mitochondrial activity, which in turn exacerbates cellular oxidative stress [5,6,9,10,40].

A detailed analysis of the molecular mechanisms underlying the brain alterations produced by Cr depletion, however, is still missing. Using bulk RNA-seq, we had the opportunity to interrogate the genomic profile of the CTD brain and we found that key metabolic and cellular stress programs are upregulated in the cerebral cortex of $CrT^{-/y}$ mice. These results corroborate the hypothesis that the inadequate supply of Cr in the brain over activates energy-generating pathways in an attempt to compensate for the chronic power shortage, likely resulting in an overload of harmful by-products of cellular metabolism corrupting physiological processes [9,10,40]. Another intriguing and novel discovery is that *Slc6a8* deletion also downregulates the expression of genes involved in protein folding and synaptic signaling, suggesting that Cr deficiency might disrupt the function and maintenance of synaptic circuits [41].

Bulk RNA-seq measures the average gene expression across the variety of cellular populations present in the sample, providing an overview of global differences in the transcriptome of the brain between the two genotypes. Given the highly heterogeneous expression of *Slc6a8* in the brain [20-22], this approach is likely to obscure the diversified and unique impact of Cr deficiency on the transcriptional programs of various cell types. Thus, we harnessed the technology of snRNA-seq to get better insight into the complexity of the effects of Cr deficiency on different cell populations [42]. With this approach we ruled out major alterations in the cellular composition of the brain of $CrT^{-/y}$ mice. This is consistent with our previous data showing that thickness and neuronal density are unaffected in the cerebral cortex of these animals [5] and with neuroimaging studies in children with CTD reporting only mild structural abnormalities [43-45]. However, we found that *Slc6a8* deletion dramatically affects gene expression in excitatory and inhibitory neurons, and oligodendrocytes. Although this observation could be limited by the number of libraries (two replicates in each group), it indicates that these cell populations might be the main players in CTD pathogenesis. Gene ontology analysis revealed that genes associated with synaptic assembly, neurotransmission

and circuit development/preservation were mostly enriched for dynamic expression across the genotypes, suggesting that alterations in the dendritic, axonal and/or synaptic compartments may strongly contribute to the neurological phenotype of CTD. Intriguingly, a significant fraction of DEGs (almost the 20% for excitatory neurons, and 30% for inhibitory cells) mapped onto the list of presynaptic and postsynaptic proteins of the SynGO database [30], suggesting that CTD might be considered a synaptopathy.

Using neurophysiological recordings, we investigated more in-depth the functional deterioration of CTD cortical circuits. The atypically high firing frequency, elevated membrane resistance and reduced rheobase that we found in pyramidal neurons indicate a hyperexcitability of the excitatory circuits that might correlate to the epileptic phenotype of $CrT^{-/y}$ mice [29]. In the absence of changes in spontaneous excitatory synaptic currents, these data suggest that this hyperexcitability might depend on altered intrinsic electrical properties of pyramidal neurons, including the membrane density and distribution of ionic conductance and receptors. However, the maintenance of a proper functional output is also influenced by inhibitory inputs. We previously reported a decrease in the number of GABAergic, but not glutamatergic, synapses in the cerebral cortex of $CrT^{-/y}$ mice [5]. Here, we identified a more specific decrease in the number of PV^+ synapses in the PFC and ACC, suggesting a dysfunction of this cell population in the CTD brain. Consistently, we found a significant hypofunction of PV^+ interneurons in the PFC. Despite future studies are needed to map the morphological and functional alteration of PV^+ synapses across multiple brain regions and throughout the different stages of CTD progression, this defective phenotype may indeed result in a global reduction of cortical inhibitory tone with potential disruption of neural circuitry efficiency [46]. One of the possible causes for the hypofunction of PV^+ interneurons might be that a lack of readily available ATP due to Cr deficiency may interfere with the maintenance of physiological ionic concentrations in the cells. The sodium–potassium ATPase (Na^+-K^+ ATPase) is the main responsible for this process, and its activity is one of the major sources of energy consumption in neurons [47]. Not surprisingly, its expression is predominant in the PV^+ subclass [48-50]. It is therefore reasonable to speculate that malfunction of the Na^+-K^+ ATPase due to energy shortage may hamper the generation of high-frequency action potentials typical of these neurons.

Remarkably, the dysfunction of PV^+ interneurons is sufficient to reproduce the cognitive deterioration and the hyperexcitability of cerebral circuits that are hallmarks of CTD. Conditional mice with *Slc6a8* deficiency restricted to this cellular population recapitulate the cognitive deficits, altered hemodynamic responses and abnormal susceptibility to KA observed in whole-body $CrT^{-/y}$ animals. The phenotypic similarity between the two murine models suggests that the depletion of Cr in PV^+ interneurons alone is sufficient to perturb the neural networks globally, leading to a CTD-like disruption of brain physiological processes.

This result is particularly remarkable considering that PV^+ interneurons represent approximately the 8-10% of the total neuronal population [32] and adds to the body of literature that identify these cells as major contributors to the etiology of several neurodevelopmental and neuropsychiatric disorders [51-60].

We need to acknowledge, however, that the replication of neurological features in PV::$CrTfl^{-/y}$ mice is not complete, because spontaneous epileptic seizures are not present in the conditional mouse model and the appearance of the behavioral phenotype is delayed to adult life. This suggests that a synergistic impairment of multiple cell types is necessary to generate the full portrait of CTD symptoms. Accordingly, snRNA-seq data highlighted that also non-neuronal cells exhibit significant gene expression changes. The high expression of *Slc6a8* in oligodendrocytes suggests that the pathophysiology of CTD might derive, at least partially, from a disruption of the tight metabolic coupling between neurons and oligodendrocytes. Despite their relatively low energy requirements, glial cells are strong Cr producers [61,62] and have been suggested to supply Cr to neurons to maintain the ionic gradient across the axolemma, propagate action potentials, and transport molecules and organelles [63]. Moreover, the decreased expression of myelin-related genes in $CrT^{-/y}$ oligodendrocytes suggests that myelin defects may contribute to the defective neuronal function in the CTD brain. Notably, recent studies showed that axon myelination is essential to the function of mature inhibitory circuits [64,65]. Thus, an impairment of oligodendrocytes function might cooperate with the specific alteration of PV^+ interneurons in the pathogenesis of CTD. Finally, it is also worth noting that terms identifying synaptic processes and assembly recurred in the GO lists of both oligodendrocytes and microglia. These cellular populations actively regulate synaptic refinement in the developing and adult mouse cortex [66-69], suggesting the possibility that an exaggerated synaptic pruning might undermine the solidity of brain circuits in CTD.

In summary, our study demonstrates that CTD pathogenesis is likely to have a complex multicellular profile with a potential network of cell-autonomous and non-autonomous effects, but the dysfunction of PV^+ interneurons is a crucial mediator of the CTD neurological phenotype. Pharmacological manipulation of PV^+ synapses can improve cortical processing in $CrT^{-/y}$ mice, indicating that therapeutic strategies selectively protecting PV^+ interneurons should be explored to prevent and/or minimize their deterioration in CTD. Drugs targeting dysfunctional PV^+ circuits are already available and have shown beneficial effects in other neuropsychiatric disorders such as schizophrenia, Fragile X syndrome and Rett syndrome [57,70]. Our results can hopefully set the background for investigating the applicability of these compounds and, more in general, for drug repurposing for the treatment of CTD.

Additional files and tables can be found in the on-line version of the article:

DOI: 10.1186/s40478-023-01533-w

8.1.5 References

1. van de Kamp JM, Mancini GM, Salomons GS (2014): X-linked creatine transporter deficiency: clinical aspects and pathophysiology. J Inherit Metab Dis 37: 715–733.

2. Joncquel-Chevalier Curt M, Voicu P-M, Fontaine M, Dessein A-F, Porchet N, Mention-Mulliez K, et al. (2015): Creatine biosynthesis and transport in health and disease. Biochimie 119: 146–165.

3. Skelton MR, Schaefer TL, Graham DL, Degrauw TJ, Clark JF, Williams MT, Vorhees CV (2011): Creatine transporter (CrT; Slc6a8) knockout mice as a model of human CrT deficiency. PLoS One 6: e16187.

4. Baroncelli L, Alessandrì MG, Tola J, Putignano E, Migliore M, Amendola E, et al. (2014): A novel mouse model of creatine transporter deficiency. F1000Res 3: 228.

5. Baroncelli L, Molinaro A, Cacciante F, Alessandrì MG, Napoli D, Putignano E, et al. (2016): A mouse model for creatine transporter deficiency reveals early onset cognitive impairment and neuropathology associated with brain aging. Hum Mol Genet 25: 4186–4200.

6. Stockebrand M, Sasani A, Das D, Hornig S, Hermans-Borgmeyer I, Lake HA, et al. (2018): A Mouse Model of Creatine Transporter Deficiency Reveals Impaired Motor Function and Muscle Energy Metabolism. Front Physiol 9: 773.

7. Duran-Trio L, Fernandes-Pires G, Simicic D, Grosse J, Roux-Petronelli C, Bruce SJ, et al. (2021): A new rat model of creatine transporter deficiency reveals behavioral disorder and altered brain metabolism. Sci Rep 11: 1636.

8. Ghirardini E, Calugi F, Sagona G, Di Vetta F, Palma M, Battini R, et al. (2021): The Role of Preclinical Models in Creatine Transporter Deficiency: Neurobiological Mechanisms, Biomarkers and Therapeutic Development. Genes 12. https://doi.org/10.3390/genes12081123

9. Perna MK, Kokenge AN, Miles KN, Udobi KC, Clark JF, Pyne-Geithman GJ, et al. (2016): Creatine transporter deficiency leads to increased whole body and cellular metabolism. Amino Acids 48: 2057–2065.

10. Giusti L, Molinaro A, Alessandrì MG, Boldrini C, Ciregia F, Lacerenza S, et al. (2019): Brain mitochondrial proteome alteration driven by creatine deficiency suggests novel therapeutic venues for creatine deficiency syndromes. Neuroscience 409: 276–289.

11. Abdulla ZI, Pennington JL, Gutierrez A, Skelton MR (2020): Creatine transporter knockout mice (Slc6a8) show increases in serotonin-related proteins and are resilient to learned helplessness. Behav Brain Res 377: 112254.

12. Chen H-R, Zhang-Brotzge X, Morozov YM, Li Y, Wang S, Zhang HH, et al. (2021): Creatine transporter deficiency impairs stress adaptation and brain energetics homeostasis. JCI Insight 6. https://doi.org/10.1172/jci.insight.140173

13. Wawro AM, Gajera CR, Baker SA, Nirschl JJ, Vogel H, Montine TJ (2021): Creatine transport and pathological changes in creatine transporter deficient mice. J Inherit Metab Dis 44: 939–948.

14. Molinaro A, Alessandrì MG, Putignano E, Leuzzi V, Cioni G, Baroncelli L, Pizzorusso T (2019): A Nervous System-Specific Model of Creatine Transporter Deficiency

Recapitulates the Cognitive Endophenotype of the Disease: a Longitudinal Study. Sci Rep 9: 62.

15. Udobi KC, Kokenge AN, Hautman ER, Ullio G, Coene J, Williams MT, et al. (2018): Cognitive deficits and increases in creatine precursors in a brain-specific knockout of the creatine transporter gene Slc6a8. Genes Brain Behav 17: e12461.

16. Bélanger M, Allaman I, Magistretti PJ (2011): Brain energy metabolism: focus on astrocyte-neuron metabolic cooperation. Cell Metab 14: 724–738.

17. Magistretti PJ, Allaman I (2015): A cellular perspective on brain energy metabolism and functional imaging. Neuron 86: 883–901.

18. Harris JJ, Jolivet R, Attwell D (2012): Synaptic energy use and supply. Neuron 75: 762–777.

19. Hyder F, Rothman DL, Bennett MR (2013): Cortical energy demands of signaling and nonsignaling components in brain are conserved across mammalian species and activity levels. Proc Natl Acad Sci U S A 110: 3549–3554.

20. Braissant O, Béard E, Torrent C, Henry H (2010): Dissociation of AGAT, GAMT and SLC6A8 in CNS: relevance to creatine deficiency syndromes. Neurobiol Dis 37: 423–433.

21. Lake BB, Ai R, Kaeser GE, Salathia NS, Yung YC, Liu R, et al. (2016): Neuronal subtypes and diversity revealed by single-nucleus RNA sequencing of the human brain. Science 352: 1586–1590.

22. Yao Z, Liu H, Xie F, Fischer S, Adkins RS, Aldridge AI, et al. (2021): A transcriptomic and epigenomic cell atlas of the mouse primary motor cortex. Nature 598: 103–110.

23. Saunders A, Macosko EZ, Wysoker A, Goldman M, Krienen FM, de Rivera H, et al. (2018): Molecular Diversity and Specializations among the Cells of the Adult Mouse Brain. Cell 174: 1015–1030.e16.

24. Ritchie ME, Phipson B, Wu D, Hu Y, Law CW, Shi W, Smyth GK (2015): limma powers differential expression analyses for RNA-sequencing and microarray studies. Nucleic Acids Res 43: e47.

25. Ge SX, Jung D, Yao R (2020): ShinyGO: a graphical gene-set enrichment tool for animals and plants. Bioinformatics 36: 2628–2629.

26. Szklarczyk D, Gable AL, Nastou KC, Lyon D, Kirsch R, Pyysalo S, et al. (2021): The STRING database in 2021: customizable protein-protein networks, and functional characterization of user-uploaded gene/measurement sets. Nucleic Acids Res 49: D605–D612.

27. Cid E, Marquez-Galera A, Valero M, Gal B, Medeiros DC, Navarron CM, et al. (2021): Sublayer- and cell-type-specific neurodegenerative transcriptional trajectories in hippocampal sclerosis. Cell Rep 35: 109229.

28. Ting JT, Lee BR, Chong P, Soler-Llavina G, Cobbs C, Koch C, et al. (2018): Preparation of Acute Brain Slices Using an Optimized N-Methyl-D-glucamine Protective Recovery Method. J Vis Exp. https://doi.org/10.3791/53825

29. Mazziotti R, Cacciante F, Sagona G, Lupori L, Gennaro M, Putignano E, et al. (2020): Novel translational phenotypes and biomarkers for creatine transporter deficiency. Brain Commun 2: fcaa089.

30. Koopmans F, van Nierop P, Andres-Alonso M, Byrnes A, Cijsouw T, Coba MP, et al. (2019): SynGO: An Evidence-Based, Expert-Curated Knowledge Base for the Synapse. Neuron 103: 217–234.e4.

31. Monyer H, Markram H (2004): Interneuron Diversity series: Molecular and genetic tools to study GABAergic interneuron diversity and function. Trends Neurosci 27: 90–97.

32. Hu H, Gan J, Jonas P (2014): Interneurons. Fast-spiking, parvalbumin+ GABAergic interneurons: from cellular design to microcircuit function. Science 345: 1255263.

33. Carter BC, Bean BP (2009): Sodium entry during action potentials of mammalian neurons: incomplete inactivation and reduced metabolic efficiency in fast-spiking neurons. Neuron 64: 898–909.

34. Klausberger T, Roberts JDB, Somogyi P (2002): Cell type- and input-specific differences in the number and subtypes of synaptic GABA(A) receptors in the hippocampus. J Neurosci 22: 2513–2521.

35. Sanna E, Busonero F, Talani G, Carta M, Massa F, Peis M, et al. (2002): Comparison of the effects of zaleplon, zolpidem, and triazolam at various GABA(A) receptor subtypes. Eur J Pharmacol 451: 103–110.

36. Katagiri H, Fagiolini M, Hensch TK (2007): Optimization of somatic inhibition at critical period onset in mouse visual cortex. Neuron 53: 805–812.

37. Wallimann T, Tokarska-Schlattner M, Schlattner U (2011): The creatine kinase system and pleiotropic effects of creatine. Amino Acids 40: 1271–1296.

38. Ellington WR (2001): Evolution and physiological roles of phosphagen systems. Annu Rev Physiol 63: 289–325.

39. Nabuurs CI, Choe CU, Veltien A, Kan HE, van Loon LJC, Rodenburg RJT, et al. (2013): Disturbed energy metabolism and muscular dystrophy caused by pure creatine deficiency are reversible by creatine intake. J Physiol 591: 571–592.

40. Li S, Bianconi S, van der Veen JW, Dang Do A, Stolinski J, Cecil KM, et al. (2021): Oxidative phosphorylation in creatine transporter deficiency. NMR Biomed 34: e4419.

41. Gorenberg EL, Chandra SS (2017): The Role of Co-chaperones in Synaptic Proteostasis and Neurodegenerative Disease. Front Neurosci 11: 248.

42. Li X, Wang C-Y (2021): From bulk, single-cell to spatial RNA sequencing. Int J Oral Sci 13: 36.

43. deGrauw TJ, Salomons GS, Cecil KM, Chuck G, Newmeyer A, Schapiro MB, Jakobs C (2002): Congenital creatine transporter deficiency. Neuropediatrics 33: 232–238.

44. van de Kamp JM, Betsalel OT, Mercimek-Mahmutoglu S, Abulhoul L, Grünewald S, Anselm I, et al. (2013): Phenotype and genotype in 101 males with X-linked creatine transporter deficiency. J Med Genet 50: 463–472.

45. Heussinger N, Saake M, Mennecke A, Dörr H-G, Trollmann R (2017): Variable White Matter Atrophy and Intellectual Development in a Family With X-linked Creatine Transporter Deficiency Despite Genotypic Homogeneity. Pediatr Neurol 67: 45–52.

46. Baroncelli L, Braschi C, Spolidoro M, Begenisic T, Maffei L, Sale A (2011): Brain plasticity and disease: a matter of inhibition. Neural Plast 2011: 286073.

47. Wong-Riley MTT (2012): Bigenomic regulation of cytochrome c oxidase in neurons and the tight coupling between neuronal activity and energy metabolism. Adv Exp Med Biol 748: 283–304.

48. Anderson TR, Huguenard JR, Prince DA (2010): Differential effects of Na+-K+ ATPase blockade on cortical layer V neurons. J Physiol 588: 4401–4414.

49. Murata K, Kinoshita T, Ishikawa T, Kuroda K, Hoshi M, Fukazawa Y (2020): Region- and neuronal-subtype-specific expression of Na,K-ATPase alpha and beta subunit isoforms in the mouse brain. J Comp Neurol 528: 2654–2678.

50. Smith RS, Florio M, Akula SK, Neil JE, Wang Y, Hill RS, et al. (2021): Early role for a Na,K-ATPase () in brain development. Proc Natl Acad Sci U S A 118. https://doi.org/10.1073/pnas.2023333118

51. Ruden JB, Dugan LL, Konradi C (2021): Parvalbumin interneuron vulnerability and brain disorders. Neuropsychopharmacology 46: 279–287.

52. Gulyás AI, Buzsáki G, Freund TF, Hirase H (2006): Populations of hippocampal inhibitory neurons express different levels of cytochrome c. Eur J Neurosci 23: 2581–2594.

53. Kann O, Papageorgiou IE, Draguhn A (2014): Highly energized inhibitory interneurons are a central element for information processing in cortical networks. J Cereb Blood Flow Metab 34: 1270–1282.

54. Whittaker RG, Turnbull DM, Whittington MA, Cunningham MO (2011): Impaired mitochondrial function abolishes gamma oscillations in the hippocampus through an effect on fast-spiking interneurons. Brain 134: e180; author reply e181.

55. Scheuer T, Endesfelder S, Auf dem Brinke E, Bührer C, Schmitz T (2022): Neonatal Oxidative Stress Impairs Cortical Synapse Formation and GABA Homeostasis in Parvalbumin-Expressing Interneurons. Oxid Med Cell Longev 2022: 8469756.

56. Inan M, Zhao M, Manuszak M, Karakaya C, Rajadhyaksha AM, Pickel VM, et al. (2016): Energy deficit in parvalbumin neurons leads to circuit dysfunction, impaired sensory gating and social disability. Neurobiol Dis 93: 35–46.

57. Patrizi A, Picard N, Simon AJ, Gunner G, Centofante E, Andrews NA, Fagiolini M (2016): Chronic Administration of the N-Methyl-D-Aspartate Receptor Antagonist Ketamine Improves Rett Syndrome Phenotype. Biol Psychiatry 79: 755–764.

58. Mukherjee A, Carvalho F, Eliez S, Caroni P (2019): Long-Lasting Rescue of Network and Cognitive Dysfunction in a Genetic Schizophrenia Model. Cell 178: 1387–1402.e14.

59. Zorrilla de San Martin J, Donato C, Peixoto J, Aguirre A, Choudhary V, De Stasi AM, et al. (2020): Alterations of specific cortical GABAergic circuits underlie abnormal network activity in a mouse model of Down syndrome. Elife 9. https://doi.org/10.7554/eLife.58731

60. Kalinowska M, van der Lei MB, Kitiashvili M, Mamcarz M, Oliveira MM, Longo F, Klann E (2022): Deletion of Fmr1 in parvalbumin-expressing neurons results in dysregulated translation and selective behavioral deficits associated with fragile X syndrome. Mol Autism 13: 29.

61. Braissant O, Henry H, Loup M, Eilers B, Bachmann C (2001): Endogenous synthesis and transport of creatine in the rat brain: an in situ hybridization study. Brain Res Mol Brain Res 86: 193–201.

62. Baker SA, Gajera CR, Wawro AM, Corces MR, Montine TJ (2021): GATM and GAMT synthesize creatine locally throughout the mammalian body and within oligodendrocytes of the brain. Brain Res 1770: 147627.

63. Bonvento G, Valette J, Flament J, Mochel F, Brouillet E (2017): Imaging and spectroscopic approaches to probe brain energy metabolism dysregulation in neurodegenerative diseases. J Cereb Blood Flow Metab 37: 1927–1943.

64. Benamer N, Vidal M, Balia M, Angulo MC (2020): Myelination of parvalbumin interneurons shapes the function of cortical sensory inhibitory circuits. Nat Commun 11: 5151.

65. Dubey M, Pascual-Garcia M, Helmes K, Wever DD, Hamada MS, Kushner SA, Kole MHP (2022): Myelination synchronizes cortical oscillations by consolidating parvalbumin-mediated phasic inhibition. Elife 11. https://doi.org/10.7554/eLife.73827

66. Paolicelli RC, Bolasco G, Pagani F, Maggi L, Scianni M, Panzanelli P, et al. (2011): Synaptic pruning by microglia is necessary for normal brain development. Science 333: 1456–1458.

67. Schafer DP, Lehrman EK, Kautzman AG, Koyama R, Mardinly AR, Yamasaki R, et al. (2012): Microglia sculpt postnatal neural circuits in an activity and complement-dependent manner. Neuron 74: 691–705.

68. Auguste YSS, Ferro A, Kahng JA, Xavier AM, Dixon JR, Vrudhula U, et al. (2022): Oligodendrocyte precursor cells engulf synapses during circuit remodeling in mice. Nat Neurosci 25: 1273–1278.

69. Guedes JR, Ferreira PA, Costa JM, Cardoso AL, Peça J (2022): Microglia-dependent remodeling of neuronal circuits. J Neurochem 163: 74–93.

70. Olmos-Serrano JL, Corbin JG, Burns MP (2011): The GABA(A) receptor agonist THIP ameliorates specific behavioral deficits in the mouse model of fragile X syndrome. Dev Neurosci 33: 395–403.

Acknowledgements

I want to thank Dr. Laura Baroncelli for being a mentor during my years of scientific training. I thank her, in particular, for the attention and care she has always shown towards her students.
A special thanks also go to Dr. Paola Tognini for encouraging and directing me in the early stages of my research activity. I would also like to thank everyone I have met working at the Istituto di Neuroscienze in Pisa. A special thanks go to Elena, Vania, and above all, Anto. Finally, I would like to thank the wonderful group I am part of, made up of people with exceptional qualities who have enriched me both from a professional point of view and from a human point of view. All my sincere gratitude goes to them.